Ultracold Dipolar Gases in Deep Optical Lattices

Von der Fakultät für Mathematik und Physik der
Gottfried Wilhelm Leibniz Universität Hannover
zur Erlangung des Grades

Doktor der Naturwissenschaften
Dr. rer. nat.

genehmigte Dissertation von

Dipl.-Phys. Michael Klawunn
geboren am 19. August 1981 in Hildesheim

Institut für Theoretische Physik
Gottfried Wilhelm Leibniz Universität Hannover

2009

Referent: Prof. Dr. Luis Santos
Koreferent: Prof. Dr. Eric Jeckelmann
Tag der Promotion: 17. Dezember 2009

to Maria

Abstract

Ultracold dilute atomic gases are highly controllable systems whose properties are fundamentally determined by the interatomic interactions. In typical experiments on ultra cold gases particles interact dominantly via a short-range isotropic potential. However, during the last years a new generation of experiments is starting to explore systems, where an additional interaction, the long-range and anisotropic dipole-dipole interaction plays a significant or possibly dominant role. The effects induced by the anisotropy of the dipole-dipole interaction are crucially enhanced if the dipolar gas is confined in a deep optical lattice. In this thesis we study novel phenomena in such systems of dipolar gases in deep optical lattices.

The nonlocal nonlinearity introduced by the dipole-dipole interaction plays a crucial role in the physics of dipolar Bose-Einstein condensates. In particular, it may distort significantly the stability of straight vortex lines. Remarkably, in the presence of a periodic potential along the vortex line, the spectrum of transverse modes shows a roton-like minimum, which eventually destabilizes the straight vortex when the BEC as a whole is still stable, opening the possibility for new scenarios for vortex line configurations in dipolar gases. We have analyzed this instability, and showed that it leads to a second-order-like phase transition from a straight vortex line into novel helical or snake-like configurations, depending on the dipole orientation.

Strong 1D lattices usually lead to unconnected two-dimensional gases. The long-range character of the dipole-dipole interactions leads to a novel scenario where non-overlapping gases at different sites may interact significantly. We show that the excitations of non-overlapping condensates in 1D optical lattices acquire a band-like character, being collectively shared by different sites. In particular, the hybridization of the modes significantly enhances the rotonization of the excitations, and may induce roton-instability. We discuss the observability of this effect in on-going experiments.

Fermionic polar molecules in deep 1D optical lattices may form self-assembled filaments when the electric dipoles are oriented along the lattice axis. These composites are bosons or fermions depending on the number of molecules per chain, leading to a peculiar and complex Bose-Fermi mixture,

which we discuss in detail for the simplest case of a three-well potential. We show that the interplay between filament binding energy, transverse filament modes, and trimer Fermi energy leads to a rich variety of possible scenarios ranging from a degenerate Fermi gas of trimers to a binary mixture of two different types of bosonic dimers. We study the intriguing zero temperature and finite temperature physics of these composites for the particular case of an ideal filament gas loaded in 1D sites, and discuss possible methods to probe these chain mixtures.

Keywords: Bose-Einstein Condensation, Dipole-Dipole Interaction, Optical Lattices.

Zusammenfassung

Verdünnte ultrakalte Gase sind gut kontrollierbare Systeme deren Eigenschaften grundlegend durch interatomare Wechselwirkungen bestimmt werden. In typischen Experimenten mit ultrakalten Gase sind diese Wechselwirkungen hauptsächlich kurzreichweitig und isotrop. Allerdings hat in den letzten Jahren eine neue Generation von Experimenten damit begonnen Systeme zu erforschen, in denen eine zusätzliche Wechselwirkung, die langreichweitige und anisotrope Dipol-Dipol Wechselwirkung, eine signifikante oder sogar dominierende Rolle spielt. Die Auswirkungen, die von der Anisotropie der Dipol-Dipol Wechselwirkung verursacht werden, werden bedeutend verstärkt, wenn sich das dipolare Gas in einem optischen Gitter befindet. In dieser Arbeit werden neuartige Phänomene studiert, die in solchen Systemen von dipolaren Gasen in optischen Gittern auftreten.

Die nonlokale Nichtlinearität, die mit der Dipol-Dipol Wechselwirkung einhergeht spielt eine entscheidende Rolle in der Physik dipolarer Bose-Einstein Kondensate. Insbesondere kann sie die Stabilität von geraden Vortex Filamenten signifikant beeinflussen. Bemerkenswerterweise weist das Spektrum transversaler Moden in Anwesenheit eines periodischen Potential entlang des Vortex Filaments ein Roton-artiges Minimum auf, das unter Umständen den geraden Vortex destabilisieren kann, während das Bose-Einstein Kondensat als ganzes stabil bleibt. Dies eröffnet in dipolaren Gasen die Möglichkeit für neue Szenarien von Vortex Filament Strukturen. Wir haben diese Instabilität studiert und gezeigt, dass sie zu einem Phasenübergang zweiter Art führt, bei dem das gerade Vortex Filament in Abhängigkeit von der Ausrichtung der Dipole in eine neuartige helix- oder schlangenlinien-artige Konfiguration übergeht.

Üblicherweise führen starke 1D Gitter zu unverbundenen zwei-dimensionalen Gasen. Der langreichweitige Charakter der Dipol-Dipol Wechselwirkung führt zu neuartigen Situationen in denen nicht-überlappende Gase auf verschiedenen Gitterplätzen signifikant wechselwirkungen können. Wir zeigen, dass Anregungen in nicht-überlappenden Kondensaten in 1D optischen Gittern einen band-artigen Charakter aufweisen, da sie von den verschiedenen Gitterplätzen gemeinsam geteilt werden. Insbesondere verstärkt die Hybridisierung dieser Moden entscheidend die Rotonisation der Anre-

gungen und kann eine Roton-Instabilität verursachen. Wir diskutieren die Beobachtbarkeit dieses Effekts in laufenden Experimenten.

Fermionische polare Moleküle in tiefen 1D optischen Gittern können selbstbildende Filamente formen, wenn ihre elektrischen Dipole in Richtung des Gitters ausgerichtet sind. Diese Verbindungen können, abhängig von der Anzahl der Moleküle pro Filament, Bosonen oder Fermionen sein, was zu einer seltsamen und komplexen Bose-Fermi Mischung führt, die wir für den einfachsten Fall eines Drei-Mulden Potentials im Detail diskutieren. Wir zeigen, dass das Wechselspiel von Filament Bindungs-Energien, transversalen Filament Moden und Trimer Fermi-Energie zu einer reichen Vielfalt von möglichen Szenarien führt. Diese reichen von einem entarteten Fermi Gas von Trimeren zu einer binären Mischung aus zwei verschiedenen Arten von bosonischen Dimeren. Wir studieren die faszinierende Physik von Verbindungen bei Null und bei endlicher Temperatur für den speziellen Fall eines idealen Filament Gases, das in 1D Gitterplätze geladen wurde, und diskutieren mögliche Methoden um diese Filament Mischungen zu untersuchen.

Schlagwörter: Bose-Einstein Kondensation, Dipol-Dipol Wechselwirkung, Optische Gitter

Contents

Chapter 1

Introduction

Since the first production of liquid Helium by H. K. Onnes in 1908 (Nobel prize 1913), low temperature physics provides promising systems for the investigaton of quantum effects related to electrons and atoms normally concealed by thermal motion. After considerations on ideal quantum gases in the 1920's lead to the prediction of a new state of matter, the Bose-Einstein condensation [1, 2], weakly interacting quantum gases has been studied as superfluid and superconducting systems intensively by the condensed matter community in the 50's and 60's [3, 4]. Thanks to new laser-based cooling and trapping techniques developed in the 70's and 80's [5, 6, 7] (Nobel prize 1997 to S. Chu, C. Cohen-Tannoudji and W.D. Phillips) it was finally possible to reveal the quantum statistics of ultra cold atoms in 1995 with the first observation of Bose-Einstein condensation [8, 9, 10], (Nobel prize 2001 to E. A. Cornell, C. E. Wieman and W. Ketterle [11, 12]). Later quantum degenerated atomic Fermi gases followed [13, 14, 15, 16].

These ultracold atomic gases generated with methods from quantum optics are highly controllable quantum many body systems and lead hence to a better understanding of the properties of condensed matter systems like weakly interacting Bose [17] and Fermi gases [18]. In our days also the regime of strongly correlated systems can be investigated with cold gases. In the last years atomic Fermi gases has been used to study classical condensed matter problems like Cooper-pairing and Fermi-superfluidity, described for weak attractive interactions by the famous BCS theory of superconductivity [19, 18], and the related BCS-BEC crossover [18, 20]. In addition it has become possible to create quantum gases with several components (e.g. different atoms or atoms in different internal states), the so called spinor gases [21, 22]. As highly controllable systems, cold atoms have important applications in e.g. quantum information [23], quantum metrology [24, 25] and atom interferometry [26, 27].

With the implementation of optical lattices a few years ago, lattice structures from condensed matter and solid state systems can be reproduced in a

highly controllable and defect-free way [28]. In this context the superfluid to Mott-insulator transition [29, 30] and the observation of Bloch oscillations [31] have been realized. Using thight traps and/or optical lattices atomic gases can be confined to low dimensional systems (Sec. 1.3.1) which opens the possibility to observe a variety of interesting condensed matter phenomena.

During the last years a new generation of experiments is starting to explore systems, where an additional interaction, the long-range and anisotropic dipole-dipole interaction offers a fascinating novel physics [32, 33]. The effects induced by the anisotropy of the dipole-dipole interaction are crucially enhanced if the dipolar gas is confined in a deep optical lattice. In this thesis we will study novel phenomena in such systems of "Dipolar gases in deep optical lattices".

In this first chapter, we start with a presentation of the basic features of ideal Bose and Fermi gases followed by a description of Bose-Einstein condensates in weakly interacting gases. Then we briefly introduce different kinds of traps and optical lattices and consider Bose-Einstein condensates in confined system. Since a large part of the thesis deals with vortex lines in Bose-Einstein condensates we also discuss the physics of such objects in an introductory section. Last but not least we specify the dipole-dipole interaction potential and some important properties of the dipolar Bose-Einstein condensate.

1.1 Ideal quantum gases

The physics of ideal quantum gases is well known and has been summarized in various textbooks [17, 34, 35]. An important quantity for a statistical analysis is the *distribution function* indicating the mean number of particles occupying a single particle state i at temperature T

$$\langle n_i \rangle = \frac{1}{e^{\beta(\epsilon_i - \mu)} \pm 1}, \tag{1.1}$$

with a $(+)$-sign if the particles are fermions and a $(-)$-sign for bosons. Here $\beta \equiv 1/k_B T$, μ is the chemical potential and ϵ_i the energy of the quantum state i. The sign in the denominator reflects the fact that in the case of fermions maximally one particle can occupy the state i, while in the bosonic case an arbitrarily high occupation number $\langle n_i \rangle$ is possible. The chemical potential acts as a variational parameter fixed by the conservation of the total particle number[1]

$$N = \sum_i \langle n_i \rangle. \tag{1.2}$$

[1] These formulas can be derived easily from the grand-canonical partition-function $\mathcal{Z}$ via $N = d(\ln \mathcal{Z})/d\mu$.

In order to make this equation more transparent we introduce a very important quantity, the *density of states*, which counts the states in an infinitesimally small energy-interval $[\epsilon, \epsilon + \Delta\epsilon]$ and is defined as

$$D(\epsilon) = \sum_i \delta(\epsilon - \epsilon_i). \tag{1.3}$$

The density of states is usually calculated in the thermodynamic limit, where the energy levels are continuously distributed and the sum can be replaced by an integral. In free space the thermodynamic limit is defined by $N \to \infty, V \to \infty$, but N/V finite, while in an isotropic harmonic trap with frequency ω it is $k_B T \ll \hbar\omega$. The density of states does not depend on the statistics, but, in addition to the energy-distribution ($\epsilon_p = p^2/2m$ (free), $\epsilon_i = \frac{d}{2}(\hbar\omega\, i + 1/2)$ (trap)) it depends crucially on the dimension d of the system. Hence we find from (1.3) $D(\epsilon) \propto \epsilon^{(d-2)/2}$ (free) and $D(\epsilon) \propto \epsilon^{(d-1)}$ (trap), respectively. Using the density of states, equation (1.2) reads

$$N = \int_0^\infty d\epsilon\, D(\epsilon)\, n(\epsilon), \tag{1.4}$$

where $n(\epsilon)$ is the mean number of particles in the energy interval $[\epsilon, \epsilon + \Delta\epsilon]$ and is given by equation (1.1). In the following section we shall analyse this equation in order to reveal some characteristic features of the Fermi and Bose gas, respectively.

1.1.1 The ideal Fermi gas

At zero temperature the Fermi distribution function (1.1) reduces to the Heaviside step function $n(\epsilon) = \Theta(\epsilon - \mu)$, so that all energy levels with $\epsilon < \mu$ are filled with one particle, while higher levels are empty. Then the gas is called a *degenerate Fermi gas* and one can determine the highest occupied energy level $\mu(T = 0) \equiv \epsilon_F$ called the *Fermi energy* from

$$N = \int_0^{\epsilon_F} d\epsilon\, D(\epsilon). \tag{1.5}$$

The Fermi energy depends only on the density of states derived for some special cases in the previous section. Hence in d dimensions $\epsilon_F \propto \frac{\hbar^2}{m} n^{2/d}$ (free) with the particle number density $n = N/V$, and $\epsilon_F \propto \hbar\omega N^{1/d}$ (trap). The Fermi energy is an important energy-scale, and gives a criterion, whether the Fermi-gas can be treated as ideal or not. If the total interaction energy is small in comparison with the Fermi energy $E_{int} \ll \epsilon_F$, the interactions can be neglected. The Fermi temperature associated with ϵ_F via $k_B T_F \equiv \epsilon_F$ is the corresponding temperature scale. That means that a Fermi-gas can be considered as degenerate at temperatures $T \ll T_F$. [2] On the other hand

[2] Note, that this temperature may be even of the order of room temperature if the density of the Fermi gas and therefore the Fermi-energy are sufficiently high.

at $T \gg T_F$ the system looses its quantum character and has to be treated classically. An important length scale is given by the inverse Fermi momentum k_F^{-1} defined by $\epsilon_F = \hbar^2 k_F^2/2m$, which is proportional to the mean interparticle distance.

The spatial density distribution $n(\vec{r})$ of N particles in an harmonic trap is given by the eigenstates of the harmonical oscillator [36], which are occupied by the N particles. At $T = 0$ the density $n(\vec{r})$ can be derived in the *local density approximation*, where $\epsilon = p^2/2m + V_{ho}(\vec{r})$ by integrating the distribution function (1.1) in momentum space [18]. Introducing the Thomas-Fermi radius $R_i = \sqrt{2\epsilon_F/m\omega_i}$, giving the width of the density distribution, in the i-th direction, where ω_i is the corresponding trap frequency we find in d dimensions the density profile as an inverted parabola

$$n(\vec{r}) \propto \frac{N}{\left(\prod_i^d R_i\right)} \left[1 - \sum_i^d \left(\frac{x_i^2}{R_i}\right)\right]^{d/2}. \tag{1.6}$$

with $R_i \propto N^{1/2d}$. A profile of this form is called *Thomas-Fermi profile*.

1.1.2 The ideal Bose gas

Remember that for a given total particle number N and temperature T equation (1.4) is a transcendental equation for the chemical potential μ and reads for bosons

$$N = \int_0^\infty d\epsilon \, \frac{D(\epsilon)}{e^{\beta(\epsilon-\mu)} - 1}. \tag{1.7}$$

Note, that this equation makes sense only if $\mu < 0$. Solving (1.7) we find that $\mu(T, N)$ changes with decreasing temperature only until a critical temperature T_c is reached. Below T_c the chemical potential remains constant $\mu_c \equiv \mu(T_c)$. (e.g. $\mu_c = 0$ (free gas)) and equation (1.7) has no solution. Interestingly the critical temperature depends only on the density of states $D(\epsilon)$ and is therefore of the same order as the temperature T_F of the corresponding Fermi-gas, hence $T_c \propto \frac{\hbar^2}{m} n^{2/d}$ (free) and $T_c \propto \hbar\omega N^{1/d}$ (trap). In order to find the reason why equation (1.7) has no solution at $T < T_c$ we have to go back to equation (1.2), where the energy-levels are not considered as continuous. At $\mu = \mu_c$ the number of particles N_0 in the ground-state ($i = 0$) formally diverges and has to be treated separately. That means that at $T < T_c$ the ground state is macroscopically occupied and N_0 is of the order of the total number of particles N_{ex} in all excited states. This phenomenon is called *Bose-Einstein condensation* [1, 2] and the particles N_0 in the ground state form the *Bose-Einstein condensate (BEC)*. The fraction of particles in the BEC can be calculated via $N_0/N = 1 - N_{ex}/N$, whereas N_{ex} is given again by (1.7) with energy levels counted as continuous and with $\mu = \mu_c$. Hence the fraction of particles in the BEC also depends only on the

density of states

$$\frac{N_0}{N} = 1 - \frac{1}{N}\int_0^\infty d\epsilon \, \frac{D(\epsilon)}{e^{\beta(\epsilon-\mu_c)}-1}, \tag{1.8}$$

and obeys as a function of temperature

$$N_0/N = 1 - (T/T_c)^{d/2} \qquad \text{(free)} \tag{1.9}$$

$$N_0/N = 1 - (T/T_c)^{d} \qquad \text{(trap)} \tag{1.10}$$

In lower-dimensional systems it may happen that the integral on the right hand site of equation (1.8) diverges, namely if the density of states is $D(\epsilon) \propto \epsilon^\lambda$ and $\lambda \leq 0$. Then the fraction of particles in the condensate and the critical temperature tend to zero and no BEC is formed. In particular it follows from the expressions for $D(\epsilon)$ given above that there is no Bose-Einstein condensation in one and two dimensions in free space and in a one-dimensional harmonic trap.

The spatial density distribution in an harmonic oscillator [17, 36] trap in the case of bosons is simple. The particles in the BEC are characterized by the ground-state wave function of the harmonic oscillator which is simply a Gaussian function and reads in d dimensions

$$\Psi(\vec{r}) = \prod_{i=1}^{d} \frac{1}{\left(\pi l_i^2\right)^{1/4}} \exp\left\{-\frac{x_i^2}{2l_i^2}\right\}, \tag{1.11}$$

where $l_i = \sqrt{\hbar/m\omega_i}$ for frequencies ω_i. The rest of the particles thermally distributed in higher oscillator levels is spacially more expanded and is called *thermal cloud*. The radius of the BEC is the averaged width of the Gaussian $l_{ho} = (\prod_i l_i)^{1/d}$, which is in typical experiments around 1 μm, while the radius of the thermal cloud is approximately $R_T \approx l_{ho}(k_b T/\hbar\omega_{ho})^{1/2}$.

1.2 The weakly interacting Bose gas

In real experiments one usually has even in the case of very dilute ultra cold gases at least weak interactions. That is why we have to ask ourselves, whether a BEC as defined in the previous section for ideal gases can develop in the case of interactions as well. Therefore we need a more general definition of Bose-Einstein condensation which still holds in the interacting case [35]. Remember that for an ideal gas a BEC was defined as a macroscopically occupied single-particle quantum state. This definition can be generalized [37] to quantum many-body states described by the density-matrix

$$\rho(\vec{r},\vec{r}',t) = \langle \hat{\Psi}^\dagger(\vec{r},t)\hat{\Psi}(\vec{r}',t)\rangle, \tag{1.12}$$

where $\hat{\Psi}(\vec{r},t)$ is the Bose field operator at position $\vec{r}$ and time t. If at time t one of the eigenvalues of the density-matrix is macroscopic, i.e. of the order

of the sum of all other eigenvalues and much larger than any of them, then this eigenvalue defines the number of particles N_0 in the BEC.[3] If on the contrary all eigenvalues of ρ are more or less of the same order a BEC does not exists. Actually macroscopic means that the eigenvalue is of the order of the total number of particles N, with $N \to \infty$ in the thermodynamic limit. But in experiments with finite sized systems this limit is strictly speaking not well defined. However, if we have for example 10^8 atoms in a trap and say 5×10^7 of them are in the ground state, while the number of particles in none of the excited state is larger than 10^3, we can confidently consider the system as Bose-condensed.

An alternative definition of Bose-Einstein condensation in quantum many-body systems is based on the concept of off-diagonal long-range order (ODLRO) [38]. Instead of diagonalizing $\rho(\vec{r}, \vec{r}')$ at time t in ODLRO one is interested in the limit $|\vec{r} - \vec{r}'| \to \infty$. If the density matrix is finite in this limit, particles far away from each other are still correlated, resembling coherence, and can be expressed by a macroscopic wave-function $\Psi(\vec{r}, t)$ via

$$\lim_{|\vec{r}-\vec{r}'|\to\infty} \rho(\vec{r}, \vec{r}') = \Psi^*(\vec{r}, t)\Psi(\vec{r}', t). \tag{1.13}$$

This wave-function $\Psi(\vec{r}, t)$ can be identified with an order parameter characterizing the BEC. The concept of order parameters appears in the context of phase transitions in ordered media and spontaneous symmetry breaking. Note, that cooling below T_c can be considered as a phase-transition from the normal phase to the BEC phase, where the U(1) gauge symmetry of the energy-functional is spontaneously broken [39, 40] and the system chooses a certain phase.[4]. It has been shown [42] that in one and two dimensions in free space, there is no ODLRO, and hence no BEC. Furthermore, the concept of ODLRO is not well defined in finite sized systems.

In a similar definition [43, 17] of the condensate wave function we take the non-vanishing vacuum expectation value of the Bose field operator $\Psi(\vec{r}, t) \equiv \langle\hat{\Psi}(\vec{r}, t)\rangle$ as an order parameter. This definition is in analogy to the relation between the electric field operator and the classical electric field and is applied usually in the context of ultra cold atom gases. We will use this *mean field approach* in the remainder of this thesis in order to describe the ground-state wave function, the condensed part of the Bose gas. The non-condensed part $\hat{\Psi}'(\vec{r}, t)$ will be still treated as an operator so that the Bose field operator can be decomposed into

$$\hat{\Psi}(\vec{r}, t) = \Psi(\vec{r}, t) + \hat{\Psi}'(\vec{r}, t) \tag{1.14}$$

At sufficiently small temperatures and densities the non-condensed part can be treated as a small perturbation.

[3] Note, that a situation with two or more (finite number) macroscopic eigenvalues describes a fragmented BEC.

[4] This is similar to the well-known example of spontaneous symmetry breaking of the magnetization in an Heisenberg ferromagnet [41]

Equation (1.14) follows also from the *Bogoliubov approximation*. The Bose field operator can be decomposed into $\hat{\Psi}(\vec{r},t) = \sum_i \Psi(\vec{r},t)_i a_i$ with single-particle wave-functions $\Psi(\vec{r},t)_i$ and annihilation operators a_i. In the presence of a condensate the expectation value of the ground-state is macroscopic ($N \to \infty$) and hence

$$\langle a_0^\dagger a_0 \rangle_0 = N_0 \approx (N_0 + 1) = \langle a_0 a_0^\dagger \rangle_0. \tag{1.15}$$

This means that a_0 and $a_0^\dagger$ commute and can be treated as c-numbers $a_0 \approx a_0^\dagger \approx \sqrt{N_0}$. Thus the condensate is described by a macroscopic complex wave-function, whereas particles in excited states still require an operator treatment as noted in (1.14).

1.2.1 The Gross-Pitaevskii equation

In order to derive an equation for the condensate wave-function $\Psi(\vec{r},t)$ we take the many-body Hamiltonian for N weakly interacting bosons [17]

$$\begin{aligned} \hat{H} &= \int d^3r \hat{\Psi}^\dagger(\vec{r},t) \left[-\frac{\hbar^2}{2m}\nabla^2 + V_{ext}(\vec{r}) \right] \hat{\Psi}(\vec{r},t) \\ &+ \frac{1}{2} \int d^3r d^3r' \hat{\Psi}^\dagger(\vec{r},t) \hat{\Psi}^\dagger(\vec{r}',t) V(\vec{r}-\vec{r}') \hat{\Psi}(\vec{r},t) \hat{\Psi}(\vec{r}',t), \end{aligned} \tag{1.16}$$

with an external potential V_{ext} confining the bosons and the two-particle interaction potential $V(\vec{r},\vec{r}')$.[5] This Hamiltonian determines the time evolution of the Bose field. From the corresponding Heisenberg equation we find (by replacing the Bose field operator with the classical field according to (1.14)) the non-linear Schrödinger-equation

$$i\hbar \frac{\partial}{\partial t}\Psi(\vec{r},t) = \left[-\frac{\hbar^2}{2m}\nabla^2 + V_{ext}(\vec{r}) + \int d^3r' V(\vec{r}-\vec{r}') |\Psi(\vec{r}',t)|^2 \right] \Psi(\vec{r},t). \tag{1.17}$$

In dilute ultra cold gases the interatomic potential is usually short-range and can be approximated by a delta-function pseudo-potential characterized by the s-wave scattering length a [17, 44, 45, 46]

$$V(\vec{r}-\vec{r}') = g\delta(\vec{r}-\vec{r}') \tag{1.18}$$

with the coupling constant $g = 4\pi a\hbar^2/m$. The scattering length a, and hence g, are positive in the case of repulsive interactions and negative if the interatomic interactions are attractive. For most atom species it can be tuned with an external magnetic field to almost every value by using Feshbach resonances [47, 48, 49, 50]. With the contact interaction potential

[5] If the Bose gas is dilute only binary collisions are relevant and three-particle collisions can be neglected.

(1.18) equation (1.17) becomes the well known *Gross-Pitaevskii equation* (GP) [51, 52]

$$i\hbar\frac{\partial}{\partial t}\Psi(\vec{r},t) = \left[-\frac{\hbar^2}{2m}\nabla^2 + V_{ext}(\vec{r}) + g|\Psi(\vec{r},t)|^2\right]\Psi(\vec{r},t). \tag{1.19}$$

The general solution is a complex function $\Psi(\vec{r},t) = \sqrt{n(\vec{r},t)}\exp[i\phi(\vec{r},t)]$, where $n(\vec{r},t)$ is the density and $\phi(\vec{r},t)$ the phase of the condensate. Later in section 1.4 we will see that the phase is related to the velocity field of the condensate. Note, that the mean-field approach leading to this equation is valid only if the gas is sufficiently dilute and weakly interacting. Since the interactions are proportional to the scattering length and the mean density n_0, a condition for the validity of equation (1.19) is given by $an_0^{1/3} \ll 1$. In order to guarantee the conservation of the total number of particles N, we demand that the condensate wave-function $\Psi(\vec{r},t)$ satisfies the constraint

$$\int d^3r|\Psi(\vec{r},t)|^2 = N. \tag{1.20}$$

Since the Bose-field operator $\hat{\Psi}(\vec{r},t)$ reduces the number of particles by one its off-diagonal matrix element $\langle N-1|\hat{\Psi}(\vec{r},t)|N\rangle$ and hence the condensate wave-function $\Psi(\vec{r},t)$ oscillates at a frequency corresponding to the chemical potential $\mu \approx E(N)-E(N-1)$, associated with removing one particle from the ground state [53]. Thus the time-dependence of the ground-state can be seperated by $\Psi(\vec{r},t) = \Psi(\vec{r})\,e^{-i\mu t/\hbar}$ leading to the time-independent Gross-Pitaevskii equation

$$\mu\Psi(\vec{r},t) = \left[-\frac{\hbar^2}{2m}\nabla^2 + V_{ext}(\vec{r}) + g|\Psi(\vec{r},t)|^2\right]\Psi(\vec{r},t). \tag{1.21}$$

As in the ideal gas the chemical potential is $\mu = \partial E/\partial N$ and acts as a Lagrangian multiplier minimizing the free energy at small temperatures $F = E - \mu N$ associated with the conservation of the total particle number. Here E is the energy functional consisting of kinetic energy, potential energy and interaction energy

$$E = \int d^3r\left[\frac{\hbar^2}{2m}|\nabla\Psi(\vec{r})|^2 + V_{ext}(\vec{r})|\Psi(\vec{r})|^2 + \frac{1}{2}g|\Psi(\vec{r})|^4\right]. \tag{1.22}$$

Note, that an energy functional of the same form appears in the famous Ginzburg-Landau theory describing superconductivity close to the critical temperature [54]. Using a variational method, one can derive the time-independent GP-equation also from this energy-functional via

$$i\hbar\frac{\partial\Psi(\vec{r},t)}{\partial t} = \frac{\delta E}{\delta\Psi^*(\vec{r},t)}. \tag{1.23}$$

The GP equation has the form of non-linear Schrödinger equations (NLSE) describing experimentally relevant non-linear phenomena [55] in various physical fields such as optics, fluid dynamics, plasma physics and condensed matter physics. These NLSEs admit soliton solutions like kinks (1D) or vortices (2D) and are hence important for studying theoretically situations, where such phenomena occur.

In the absence of interactions ($g = 0$) the GP equation (1.19) reduces to the well-known single particle Schrödinger equation. In the absence of an external potential ($V_{ext} = 0$) the time-independent GP equation has a simple homogeneous solution of constant density n_0 obeying

$$\mu = gn_0. \tag{1.24}$$

1.2.2 Excitations of the BEC and stability analysis

The ground state of a weakly interacting Bose gas is at sufficiently low temperatures described by the macroscopic order parameter Ψ_0, obtained as a solution of equation (1.19). Following Bogoliubov [43] and Landau [56] we study collective elementary excitations corresponding to small oscillations around the ground state value as quasi-particles with energy ϵ and wave number $p = \hbar q$. The behaviour of the system under excitations is characterized by the dispersion law $\epsilon(q)$ and provides useful information about the stability of the ground state. Considering the excitations as small perturbations the wave function

$$\Psi(\vec{r}, t) = \left[\Psi_0(\vec{r}) + u(\vec{r})e^{-i\epsilon t/\hbar} + v^*(\vec{r})e^{i\epsilon^* t/\hbar}\right] e^{-i\mu t/\hbar} \tag{1.25}$$

with complex functions $u(\vec{r})$ and $v(\vec{r})$ is still a solution of the GP equation (1.19). Inserting this ansatz in (1.19) and linearizing in u and v we obtain coupled eigenvalue equations for the excitation energy ϵ

$$\epsilon u(\vec{r}) = \left[-\frac{\hbar^2}{2m}\nabla^2 + V_{ext}(\vec{r}) - \mu + 2g|\Psi_0(\vec{r})|^2\right] u(\vec{r}) + g\Psi_0(\vec{r})^2 v(\vec{r}) \tag{1.26}$$

$$-\epsilon v(\vec{r}) = \left[-\frac{\hbar^2}{2m}\nabla^2 + V_{ext}(\vec{r}) - \mu + 2g|\Psi_0(\vec{r})|^2\right] v(\vec{r}) + g\Psi_0(\vec{r})^2 u(\vec{r}) \tag{1.27}$$

called *Bogoliubov-de Gennes equations (BdG)*. This formalism decribing the quasi-particle excitations by macroscopic wave functions u and v was introduced by Pitaevskii in the context of vortex-lines excitations, the so called Kelvin-modes [52]. Later in chapter 2 we will investigate Kelvin-modes by using the same formalism. As noted earlier, in the case without trapping ($V_{ext} = 0$) the homogeneous solution $\Psi_0 = \sqrt{n_0}$ of equation (1.19) obeys $\mu = gn_0$. In this case the complex functions u and v can be approached as plane-waves $u, v \propto \exp\{-i\vec{q}\vec{r}\}$ with wave-number $\vec{q}$ and the BdG equations can be solved analytically. This leads to the dispersion law of the famous

Bogoliubov form, well known in the context of quantum fluctuations of the Bose field operator derived by diagonalizing the Hamiltonian (1.16) of the weakly interacting Bose gas with Bogoliubov transformations [57]. This dispersion relation reads

$$\epsilon(q) = \pm\sqrt{\frac{\hbar^2 q^2}{2m}\left(\frac{\hbar^2 q^2}{2m} + 2gn_0\right)}, \tag{1.28}$$

and goes quadratically in q for large momenta since the interaction term can be neglected in this regime. For small q the dispersion law is approximately linear, resembling phonons,with sound velocity $c = \sqrt{gn_0/m}$. The dispersion relation has a positive and a negative energy branch. The corresponding eigenfunctions $u(\vec{r})$ and $v(\vec{r})$ are normalized with respect to

$$\int d^3r \left(|u(\vec{r})|^2 - |v(\vec{r})|^2\right) = \pm 1 \tag{1.29}$$

whereas the states with norm (+1) normally correspond to the positive energies, while norm (-1) states belong to negative energies. The (+) and the (-) families are physically equivalent and discussed in detail in [58].

As mentioned earlier a homogeneous BEC with attractive interactions ($a < 0$) is unstable against collapse. This may be understood now from equation (1.28) considering the phonon regime. If $q \to 0$ for negative coupling constant, the excitation energy will be imaginary $\epsilon \to \pm i\epsilon$, leading to an exponential increase $\Psi \propto \exp\{+\epsilon t/\hbar\}$ of the wave function, which is the reason for the collapse of an attractively interacting Bose-Einstein condensate. This phenomenon is called *phonon instability* and is an example for a *dynamical instability* occuring in many different situations.

Another type of instability is called *thermodynamical instability* and decribes a situation, where the assumed ground state Ψ_0 is not the state of lowest energy but possibly only a local minimum of the energy functional. In order to analyze this more quantitatively, we consider the total free energy of the system following from expression (1.22). Inserting the wave-function (1.25) and linearizing again in u and v we obtain the energy contribution of the excitations

$$E_{u,v} = \left[\int d^3r \left(|u(\vec{r})|^2 - |v(\vec{r})|^2\right)\right] \epsilon. \tag{1.30}$$

This energy can be negative if $\epsilon < 0$ in the case of a positive norm state (or equivalently for negative norm states and $\epsilon > 0$)). This means that the excited state is energetically more favorable than the originally assumed ground state. Thus Ψ_0 becomes energetically unstable under small perturbations, against the lower energy configuration. In the remainder of the thesis we will encounter both types of instability the thermodynamical one in the context of vortex-line in chapter 2 and the dynamical instability in chapter 4.

1.3 Traps and optical lattices

In the previous section we approximated the external potential confining neutral atoms in a trap by an harmonical oscillator potential. In real experiments different kinds of traps occur, classified as dissipative and conservative traps. Dissipative traps like the magneto-optical trap (MOT) [59] exploit radiation pressure and are used to cool atoms down to a few microkelvin. Then in order to reach Bose-Einstein condensation evaporative cooling techniques are applied and one can cool to temperatures of the order of nanoKelvin. In evaporative cooling the atoms in high energy levels are basically thrown away, so that only the cool low-energy atoms remain in the trap and the temperature of the gas is reduced. However, by removing the hot particles from the trap one looses atoms and to prevent high losses one cannot start with these methods at too high temperatures. These techniques are applied in conservative traps like magnetic or optical traps.

Magnetic traps [11, 12, 60, 61] are based on the Zeeman effect depending on the internal states of the atoms. In order to avoid losses caused by Majorana spin-flips, usually *Ioffe-Pritchard-like* traps with finite local minima are used. These traps can be approximated by an harmonic oscillator potential.

Optical traps have the big advantage that the trapping does not depend on an internal atom state since the atoms are trapped with far detuned laser light. The laser as an external electric field induces an electric atomic dipole moment which leads to an energy shift (Stark shift [62]) proportional to the intensity profile of the laser and hence pushes the atoms to the regions with high (low) light intensity for a red-(blue-)detuned laser. In *optical dipole traps* [63, 64, 65, 66] the light beam usually has a Gaussian profile and the potential around the extremum can therefore again be approximated by an harmonic oscillator potential. However, it is possible to realize in this way various trapping geometries, and sometimes it can be also useful to combine magnetic and optical traps, for example to create double-well potentials [69].

Similar to an optical dipole trap, two counter-propagating laser beams with the same amplitude, wave-length and polarization, forming a standing wave, create an *optical lattice* potential [67, 68, 28]. The atoms are trapped in the minima[6] of the standing wave resembling lattice structures well known from condensed matter physics. Later we will discuss atoms in optical lattices in more detail.

1.3.1 Lower dimensional systems

By confining atomic gases strongly in one (pancake-shape) or two (cigar-shape) directions using highly anisotropic traps one can generate system of reduced dimensionality. Such low dimensional systems of ultracold atomic

[6] This is valid for blue-detuned lasers only, whereas for red-detuned lasers the atoms are trapped analogeously in the maxima of the standing wave.

gases provide rich physical phenomena, investigated already theoretically [70, 71, 72, 73, 74] and experimentally [75, 76, 77, 78, 79] and play an important role in the field of condensed matter physics [80, 81]. We shall now analyse the physics of BECs in a quasi two-dimensional geometry and derive the corresponding GP equation.

A system is effectively *two-dimensional* if $\hbar\omega_z \gg \mu$, meaning that the system is frozen in the ground-state of the trap in the confined z-direction. Since the trapping potential is approached as an harmonic oscillator the wave-function of the BEC reads

$$\Psi(\vec{r},t) = \psi(x,y,t)\,\phi_0(z) \quad \text{with} \quad \phi_0(z) = \frac{1}{(\pi l_z^2)^{1/4}}\,\exp\left(-\frac{z^2}{2l_z^2}\right), \quad (1.31)$$

where l_z is the very small width of the system in z-direction. Inserting this ansatz in the three-dimensional GP equation (1.19) and multiplying with $\phi_0(z)$ we can carry out the z-integration and obtain the two-dimensional GP equation

$$i\hbar\frac{\partial}{\partial t}\psi(x,y,t) = \left[-\frac{\hbar^2}{2m}\nabla_{x,y}^2 + V_{ext}(x,y) + g_{2D}|\psi(x,y,t)|^2\right]\psi(x,y,t), \quad (1.32)$$

where we have introduced an effective two-dimensional coupling constant $g_{2D} = g/\sqrt{2\pi}l_z$. In free space with homogeneous density this equation can be solved easily as in (1.24) and the 2D condition becomes $\hbar\omega_z \gg g_{2D}n_0$. Note, that in two dimensions the coupling constant is a dimensionless quantity, obtained directly from the three-dimensional scattering length. Considering the scattering process in three dimensions is necessary for $a \ll l_z$. We do not consider situations with $a \sim l_z$, where one should employ a 2D scattering theory. Note further, that this procedure is much more restrictive for the case of fermions [74], since one can employ it only if all particles are in the ground state of the trap in z-direction. This is the case only if $\epsilon_F \ll \hbar\omega_z$.

1.3.2 Optical lattices

As noted earlier, optical traps can be used to give an atomic gas a lattice structure similar to electrons in metals. This opens novel interesting possibilities for theoretical and experimental research on ultracold atomic Bose as well as Fermi gases [18, 28, 82, 83]. Contrary to traditional crystals in condensed matter physics, atoms in optical lattices are highly controllable systems. The optical lattice is defect-free and can be changed in intensity and wave length, which is usually large enough to make experimental observations. Since the atoms are neutral, also interactions are easier to control (via Feshbach resonances) than in the case of charged electrons.

A one dimensional optical lattice generated by two counterpropagating laser beams with wave-length λ_{ol} and amplitude V_0 is described by the po-

tential

$$V_{ol}(z) = sE_R \sin^2(Qz), \tag{1.33}$$

where $Q = 2\pi/\lambda_{ol}$ is the wave number and $E_R = \hbar^2 Q^2/2m$ the recoil energy of the lattice. The parameter s is the amplitude of the lasers in units of the recoil energy ($s = V_0/E_R$) and gives the depth of the optical lattice potential. For deep optical lattices, one may approximate the individual lattice wells (lattice sites) as harmonic ocsillators, with a characteristic oscillator length l_z associated to the lattice parameters via $l_z \approx bs^{-1/4}/\pi$, where $b = \lambda/2$ is the period of the lattice.

Similarly, in three dimensions the optical lattice potential reads

$$V_{ol}^{3D}(\vec{r}) = sE_R \left[\sin^2(Q_x x + \phi_x) + \sin^2(Q_y y + \phi_y) + \sin^2(Q_z z + \phi_z)\right], \tag{1.34}$$

with arbitrary phases ϕ_i. Note that an optical lattice is used normally in combination with an overall trap confining the whole system.

If the lattice is sufficiently strong the system is in the so called *tight-binding regime*, where the atoms are localized at the lattice sites and the overlap between wave-functions in different sites is small. Hence, the wave-function of a Bose-Einstein condensate in a strong one dimensional lattice (1.33) may be written as

$$\Psi(\vec{r}, t) = \sum_j w(z - bj)\psi_j(x, y, t), \tag{1.35}$$

where $\psi_j(x, y, t)$ is the wave function of the condensate on the j-lattice site, and $w(z)$ is the Wannier-function associated with the lowest energy-band. In the tight binding regime an occupation of higher bands is energetically too costly. In this sense a lattice site can be considered as a quasi 2D system studied in the previous subsection, where the system is always in the ground state of the harmonical oscillator in the strongly confined direction. Inserting this ansatz into the GP equation (1.19), we obtain a discretized non-linear Schrödinger equation [84]

$$\begin{aligned} i\hbar\frac{\partial}{\partial t}\psi_j(x, y, t) = &\left[-\frac{\hbar^2}{2m}\nabla_{x,y}^2 + V_{ext}(x, y) + \bar{g}|\psi_j(x, y, t)|^2\right]\psi(x, y, t) \\ &-J(\psi_{j-1}(x, y, t) - 2\psi_j(x, y, t) + \psi_{j+1}(x, y, t)), \end{aligned} \tag{1.36}$$

where $\bar{g} = gb\int dz\, w(z)^4$ is the renormalized coupling constant of the contact interaction and the last term gives the reduced kinetic energy in lattice direction describing hopping between neighbouring sites. The higher inertia induced by the lattice can be expressed by an effective mass $m^* \equiv \hbar^2/2b^2J$, which is inverse proportional to the hopping parameter (tunneling energy)

$$J = \int dz\, w(z)\left[-\frac{\hbar^2}{2m}\frac{d^2}{dz^2} + V_{ol}(z)\right]w(z + b) \equiv \frac{2b^2}{\hbar^2}\frac{m}{m^*}. \tag{1.37}$$

A simple calculation shows that J and hence m/m^* depends exponentially on the lattice width l_z, such that $J \to 0$ if $l_z \lesssim 1/6$. In terms of the effective mass the tight binding approximation becomes wrong if $m/m^* \to 1$, since the wave-function is not well localized and the gap between the lowest energy-band and the second energy-band is of the order of other relevant energy scales in the system. In that case a restriction on the lowest band is not valid anymore.

1.4 Vortex filaments

When rotated at sufficiently large angular frequency, a superfluid develops vortex lines of zero density [85, 56], around which the circulation is quantized due to the single-valued character of the corresponding wavefunction [86]. Quantized vortices constitute indeed one of the most important consequences of superfluidity, playing a fundamental role in various physical systems, as superconductors [19, 87] and superfluid Helium [88]. Due to the enormous progress in the control and manipulation of ultra cold gases, Bose-Einstein condensates offer an extraordinarily controllable system for the analysis of superfluidity, and in particular quantized vortices [53, 89]. Vortices and even vortex lattices have been created in BECs in a series of milestone experiments [90, 91, 92].

First of all we shall investigate the mathematical nature of vortex filaments from a topological point of view [41, 93]. In condensed matter systems vortex filaments are defined as line-defects in ordered media [94, 95, 96] in three dimensions[7] with finite core ξ. Let the complex scalar field

$$\Psi(\vec{r}, t) = |\Psi(\vec{r})|\, e^{-i\Phi(\vec{r})}, \tag{1.38}$$

be the order parameter of such a system, where $|\Psi(\vec{r})| \to$ const. and the phase depends only on the polar angle $\Phi(\vec{r}) \to \Phi_\infty(\theta)$ at large $\rho \gg \xi$ [93]. Far away from the core the order parameter space is $\mathrm{U}(1) \cong S^1$ and $\Psi_\infty \propto e^{i\Phi_\infty(\theta)}$. Now consider points on a circle at infinity S^1_∞ around the vortex line such that Ψ_∞ is a map $S^1_\infty \to \mathrm{U}(1)$. Since this map describes loops in the topological space U(1) it is classified by homotopy classes. The set of these equivalence classes π_1 is called the fundamental group or first homotopy group [41]. Using $\pi_1(\mathrm{U}(1)) = \mathbb{Z}$ we classify the map Ψ_∞ by an integer $N \in \mathbb{Z}$ [41]. Equivalently, if the order parameter is single valued the phase $\Phi_\infty(\theta)$ must satisfy

$$\Phi_\infty(2\pi) = \Phi_\infty(0) + 2\pi N, \tag{1.39}$$

so that for θ encircling S^1 once $\Phi_\infty(\theta)$ encircles S^1 N times. The integer N is called the winding number or degree of the map Ψ_∞. Two vortex lines

[7] Actually vortices are two-dimensional topological solitons [93]. The third dimension is not important for the topological character.

are equivalent under homotopy if they can be continuously transformed into each other, requiring that they have the same winding number. Since the winding number is a topological invariant of $S^1_\infty \to \mathrm{U}(1)$, it is also called the topological charge of the field configuration [93]. It is a very important quantity, because it gives a deep insight in the physics of vortex filaments. If two vortex lines with winding numbers N_1 and N_2 are merged together one gets a vortex line with total winding $N = N_1 + N_2$. However, we will show later that multi-vortex lines with winding $N > 1$ are thermodynamically unstable under small perturbations against a field configuration of N single vortex lines having winding number $N = \pm 1$. If two defects with opposite winding numbers $+N$ and $-N$ merge together the resulting field configuration has zero winding and is homotopycally equivalent to the homogeneous medium. Note, that a field configuration of non-zero winding has always a divergent energy-contribution. The centrifugal part of the kinetic energy is proportional to

$$\frac{1}{2}\int_0^{2\pi} d\theta \int_{\rho_0}^{\infty} \rho d\rho \frac{\left(\partial_\theta \Phi_\infty(\theta)\right)^2}{\rho^2}, \tag{1.40}$$

with $\rho_0 \gg \xi$ where the ρ-integral is logarithmically divergent. However, fortunately the divergent energy depends only on N and not on the positions of the vortices. Therefore it can be regularized just by removing a divergent constant [97, 98].

Other topological defects can be classified similarly. For an order parameter space M an m-dimensional defect in d dimensions is classified by the n-th homotopy group $\pi_n(M)$, where $n = d - m - 1$ (e.g. the vortex filament is a 1D defect (m=1) in 3D (d=3) classified by $\pi_1(S^1)$). Examples for other topological defects are textures in ^{3}He [99], monopoles [100], skyrmions [101, 102, 103] and domain walls, recently created in experiments using spinor condensates [104].

The definition of the vortex line we gave at the beginning of the chapter is quite general. It is applicable not only to condensed matter systems but also to cosmological global U(1)-strings occuring in the context of phase-transitions in the early universe [105], described by the Goldstone model [106] or the abelian Higgs model [107]. In both cases the Higgs field should be interpreted as an phenomenological order parameter. Note, that there are subtle differences between global U(1)-strings and vortex filaments in superfluids [108, 109]. The vortex line has a non-relativistic superfluid backround and carries angular momentum, while the global U(1)-string is defined in a Lorentz-invariant vacuum backround. However, it has been shown that introducing a special external background field spinning global U(1)-strings can describe a system of superfluid vortices [108].

In addition vortices or vortex-like excitations appear in the context of hydrodynamics [110], in the earth's atmosphere [111], and even in neutron stars [112].

In this thesis we are interested in vortices in superfluids and Bose-Einstein condensates. At first we shall derive results coming from the fact that the motion of a superfluid liquid is a potential flow. Later, considering Bose-Einstein condensates, we will study the quantum nature of the vortex lines.

1.4.1 Rotating superfluids

Let us consider a liquid in a rotating cylindrical vessel[56], [88]. An ordinary liquid rotates as a whole together with the vessel due to the friction against the vessel walls. In a superfluid only the normal component ρ_n is brought into rotation, while the superfluid component ρ_s remains at rest ($\mathrm{rot}\,\vec{v}_s = 0$). Hence superfluid motion is a potential flow with a velocity potential ϕ defined via $\vec{v}_s = \mathrm{grad}\,\phi$.

However, for sufficiently large Ω such a state becomes energetically unfavorable. In a frame rotating with Ω the energy to minimize is

$$E_{rot} = E - \vec{\Omega}\vec{L}. \tag{1.41}$$

Hence for sufficiently large Ω the term $-\vec{\Omega}\vec{L}$ causes the state with $\vec{\Omega}\vec{L} > 0$ to be thermodynamically more favorable than that with $\vec{L} = 0$. This leads to a rotation of the liquid as a whole with

$$\vec{v} = \vec{\Omega} \times \vec{r} \qquad \Rightarrow \qquad \mathrm{rot}\,\vec{v} = 2\Omega. \tag{1.42}$$

This seems to be a contradiction to the fact that superfluid motion is a potential flow. The solution of this problem is the assumption that potential flow is lost only at certain lines of singularity in the liquid called *vortex lines* or *vortex filaments*.[8] Outside these lines the potential flow ($\mathrm{rot}\,\vec{v}_s = 0$) is conserved. This motion is called potential rotation.

Considering vortex filaments from a purely kinematic point of view, as lines of singularity in the irrotational velocity distribution of the liquid we find their velocity circulation as

$$\oint d\vec{l}\,\vec{v}_s \equiv 2\pi\chi. \tag{1.43}$$

Since $\vec{v}_s$ is irrotational the circulation is independent of the choice of integration. There are no free ends of a vortex filament. (They end at the boundary of the vessel, at infinity in infinite systems or they build vortex rings.) Now we are able to calculate the velocity distribution in a liquid moving around the vortex filament. The simplest case is a straight vortex line in an infinite liquid, where the streamlines are circles perpendicular to the line

$$\oint d\vec{l}\,\vec{v}_s = 2\pi r v_s \equiv 2\pi\chi. \tag{1.44}$$

[8] This was proposed by Onsager in 1949 [86] and developed by Feynman in 1955 [85].

This implies the velocity distribution of a straight vortex line

$$v_s = \frac{\chi}{r}, \tag{1.45}$$

where r is the distance from the line. For a vortex filament of any shape a formula is found in analogy to the familiar Biot-Savart law, since a line current J obeys $\oint \vec{H}\, d\vec{l} = 4\pi J/c$. Substituting $v_s \leftrightarrow H$ and $\chi/2 \leftrightarrow J/c$ this is exactly (1.43). Hence the velocity distribution for a vortex filament of an arbitrary shape is

$$\vec{v}_s = \frac{1}{2}\chi \int \frac{d\vec{l} \times \vec{R}}{R^3}, \tag{1.46}$$

where the integration is along the filament and $\vec{R}$ is the radius vector from $\mathrm{d}\vec{l}$ to the point where the velocity is observed.

1.4.2 Vortex filaments in Bose-Einstein condensates

So far we derived our results from the fact that the motion of the liquid is a potential flow. Now we have a look on the quantum nature of the vortex lines. The fraction of particles in the ground state (BEC) belongs to the superfluid part of the liquid ρ_s [56] and hence the velocity of the condensate is the velocity of the superfluid part $\vec{v}_s$. In general, the time-independent condensate wave function is the complex scalar field

$$\Psi(\vec{r}) = \sqrt{n_0(\vec{r})}\ \mathrm{e}^{-\mathrm{i}\,\Phi(\vec{r})}, \tag{1.47}$$

with $n_0(\vec{r}) = |\Psi_0(\vec{r})|^2$ being the density of the condensate. For a homogeneous condensate with constant density this leads to the current density

$$\vec{j}_{cond} = \frac{\mathrm{i}\,\hbar}{2m}\left(\Psi\,\nabla\Psi^* - \Psi^*\,\nabla\Psi\right) = \frac{\hbar}{m} n_0 \nabla\Phi, \tag{1.48}$$

and with $\vec{j}_{cond} = n_0 \vec{v}_s$ one obtains the superfluid velocity

$$\vec{v}_s = \frac{\hbar}{m}\nabla\Phi. \tag{1.49}$$

The corresponding velocity potential is for the case of a BEC simply the phase of the condensate wave function $\phi = \frac{\hbar}{m}\Phi$. Now we use the condensate-velocity (1.49) to calculate the circulation defined by (1.43)

$$\chi = \frac{1}{2\pi}\oint d\vec{l}\,\vec{v}_s = \frac{\hbar}{2\pi m}\Delta\Phi = n\,\frac{\hbar}{m}, \tag{1.50}$$

where $\Delta\Phi$ is the change of phase going around the contour. Returning to the original point (closed contour) $\Delta\Phi$ must be an integer multiple of 2π.[9]

[9] Note,that the condensate wave function Ψ is single-valued.

Hence the circulation is quantized in units of $\frac{\hbar}{m}$ with quantum number n. This quantum number corresponds to the winding number N introduced before, since it counts how many times the condensate wave-function, which is the order-parameter of this system encircles the vortex line. A straight vortex filament has the velocity field (1.45) with circulation given by (1.50)

$$\vec{v}_s = \frac{\hbar}{m}\frac{n}{r}\,\vec{e}_\varphi, \tag{1.51}$$

Comparing this with the phase of the condensate via equation (1.49) yields $\Phi(\vec{r}) = n \cdot \varphi$. Then the wave-function of a Bose-Einstein condensate with n circulation quanta is

$$\Psi(\vec{r}) = \sqrt{n_0(\rho)}\;\mathrm{e}^{-\mathrm{i}n\varphi}, \tag{1.52}$$

where we assume that the density $n_0(\rho) = |\Psi(\rho)|^2$ is rotationally invariant. It is not surprising that this order parameter satisfies the asymptotic conditions given below equation (1.38), since it describes a medium with topological line-defects.

Remember that a BEC with weak contact interactions is generally described by the Gross-Pitaevskii equation (1.19). For a condensate with n vortex lines it takes the form [113, 46]

$$\left[-\frac{\hbar^2}{2M}\left(\partial_\rho^2 + \frac{1}{\rho}\partial_\rho\right) + \frac{\hbar^2 n^2}{2m\rho^2} - \mu + g|\Psi(\rho)|^2\right]|\Psi(\rho)| = 0. \tag{1.53}$$

Note, that this is a one-dimensional differential equation in the radial coordinate. The other coordinates have been integrated out, already. Using $\lim_{\rho\to\infty}|\Psi(\rho)| = \sqrt{n_0}$ we go to dimensionless units via

$$|\Psi_0(\rho)| = \sqrt{n_0}\,f(\rho) \qquad \text{with} \qquad \rho \to \frac{\rho}{\xi} \qquad \text{and} \qquad \xi^2 = \frac{\hbar}{mgn_0},$$

where ξ is the healing length and gives the width of the vortex core. We obtain

$$\frac{1}{2}\left(\partial_\rho^2 + \frac{1}{\rho}\partial_\rho\right) f + \left(1 - \frac{n^2}{2\rho^2}\right) f - f^3 = 0. \tag{1.54}$$

The limits are $\lim_{\rho\to\infty} f = 1$ and $\lim_{\rho\to 0} f \approx \rho^{|n|}$ so that $n_0(\vec{r})$ tends to zero on the vortex line. We rescale $f(\rho) = \rho^n\phi(\rho)$ in order to simplify numerical calculations and get rid of the centrifugal barrier

$$\frac{1}{2}\left(\partial_\rho^2 + \frac{2n+1}{\rho}\partial_\rho\right)\phi + \phi - \rho^{2n}\phi^3 = 0. \tag{1.55}$$

The singularity at $\rho \to 0$ in the second term is spurious since $\partial_\rho\phi(\rho) \to \rho^{2n-1}$ and can be evaluated by using the de l'Hospital rule. Figure 1.1 shows the numerical solution of equation (1.55) for $n = 1$ obtained with the imaginary time evolution method (appendix A).

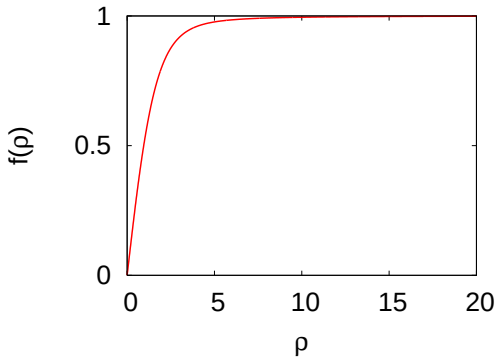

Figure 1.1: Dimesionless condensate wave-function f as a function of ρ in units of the healing length ξ for $n = 1$.

From equation (1.54) one can derive an interesting relation between the total dimensionless potential energy density U of the system and the winding number n of the field configuration (Virial theorem) [93]. By multiplying with $2\rho^2\, df/d\rho$ and integrating over the hole plane we find

$$U \equiv \int d^2x(1 - |f(\rho)|^2)^2 = 2\pi n^2. \tag{1.56}$$

1.4.3 Critical angular velocity

In section 1.4.1 we have discussed that vortex lines occur only if the angular velocity Ω of the rotating vessel is sufficiently large. In order to determine the critical angular velocity Ω_c where a straight vortex line ($n = 1$) is energetically favorable we consider the change of energy caused by such a straight vortex filament [56]

$$\Delta E = E_{1vortex} - E_0 = \int dV\, \frac{1}{2}\rho_s\, v_s^2 \tag{1.57}$$

$$= \frac{1}{2}\rho_s L_z \int dr\, r v_s^2\, 2\pi = L_z \rho_s \pi \chi^2 \int dr\, \frac{1}{r}. \tag{1.58}$$

Under a macroscopic treatment we can assume that the lower integration limit a is of the order of atomic distances to get rid of the logarithmic divergence. The upper limit is the radius R of the vessel. In the region of integration the density ρ_s is almost constant. This gives the energy

$$\Delta E = L_z \rho_s \pi \frac{\hbar^2}{m^2} \ln \frac{R}{a}. \tag{1.59}$$

The angular momentum of the liquid is

$$L = \int dV\, \rho_s v_s r = \rho_s \chi \int dV = L_z \rho_s \pi \frac{\hbar}{m} R^2. \tag{1.60}$$

Inserting the expressions (1.59) and (1.60) in the equation for the energy in the rotating frame (1.41), we obtain the critical angular velocity

$$\Omega_c = \frac{\hbar}{mR^2} \ln \frac{R}{a}. \tag{1.61}$$

This means that for $\Omega > \Omega_c$ the change of energy in the rotating frame ΔE_{rot} becomes negative and the one-vortex configuration is favorable.

From these formulas one can also estimate why only vortex lines with $n = 1$ are thermodynamically stable. For larger n, ΔE increases with n^2 while ΩL evolves with n. Hence ΔE_{rot} increases and a vortex line with $n > 1$ is energetically unfavorable.

But what happens in the case of faster rotations? More and more vortex lines will appear distributed over the liquid. If the density of the vortex lines ν is sufficiently large, rigid body rotation of the superfluid part is simulated

$$\mathrm{rot}\, \vec{v}_s = 2\Omega \qquad \Rightarrow \qquad 2\pi\chi = 2\Omega. \tag{1.62}$$

Using (1.43), we determine the number of vortex lines

$$\oint d\vec{l}\, \vec{v}_s = \nu \cdot 2\pi\chi_\cdot = 2\pi\nu \frac{\hbar}{m} \tag{1.63}$$

From these two equations it follows that

$$\nu = \frac{m\Omega}{\pi\hbar}, \tag{1.64}$$

which means that by increasing the angular velocity the number of vortices grows. Thereby one can observe scattering between the vortex lines and the quasi-particles from the normal part of the liquid ρ_n. Thus, there is a momentum transfer between ρ_s and ρ_n, which leads to friction and superfluidity disappears.

However, superfluids rotating with high angular velocity are remarkable physical systems, where a variety of novel quantum phases may occur [89]. Normally the vortices arrange in a triangular lattice (Abrikosov lattice) predicted first in the context of superconductors by Abrikosov [114] and recently experimentally imaged in an atomic BEC [92]. Novel lattice structures has been observed in two-component BECs [115], at very high vortex density regimes [116] and theoretically predicted in dipolar BECs [117]. Further, at very high vortex density a phase transition from the triangular vortex lattice into novel uncondensed phases (e.g. a vortex liquid phase [118]) has been predicted. These novel phases are closely related to the incompressible liquids of the fractional quantum Hall effect [118, 119, 120].

1.5 Dipolar quantum gases

The physics of ultracold atomic and molecular gases is crucially determined by the interparticle interactions. Typical experiments in quantum gases have studied up to now particles which interact dominantly via short-range isotropic potentials. At the very low energies involved in these experiments, such interactions are characterized by a single parameter, namely the s-wave scattering length. However, a new generation of recent experiments is opening a fascinating new research area, namely that of dipolar gases [32, 33], for which the *dipole-dipole interaction* (DDI) plays a significant or even dominant role. These experiments include on one hand those dealing with the DDI effects due to magnetic dipoles in degenerate atomic gases, as it is the case of recent exciting experiments especially in Chromium Bose-Einstein condensates [121, 122], but also on Rubidium spinor BECs [123], Potassium [124] and Lithium [125]. On the other hand, recent experiments on cold molecules [126, 127, 128, 129] like the creation of heteronuclear molecules in the lowest vibrational states [130, 131, 132], although not yet brought to quantum degeneracy, open fascinating perspectives for the generation of polar molecules with very large electric dipole moments. These gases are expected to be largely dominated by the DDI. Last but not least, the DDI in Rydberg atoms is extremely large [133] and may allow for e.g. the construction of fast quantum gates [134].

Contrary to the isotropic van-der-Waals-like short-range interactions, the DDI is long-range and anisotropic (partially attractive) and leads to fundamentally new physics in ultra cold gases, modifying e.g. the stability [135, 136, 137] and excitations of BECs [138, 139, 140, 141]. Similarly, the DDI significantly changes the properties of Fermi gases in three [142, 143, 33] or lower dimensions [144, 145, 146] and the physics of strongly-correlated gases [147, 148, 149, 150, 151]. Time-of-flight experiments in Chromium condensates allowed for the first observation of DDI effects in quantum degenerate gases [152]. They have been remarkably enhanced by means of Feshbach resonances [153], where it is possible to supress short-range interactions completely in order to generate a pure dipolar gas. In addition, the DDI has been recently shown to play an important role in the physics of spinor Rubidium BEC [123], and to lead to an observable damping of Bloch oscillations of Potassium atoms in optical lattices [124].

The long-range character of the DDI leads to nonlocal nonlinearity in dipolar BECs that resembles that encountered in plasmas [154] and nematic liquid crystals [155]. This nonlocality leads to novel nonlinear physics in dipolar BECs, including the possibility of obtaining stable 2D bright solitons [159, 160] and stable 3D dark solitons [161]. Long-range anisotropic interactions also lead to interesting phenomena in the physics of classical ferrofluids [157, 158].

In addition, the partially attractive character of the nonlocal nonlinear-

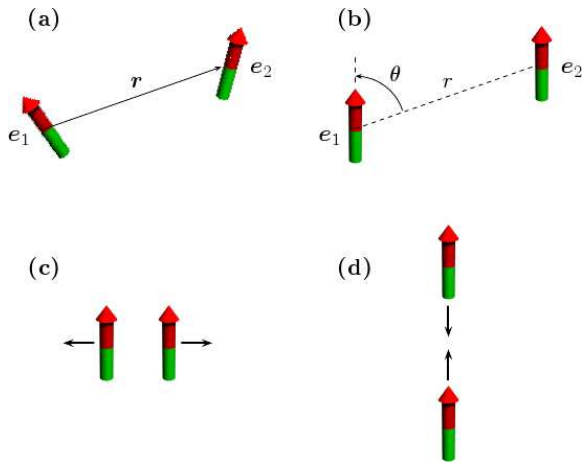

Figure 1.2: Anisotropy of the dipole-dipole interaction [32]: (a) Non-polarized dipoles; (b) Dipoles oriented in z-direction; (c) Two dipoles side by side repel each other; (d) Two dipoles on top of each other attract each other.

ity due to the anisotropy of the DDI has remarkable consequences for the stability of dipolar BECs, which may become unstable against collapse in 3D traps, as recently shown in experiments with Chromium BECs [162]. On the contrary, 2D traps may allow for an instability without collapse, characterized by the formation of a gas of inelastic 2D solitons [163]. Interestingly, the momentum dependence of the DDI allows for a second type of instability, called *roton instability*. It is related to the appearance of a roton-like minimum in the dispersion law of elementary excitations [138]. This minimum resembles the roton minimum in the dispersion law of liquid helium [164], which is related to the structure factor of the liquid [165]. Roton instability leads to local collapses [140] or stabilized modulated density profiles in sufficiently tight traps [141].

1.5.1 The dipole-dipole interaction potential

In general, two particles with dipole moments oriented in the directions $\vec{e}_1$ and $\vec{e}_2$ and with relative distance $\vec{r}$ as shown in Fig. 1.2 (a) interact via the dipole-dipole potential [32]

$$V_d(\vec{r}) = d^2 \frac{(\vec{e}_1 \cdot \vec{e}_2)r^2 - 3(\vec{e}_1 \cdot \vec{r})(\vec{e}_2 \cdot \vec{r})}{r^5} \tag{1.65}$$

with coupling constant d^2. For atoms with a permanent magnetic dipole moment μ the coupling constant is $d^2 = \mu_0\mu^2/4\pi$, while for polar molecules with electric dipole moment d_ϵ it reads $d^2 = d_\epsilon^2/4\pi\epsilon_0$. The electric dipole

moment of polar molecules is usually of the order of $d_\epsilon \propto ea_0$, where e is the electron charge and a_0 the Bohr radius. It is therefore much larger than the magnetic dipole moment of an atom, which is typically of the order of the Bohr magneton μ_B. One can estimate the ratio $d_\epsilon^2/\epsilon_0 : \mu_0\mu^2$ to be of the order of 10^4. Typical values appearing in the experiments noted earlier are for example $\mu = 6\mu_B$ for Chromium [121] and $\mu = 1\mu_B$ for Rubidium [123] and Potassium [124]. Potassium-Rubidium [130] molecules have a permanent dipole moment $d_\epsilon \simeq 0.6$ D and the dipole moment of Lithium-Caesium [131] is close to 6 D.[10]

If all dipoles are oriented in the same direction (Fig. 1.2 (b)) by an external field, say the z-direction, the potential (1.65) simplifies to

$$V_d(\vec{r}) = d^2 \frac{1 - 3\cos^2\theta}{r^3}, \tag{1.66}$$

where θ is the angle between the relative position of the particles and the dipole direction. From this expression the long-range character ($\propto 1/r^3$) and the anisotropy of the DDI becomes obvious. For two particles placed on top of each other (head-to-tail configuration) the angle θ is 0, the factor in (1.66) is $(1 - 3\cos^2\theta) = -2$ and the interaction is maximally attractive (Fig. 1.2 (d)), while particles sitting side by side ($\theta = \pi/2$) repel each other (Fig. 1.2 (c)), since the factor $(1-3\cos^2\theta) = 1$ is positive. For intermediate values of θ the term takes values between 1 and -2 and for the special case of the so called *magic angle* $\theta = \arccos(1/\sqrt{3}) \approx 54.7$, the DDI vanishes.

The dipole-dipole interaction can be tuned [166, 32] by rotating an external field that orients the dipoles much faster than any other relevant time-scale in the system. This leads to a time-averaged DDI

$$V_d(\vec{r}) = d^2 \frac{1 - 3\cos^2\theta}{r^3} \, \frac{3\cos^2\phi - 1}{2}, \tag{1.67}$$

where ϕ is the polar angle between the rotation axes and the orientation of the dipole (see Fig 1.3). The prefactor $\alpha(\phi) \equiv (3\cos^2\phi - 1)/2$ takes values within the range from 1 to -1/2. The total DDI averages to 0 if ϕ is the magic angle and changes sign for larger values of ϕ. Note, that in this case the averaged DDI becomes attractive for dipoles sitting side by side and repulsive for dipoles in a head to tail configuration leading to otherwise inaccessible physics as we will see in chapter 2.

In the remainder of this thesis we will often use the Fourier transform of the DDI. This has several advantages and is convenient for numerical calculations (e.g. one gets rid of the singularity at the origin in expression (1.66)). The Fourier transform of the DDI can be calculated easily by identifying the angular dependence of the DDI with the spherical harmonics

[10] One Debye is 1 D $\simeq 3.335 \times 10^{-30}$ C·m .

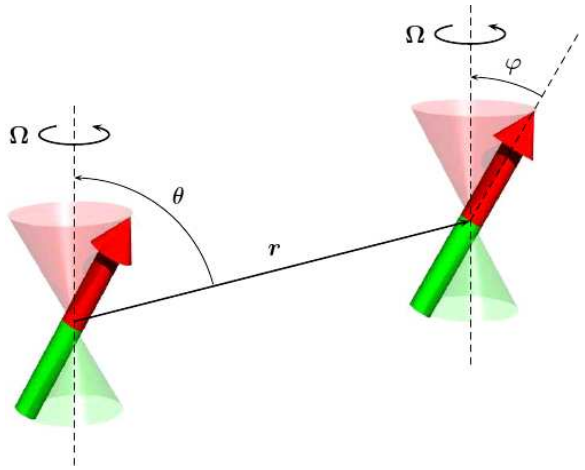

Figure 1.3: Tuning [166] of the dipole-dipole interaction with an external field rotating with frequency Ω much larger than any other time-scale in the system.

$(1-3\cos^2\theta) = \sqrt{16\pi/5}\, Y_{20}$ and reads

$$\tilde{V}_d(\vec{k}) = d^2 \frac{4\pi}{3}\,(3\cos^2\theta_k - 1), \tag{1.68}$$

where θ_k is the angle between $\vec{k}$ and the dipole direction.

1.5.2 Dipolar Bose-Einstein condensates

Dipolar Bose-Einstein condensates obey an extended version of the Gross-Pitaevskii equation (1.19), where an extra potential term taking the dipole-dipole interaction into account is added. Thus at sufficiently low temperatures and away from shape resonances[11] the physics of a dipolar BEC [135, 168] is provided by a non-local non-linear Schrödinger equation (NLSE) of the form

$$\begin{aligned} i\hbar\frac{\partial\Psi(\vec{r})}{\partial t} &= \left[-\frac{\hbar^2\nabla^2}{2m} + V_{ext}(\vec{r}) + g|\Psi(\vec{r})|^2 \right. \\ &\quad \left. + \int d\vec{r}'\,|\Psi(\vec{r}')|^2\, V_d(\vec{r}-\vec{r}')\right]\Psi(\vec{r}), \end{aligned} \tag{1.69}$$

where the last term is the dipolar contribution to the mean field interaction and is usually calculated in Fourier space. Using the convolution theorem

[11] Close to the shape resonances, the form of the pseudo-potential must be in general corrected. See [167] and reference therein.

of the Fourier transformation the dipolar term simplifies to

$$\int d\vec{r}' \, |\Psi(\vec{r}')|^2 \, V_d(\vec{r} - \vec{r}') = \int \frac{d^3k}{(2\pi)^3} \, \widetilde{|\Psi(\vec{r}')|^2} \, \tilde{V}_d(\vec{k}) \, e^{i\vec{k}\vec{r}}, \tag{1.70}$$

with the Fourier transform of the density $\widetilde{|\Psi(\vec{r}')|^2}$. However, it is very difficult even numerically to solve this non-local non-linear equation for arbitrary cases, since it has both differential and integral terms.

In the absence of an external potential, equation (1.69) has a homogeneous solution $\Psi_0(\vec{r}, t) = \sqrt{n_0} \, e^{-i\mu t/\hbar}$ with constant density n_0 and similar to equation (1.24) it reduces to

$$\mu = \left(g + \tilde{V}(q = 0) \right) n_0, \tag{1.71}$$

specifying the chemical potential μ of a gas with a relevant contribution $\tilde{V}(q = 0)$ from the dipole-dipole interaction.

Considering elementary excitations in section 1.2.2 we obtained that only a gas with repulsive contact interactions is stable, while attractive interactions lead to phonon instability. Since the dipole-dipole interaction is partially attractive we shall investigate in which cases a dipolar BEC is unstable with respect to phonon instability. Proceeding as for the case of short-range interacting gases, we study elementary excitations of the free homogeneous dipolar Bose-Eintein condensate. From the corresponding Bogoliubov-de Gennes equations we obtain a dispersion relation similar to (1.28)

$$\epsilon(q) = \pm \sqrt{\frac{\hbar^2 q^2}{2m} \left[\frac{\hbar^2 q^2}{2m} + 2 \left(g + \tilde{V}(\vec{q}) \right) n_0 \right]}. \tag{1.72}$$

In order to discuss stability conditions following from this dipersion relation we express the strength of the DDI in units of the coupling constant of the contact interaction g by the dimensionless parameter

$$\beta = \frac{g_d}{g}, \tag{1.73}$$

Here $g_d = \alpha 8\pi d^2/3$ is the dipolar coupling and α is a possible prefactor associated with the dipolar tuning. Stable phonons, excitations with low momenta q are only possible if the total contribution induced by interactions is positive for all directions $2 + \beta(3q_z^2/|\vec{q}|^2 - 1) > 0$. If $g_d > 0$ phonons with $\vec{q}$ lying on the xy plane are unstable if $\beta > 2$, while for $g_d < 0$ phonons with $\vec{q}$ along z are unstable if $\beta < -1$. Hence, absolute phonon stability demands $-1 < \beta < 2$.[12]

Note, that ground state properties and stability of dipolar condensates can be different in the trapped case, depending crucially on the particular trap geometry [137, 169, 170].

[12] The phonon instability is well explained in more detail with an intuitive physical picture in [32].

1.6 Overview

The Thesis is organized as follows:

In chapter 2 we analyze the case of a dipolar BEC in a one-dimensional optical lattice, and in particular the physics of straight vortex lines perpendicular to the two-dimensional planes defined by the lattice sites. We show that due to the long-range character of the DDI, different parts of the vortex line interact with each other, and hence the 3D character of the vortices plays a much more important role in dipolar gases than in usual short-range interacting ones. Specifically, we discuss that the DDI may severely modify the dispersion law for transverse modes, which may even acquire a roton-like minimum. This minimum may touch zero energy for sufficiently large and tuned DDI and strong lattices, leading to a thermodynamical instability of the straight vortex line. We show that this instability may occur in situations in which the whole BEC is stable, opening the possibility for the observation of twisted vortex line configurations in dipolar BECs.

In chapter 3 we continue the investigation of vortex lines in dipolar BEC. We consider again a vortex line in a one-dimensional optical lattice and dipoles oriented parallel or perpendicular to vortex line and lattice direction. With an intensive numerical analysis we determine the ground state of the system for different values of the dipolar strength and the lattice depth. We show that the thermodynamical instability found in chapter 2 leads to a second-order-like phase transition from a straight vortex line into an helical or snake-like vortex line depending on the dipole orientation. In particular, we calculate the width of the helix or snake as a function of the dipolar coupling and the effective mass associated with the lattice. In addition we investigate whether the dipole-dipole interaction can stabilize a doubly-quantized vortex against splitting into two single ones.

Chapter 4 is devoted to the analysis of non-overlapping dipolar BECs placed at different sites of a deep two-well potential or 1D optical lattice. Due to the long-range character of the DDI, contrary to the case of purely short-range interacting gases, the deep potential does not lead to independent 2D BECs. In particular, we show that the elementary Bogoliubov excitations of disconnected BECs placed in a two-well potential couple through the DDI leading to hybrid modes which are collectively shared by both wells. Interestingly this hybridization may significantly alter the stability of the system against roton instability. We show that this effect is significantly enhanced for the case of a 1D optical lattice with multiple sites, where a band-like spectrum is induced by the inter-site DDI. We analyze in detail the stability diagram, and finish with a discussion of the experimental observability in different experiments.

In chapter 5 we consider dipolar induced filamentation of fermionic polar

molecules in a deep one-dimensional optical lattice. We show that due to the attractive intersite DDI polar molecules in different lattice sites placed on top of each other can bind into self-assembled chains of different length. Depending on the number of molecules in the chain, the filament has fermionic or bosonic character. This has particularly relevant consequences when the number of available lattice sites is odd. Here we focus on the simplest non-trivial case, namely a three-well potential. We show that the competition between trimer/dimer binding and trimer Fermi energy results in a non-trivial dependence of the character of the dipolar chain liquid as a function of the number of molecules per site and as a function of temperature.

Chapter 2

Transverse instability of straight vortex lines in dipolar Bose-Einstein condensates

As discussed in the introduction dipolar gases present a rich non-linear physics, since the dipole-dipole interaction leads to nonlocal nonlinearity. This nonlocal character also has remarkable consequences for the physics of rotating dipolar gases. It has been shown that the critical angular frequency for vortex creation may be significantly affected by the dipole-dipole interaction [171]. In addition, dipolar gases under fast rotation develop vortex lattices, which due to the dipole-dipole interaction may be severely distorted [172], and even may change its configuration from the usual triangular Abrikosov lattice into other arrangements [173, 174]. However, the previous analysis of vortices in dipolar BEC have been constrained to situations where the 3D character of the vortex is unimportant.

Vortex lines are indeed 3D structures, which, resembling strings, may present transverse helical excitations, which were studied for classical vortices by Lord Kelvin already in 1880, and are thus known as *Kelvin modes* [175]. These excitations have been also studied for quantized vortices in superfluids by Pitaevskii [52]. Interestingly, the dispersion law for Kelvin modes at small wave vector q follows a characteristic dependence [56] $\epsilon(q) \sim -q^2 \ln q\xi$, where ξ is the healing length. Kelvin modes play an important role in the physics of superfluid Helium [88, 176], and even of neutron stars [177]. Recently, Kelvin modes were experimentally observed in BEC [178].

In this chapter we analyze the influence of the dipole-dipole interaction on vortex lines in a one dimensional optical lattice and in particular on the dipersion relation for the Kelvin modes as shown in figure 2.1.

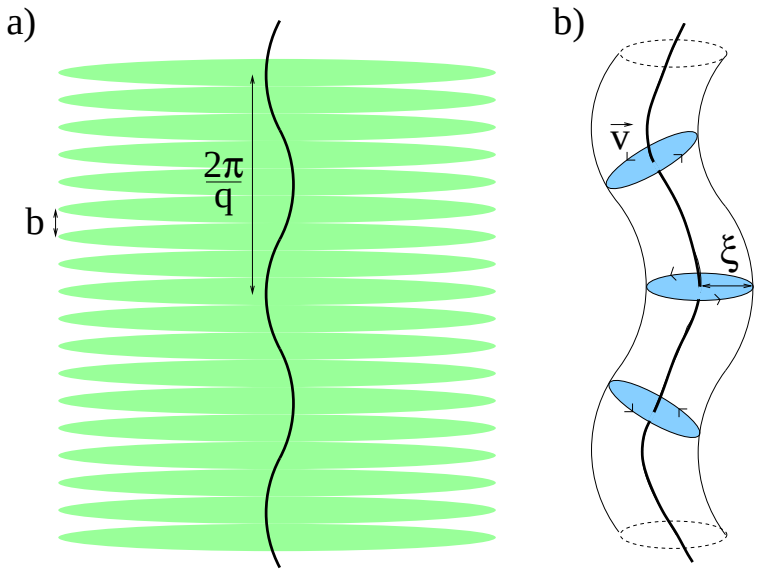

Figure 2.1: (a) Vortex line in an optical lattice with lattice spacing b. The wave-number of the Kelvin mode is q, whereas the corresponding wavelength satisfies $2\pi/q \gg b$. (b) The vortex line has a finite core with healing length ξ and a velocity field $\vec{v}$ perpendicular to the line.

2.1 Dipolar BEC in an 1D optical lattice

In the following, we consider a dipolar BEC of particles with mass m and electric dipole d (the results are equally valid for magnetic dipoles) oriented in the z-direction by a sufficiently large external field, and that hence interact via a dipole-dipole potential: $V_d(\vec{r}) = \alpha d^2(1-3\cos^2\theta)/r^3$, where θ is the angle formed by the vector joining the interacting particles and the dipole direction. As mentioned in the introduction the coefficient α can be tuned within the range $-1/2 \leq \alpha \leq 1$ by rotating the external field that orients the dipoles much faster than any other relevant time scale in the system [166]. At sufficiently low temperatures (and away from shape resonances [1]) the physics of the dipolar BEC is provided by a non-local non-linear Schrödinger equation (NLSE) of the form (1.69)

$$i\hbar\frac{\partial\Psi(\vec{r})}{\partial t} = \left\{-\frac{\hbar^2\nabla^2}{2m} + V_{\rm ol}(z) + g|\Psi(\vec{r})|^2 \int d\vec{r}'|\Psi(\vec{r}')|^2 V_d(\vec{r}-\vec{r}')\right\}\Psi(\vec{r}), \tag{2.1}$$

where $g = 4\pi\hbar^2 a/m$, with $a > 0$ the s-wave scattering length. The BEC is in a 1D optical lattice, $V_{\rm ol}(z) = sE_R\sin^2(Qz)$, where $E_R = \hbar^2Q^2/2m$ is the

[1] Close to the shape resonances, the form of the pseudopotential must be in general corrected. See [167] and reference therein.

recoil energy and Q is the laser wave vector. In the tight-binding regime (sufficiently strong lattice) we can write $\Psi(\vec{r},t) = \sum_j w(z-bj)\psi_j(\vec{\rho},t)$, where $b = \pi/Q$, $\vec{\rho} = \{x,y\}$ and $w(z)$ is the Wannier function associated to the lowest energy band. Substituting this ansatz in equation (2.1) we obtain a discrete NLSE (1.36) with an additional dipolar term, which shall be discussed in detail in appendix B. We may then return to a continuous equation (see appendix B), where the presence of the lattice amounts for an effective mass along the lattice direction and for a renormalized coupling constant [179]:

$$i\hbar\frac{\partial\Psi(\vec{r})}{\partial t} = \left\{-\frac{\hbar^2\nabla_\perp^2}{2m} - \frac{\hbar^2\nabla_z^2}{2m^*} + \tilde{g}|\Psi(\vec{r})|^2 + \int d\vec{r}'|\Psi(\vec{r}')|^2 V_d(\vec{r}-\vec{r}')\right\}\Psi(\vec{r}), \tag{2.2}$$

where $\Psi(\vec{r}) = \psi_j(\vec{\rho})/\sqrt{b}$ is the coarse-grained wavefunction. The renormalized coupling constant is $\tilde{g} = bg\int w(z)^4dz + g_d\mathcal{C}$, [2] with the dipolar coupling constant $g_d = \alpha 8\pi d^2/3$, and m^* is the effective mass as defined in the introduction 1.3.2 (equation (1.37)). Recall that m^* increases with the lattice depth s and that the tight binding approximation looses its validity if $m/m^* \to 1$. In addition the validity of equation (2.2) is limited to z-momenta $k_z \ll 2\pi/b$, in which one can ignore the discreteness of lattice.

We consider first an homogeneous solution $\Psi(\vec{r},t) = \sqrt{n_0}\exp[-i\mu t/\hbar]$, as discussed in the introduction 1.5.2. Analogeously we define a dimensionless parameter $\beta = g_d/\tilde{g}$, but now with the rescaled coupling constant $\tilde{g}$. In 1.5.2 we have found that the BEC is stable only if

$$-1 < \beta < 2. \tag{2.3}$$

Otherwise, the attractive part of the dipole-dipole interaction would lead to phonon instability and the collapse of the condensate. This condition is still valid for the dipolar gas in a one dimensional optical lattice discussed in this chapter, because the lattice mainly effects the kinetic energy due to the effective mass.

2.2 Straight vortex line

We consider at this point a condensate with a straight vortex line (n=1) along the z-direction as introduced in section 1.4.2. The corresponding ground-state wavefunction is of the form (1.52)

$$\Psi_0(\vec{r},t) = \phi_0(\rho)\, e^{i\varphi}\, e^{-i\mu t/\hbar}, \tag{2.4}$$

[2] $\mathcal{C} \simeq \sum_{j\neq 0}|\tilde{w}(2\pi j/b)|^4$, where $\tilde{w}$ is the Fourier-transform of $w(z)$.

where φ is the polar angle on the xy plane. For the case of a vortex line the NLSE (2.2) reduces to equation (1.53) with an additional dipolar term

$$\int d\vec{r}' \, |\Psi_0(\vec{r}')|^2 \, V_d(\vec{r} - \vec{r}') = -\frac{\alpha d^2 4\pi}{3} |\phi_0(\rho)|^2. \tag{2.5}$$

This result is derived in detail in appendix C Hence, the function $\phi_0(\rho)$ fulfills

$$\mu\phi_0(\rho) = \frac{\hbar^2}{2m}\left(-D_\rho + \frac{1}{\rho^2}\right)\phi_0(\rho) + \bar{g}|\phi_0(\rho)|^2\phi_0(\rho), \tag{2.6}$$

where $D_\rho = \frac{1}{\rho}\partial_\rho \rho \partial_\rho$ and we have introduced the regularized coupling constant

$$\bar{g} \equiv \tilde{g} - \frac{g_d}{2}. \tag{2.7}$$

Note that, due to the homogeneity of Ψ in the z-direction, in equation (2.6) the dipole-dipole interaction just regularizes the local term (a similar feature was observed in Ref. [138]). The density of the vortex core is given by $|\phi_0(\rho)|^2$, which goes to zero at $\rho = 0$, and becomes equal to the bulk density n_0 at distances larger than the corresponding healing length $\xi = \hbar/\sqrt{m\bar{g}n_0}$. We can solve equation (2.6) numerically (appendix A), as shown in section 1.4.2 when discussing vortex lines in usual short-range interacting BECs. Analogeously, we find a solution as shown in figure 1.1.

Note that due to the regularization of the contact interaction, the size ξ of the vortex core depends on the dipole-dipole interaction. In particular, this dependence is exactly the opposite as that expected for 2D vortices, since in 2D similar arguments provide $\bar{g} = g + g_d$. Hence, even for equal densities, the cores of 2D and 3D vortices can be remarkably different in a dipolar gas, differing significantly from the behavior of short-range interacting gases, where both 2D and 3D vortices would have the same core size.

2.3 Kelvin modes

The effects of the long-range character of the dipole-dipole interaction become even more relevant in the physics of Kelvin modes. We consider excitations of the straight vortex line ($n = 1$) of the form

$$\Psi(\vec{r}, t) = \Psi_0(\vec{r}, t) + \chi(\vec{r}, t)\, e^{i\varphi}\, e^{-i\mu t/\hbar}, \tag{2.8}$$

Introducing this ansatz into (2.2) and linearizing in χ, one obtains

$$\begin{aligned} i\hbar\partial_t\chi(\vec{r}, t) \;=\; & \Big[-\frac{\hbar^2}{2m}\nabla_\perp^2 - \frac{\hbar^2}{2m^*}\nabla_z^2 - i\frac{\hbar^2}{m\rho^2}\partial_\varphi + \frac{\hbar^2}{2m\rho^2} - \mu \\ & + (2\tilde{g} - \frac{g_d}{2})\,|\phi_0(\rho)|^2\Big]\,\chi(\vec{r}) \;+ \tilde{g}\phi_0^2(\rho)\chi^*(\vec{r}) \\ & + \int d\vec{r}' V(\vec{r} - \vec{r}')\phi_0(\rho')\phi_0(\rho)\left[\chi^*(\vec{r}') + \chi(\vec{r}')\right], \end{aligned} \tag{2.9}$$

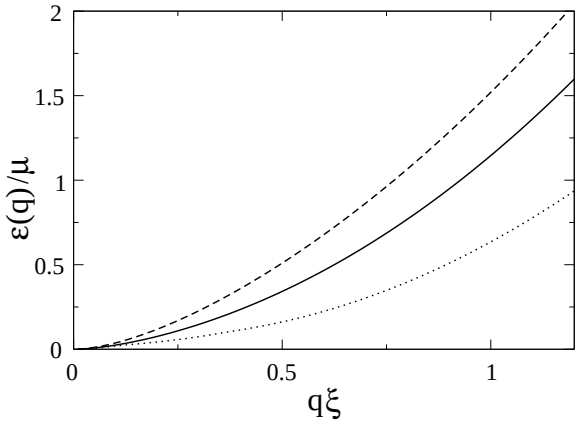

Figure 2.2: Dispersion $\epsilon(q)$ as a function of $q\xi$, in the absence of an additional optical lattice, and various values of $\beta = 0$ (solid line), 1.0 (dashed line), and -0.98 (dotted line).

where $\phi_0(\rho)$ is the ground state solution (straight vortex line) obtained numerically in the previous section. Following the famous work of Pitaevskii [52] we write the excitations as a sum over all possible modes characterized by the quantum numbers l and q

$$\chi(\vec{r},t) = \sum_{l,q} \left[u_l(\rho)\, e^{i(l\varphi+qz-\epsilon t/\hbar)} - v_l^*(\rho)\, e^{-i(l\varphi+qz-\epsilon^* t/\hbar)} \right], \tag{2.10}$$

where ϵ is the excitation energy assiciated with l and q. Several simplification based on the integral representations of the Bessel functions of the first kind $J_l(q\rho)$ [180, 181] (appendix C), finally yield the corresponding Bogoliubov-de Gennes equations for ϵ

$$\begin{aligned}
\epsilon u_l(\rho) &= \left[\frac{\hbar^2}{2m} \left(-D_\rho + \frac{(l+1)^2}{\rho^2} + \frac{m}{m^*} q^2 \right) - \mu + 2\bar{g}\phi_0(\rho)^2 \right] u_l(\rho) \\
&\quad -\bar{g}\phi_0(\rho)^2 v_l(\rho) \qquad (2.11) \\
&\quad +\frac{3\beta}{2-\beta}\bar{g}q^2 \int_0^\infty d\rho' \rho' \phi_0(\rho')\phi_0(\rho) \left[u_l(\rho') - v_l(\rho') \right] F_l(q\rho, q\rho') \\
\epsilon v_l(\rho) &= -\left[\frac{\hbar^2}{2m} \left(-D_\rho + \frac{(l-1)^2}{\rho^2} + \frac{m}{m^*} q^2 \right) - \mu + 2\bar{g}\phi_0(\rho)^2 \right] v_l(\rho) \\
&\quad +\bar{g}\phi_0(\rho)^2 u_l(\rho) \qquad (2.12) \\
&\quad +\frac{3\beta}{2-\beta}\bar{g}q^2 \int_0^\infty d\rho' \rho' \phi_0(\rho')\phi_0(\rho) \left[u_l(\rho') - v_l(\rho') \right] F_l(q\rho, q\rho'),
\end{aligned}$$

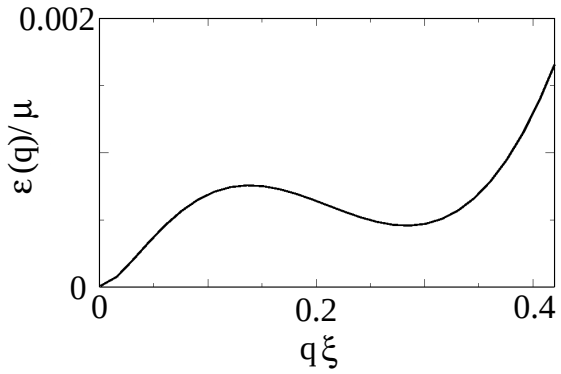

Figure 2.3: Dispersion $\epsilon(q)$ as a function of $q\xi$ for $m/m^* = 0.143$ and $\beta = -0.8$.

with $F_l(x,x') = I_l(x_<)K_l(x_>)$, where I_l and K_l are modified Bessel functions, and $x_>$ =max(x,x'), $x_<$ =min(x,x'). The transverse vortex line excitations with $l=-1$ are called Kelvin modes and we want to analyze this case in detail (note appendix C). By numerical diagonalization we determine for every q the lowest eigenenergy ϵ, that provides the dispersion law discussed below. The first line at the right-hand site of equations (2.11) and (2.12) is exactly the same as that expected for a vortex in a short-range interacting BEC [52], but with the regularized value $\bar{g}$. The last term at the right-hand site of both equations is directly linked to the long-range character of the dipole-dipole interaction and, as we show below, leads to novel phenomena in the physics of Kelvin modes in dipolar BECs.

In absence of dipole-dipole interaction (or equivalently from equations (2.11) and (2.12) without the last integral term) the dispersion law at low momenta ($q\xi \ll 1$) is provided by the well-known expression

$$\epsilon(q) = -\frac{\hbar^2 q^2}{2m^*}\,\ln\left[\sqrt{\frac{m}{m^*}}\,q\xi\right]. \tag{2.13}$$

The integral terms of equations (2.11) and (2.12) significantly modify the Kelvon spectrum in a different way depending whether β is positive or negative. In order to isolate the effect of the dipole-dipole interaction on the core size with respect to the effect of the integral terms in equations (2.11) and (2.12) we fix $\bar{g}$ and change the parameter β which is proportional to the dipole-dipole coupling constant. Figure 2.2 shows that for increasing $\beta > 0$ the excitation energy clearly increases, i.e. the vortex line becomes stiffer against transverse modulations.

In order to obtain an intuitive picture of why this is so, one may sketch the vortex core as a 1D chain of dipolar holes. Dipolar holes interact in exactly the same way as dipolar particles, and hence maximally attract each other when aligned along the dipole direction, i.e. the z-direction. In this sense, the configuration of minimal dipolar energy is precisely that of a straight vortex line along z. A wiggling of the line produces a displacement of the dipolar holes to the side, and hence an increase of the dipolar energy. As a consequence, the dipole-dipole interaction leads to an enhanced stiffness of the vortex line. From this intuitively transparent picture, we can easily understand that exactly the opposite occurs when $\beta < 0$. In that case, the dipolar holes maximally repel each other when aligned along the z-direction. Hence it is expected that the dipolar energy decreases when departing from the straight vortex configuration. This results in a reduced energy of the excitations for $\beta < 0$ (figure 2.2), i.e. it becomes easier to wiggle the vortex line.

In principle, a sufficiently large dipole-dipole interaction could destabilize the straight vortex line. However, in the absence of an addiontional optical lattice along the z-direction, the destabilization would occur for values of $\beta < -1$, i.e. in the regime of phonon instability in which the whole dipolar BEC is unstable against local collapses. An increase of the potential depth of the additional lattice leads to a reduction of the role of the kinetic energy term mq^2/m^* in equations (2.11) and (2.12) that enhances the effect of the dipolar interaction on the dispersion law. As a consequence, as shown in figure 2.3, in addition to the $-q^2 \ln(q\xi)$ dependence at low q, a roton-like minimum eventually appears at intermediate q. This changes the character of the lowest Bogoliubov modes at this value of q. For a sufficiently small $(m/m^*)_{cr}$ the roton minimum eventually reaches zero or negative energy, and the straight vortex line becomes unstable against a novel type of instability.

Figure 2.4 summarizes our results. As mentioned above, for $\beta < -1$ and $\beta > 2$ the whole BEC collapses due to phonon instability. For $0 < \beta < 2$, the dipole-dipole interaction makes the vortex stiffer against Kelvin modes (i.e. $\epsilon(q)$ grows for all q, as shown for a particular case in figure 2.2). For $-1 < \beta < 0$ the vortex is softer against transverse excitations (i.e. $\epsilon(q)$ decreases), and $\epsilon(q)$ develops a roton feature when m/m^* decreases approaching the curve $(m/m^*)_{cr}$ (thick curve in figure 2.4 obtained by calculating for each value of β the value of m/m^* for which $\epsilon(q)$ vanishes at least for some q). For $m/m^* < (m/m^*)_{cr}$ the excitation energy of the Kelvin waves is negative for some values of q. Excited vortex lines with these wave numbers q are energetically more favourable than the straight line. Hence the straight vortex filament becomes thermodynamically unstable.

Roton minima occur in superfluid Helium [85], and have been also predicted in trapped dipolar BECs [138, 139]. In the latter case, roton instability leads to local collapses which destabilize the whole BEC [140] (although a trap may stabilize the gas leading to novel ground states [141]). We stress

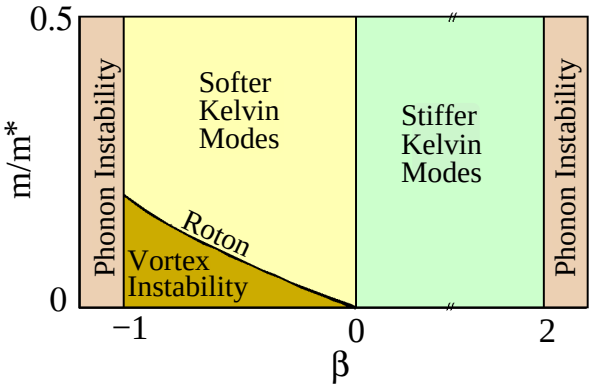

Figure 2.4: Stable/unstable regimes for straight vortex lines.

that although the roton feature in the Kelvin wave spectrum is also induced by the dipole-dipole interaction, its physics fundamentally differs from the roton-maxon feature discussed in Refs. [138, 139, 141]. The roton-like minimum occurs due to the long-range interaction between different positions in the vortex line, and the related instability is not linked to a destabilization of the whole gas, which is indeed stable when the Kelvin wave instability appears, but to an instability of the vortex line against twisting.

2.4 Conclusion

Because of the nonlocal interaction between different parts of the vortex line, the 3D character of the vortices is more crucial in dipolar BECs than in short-range interacting ones. Remarkably, the DDI significantly distorts the stability of the vortex line. In particular, under appropriate conditions (involving an additional 1D lattice), the Kelvin modes become unstable. This intrinsically dipole-induced instability opens the possibility for novel vortex line configurations in dipolar BECs, which we discuss in the following chapter.

Chapter 3

Phase-transition from straight into twisted vortex lines in dipolar Bose-Einstein condensates

In the previous chapter and in [182] we have analyzed the case of a dipolar Bose-Einstein condensate in an one-dimensional optical lattice, and in particular the physics of straight vortex lines perpendicular to the two-dimensional planes defined by the lattice sites. We have shown that due to the long-range character of the dipole-dipole interaction, different parts of the vortex line interact with each other, and hence the three-dimensional character of the vortices plays a much more important role in dipolar gases than in usual short-range interacting ones. Specifically, we discussed that, interestingly, the dipole-dipole interaction may severely modify the Kelvin-wave dispersion, which may even acquire a roton-like minimum. This minimum may touch zero energy for sufficiently large dipole-dipole interaction and strong lattices, leading to the instability of the straight vortex line even for those situations in which the BEC as a whole is stable. However, the certainly very relevant question concerning the nature of this instability was not addressed. In this chapter we discuss in detail this instability, showing that, interestingly, it has a thermodynamical character, and it is linked to a second-order-like phase transition from a straight vortex line into an helical or snake-like vortex line depending on the dipole orientation.

3.1 System and numerical method

In this chapter we consider the same configuration as in the previous chapter (figure 2.1). The dipoles are oriented along the z-direction parallel to

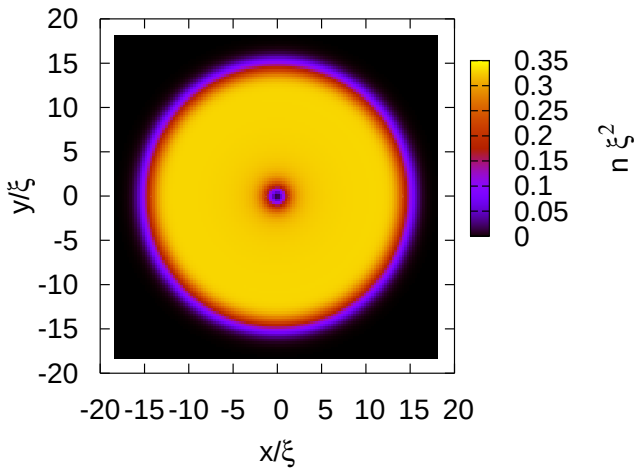

Figure 3.1: Density distribution $n(x, y, z = 0)$ in the xy-plane of the ground state with a vortex for $\beta = -0.8$ and $m/m^* = 0.15$. The dipole is assumed in the z-direction and the unit of length is the healing length ξ.

the vortex line by an external field and hence the dipolar Bose-Einstein condensate in the optical lattice obeys the non-linear Schrödinger equation (2.2)

$$i\hbar\frac{\partial\Psi(\vec{r})}{\partial t} = \left\{-\frac{\hbar^2\nabla_\perp^2}{2m} - \frac{\hbar^2\nabla_z^2}{2m^*} + \tilde{g}|\Psi(\vec{r})|^2 + \int d\vec{r}'|\Psi(\vec{r}')|^2 V_d(\vec{r}-\vec{r}')\right\}\Psi(\vec{r}), \tag{3.1}$$

with the dipolar potential $V_d(\vec{r}) = \alpha d^2(1-3\cos^2\theta)/r^3$. In addition the dipole-dipole interaction is tuned by a very fast rotating field such that it changes its sign as discussed in section 1.5.1 ($\alpha < 0$). This tuning we have used already in the previous chapter in order to obtain the instability of the vortex line.

In order to determine the new lowest-energy configuration of the vortex line, we have performed fully three-dimensional numerical calculations of the non-linear Schrödinger equation (2.2). We start our calculations from an initially imposed straight vortex line and let the system evolve in imaginary time (appendix A). Since the straight line configuration is always a local minimum one has to add a small random noise to perturb the system and find the global minimal energy configuration. We performed our calculations employing a cylindrical numerical box placed several healing lengths apart from the vortex core to minimize boundary effects (figure 3.1).

Outside the numerical box, there is no velocity field and no circulation. This has the same effect as an image vortex (with opposite winding number) at a distance of twice the cylinder radius. The potential energy of two well seperated vortices with winding number n_1 and n_2 at distance $L \gg \xi$ is proportional to [93, 183]

$$V(L) \propto 2V_1 - 2\pi n_1 n_2 \log L \tag{3.2}$$

where V_1 is the potential energy of a single vortex. Hence the interaction between a vortex and an antivortex is attractive and the potential energy decreases logarithmically with L. These attraction to the image vortex would move the vortex away from the trap center. However, if the cylinder is sufficiently large the image vortex is far away and its influence is negligible.

The employ of the fast fourier transformations [184] in our numerical calculations (see appendix A) implies the use of periodic boundary conditions, which could induce spurious effects due to the long-range character of the dipole-dipole interaction. This may be avoided by placing the boundary of the numerical box (black in figure 3.1) sufficiently far from the condensate. Another possibility technique would be to introduce a cut-off for the dipole-dipole interaction (as suggested in [185]).

As shown in figure 3.1 the cylindrical box configuration permits a sufficiently flat density in the region where the vortex core is created. This allows us to avoid unwanted density effects, which will obscure the analysis of the vortex stability.

3.2 Helical vortex lines

In this section we perform the numerical analysis of the system discussed in the previous chapter in order to confirm and extend the results and study the impact of the Kelvin-mode instability. The intriguing dependence of the dispersion of Kelvin-waves on the lattice characterized by m/m^* and the dipole strength $\beta = 8\pi\alpha d^2/3g$ as discussed in section 2.3 is explained by the competition of the two processes involved in the inter-site physics, namely tunneling and intersite dipole-dipole interaction. On one hand, the hopping energy is minimized when vortex cores at neighboring sites are placed right on top of each other. Hence tunneling tends to maintain the vortex line straight. On the other hand, for $\beta < 0$ the cores maximally repel each other when aligned along the z-direction. Hence dipole-dipole interaction and tunneling compete, and the vortex line becomes softer.

From this intuitive picture it becomes clear that when m/m^* becomes sufficiently small the tunneling cannot balance the dipole-dipole interaction any longer, and as a consequence the straight vortex line becomes thermodynamically unstable, as already mentioned in our discussion of the Bogoliubov

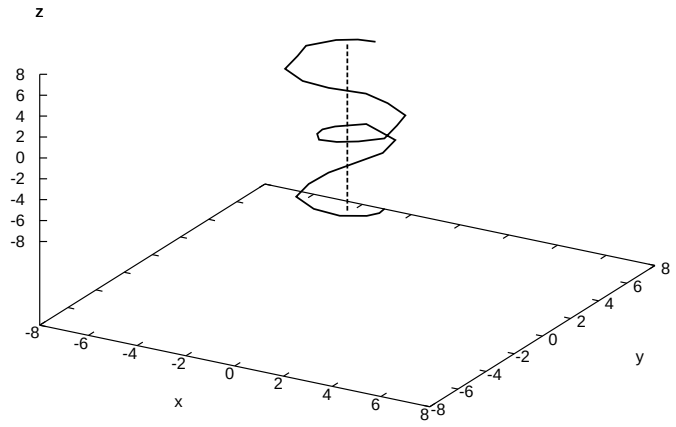

Figure 3.2: Vortex line configurations of the ground state for $\beta = -0.8$ and $m/m^* = 0.15$ (straight) and $m/m^* = 0.04$ (helical), respectively. For both cases the dipole is assumed in the z-direction. The unit of length is $\sqrt{2}\xi$.

analysis in the previous chapter. In this section we show that this instability is related to a transition from a straight vortex into a twisted vortex line. This twisting, which we confirm below numerically, may be expected by analyzing the dipole-dipole interaction between vortex cores at neighboring sites. The energy is minimized by laterally displacing the vortices with respect to each other a finite distance on the xy-plane. These lateral displacements between nearest neighbors lead to a twisting of the vortex line. Note that due to the symmetry of the problem, we may expect an helical structure, as we confirm with the numerical calculation.

As expected, the imaginary time evolution leads to a ground state configuration of a straight vortex line for those values of β and m/m^* lying inside the stable regime of figure 2.4. On the contrary, for those regions within the instability regime a qualitatively new ground state is found, where we observe a departure from the straight form into an helical configuration, as in figure 3.2.

Hence at the line $(m/m^*)_{cr}$ there is a phase transition from straight into helical ground state vortex lines. In order to characterize this phase transition we have performed an exhaustive analysis of the helical configurations, which may be characterized by a pitch with wavenumber Q and a radius r_0. We confirmed that the wave number Q is indeed comparable to the minimum $q_{\rm rot}$ in the dispersion law obtained from the Bogoliubov analysis of section 2.3. For several fixed values of β we performed a large number of three-dimensional numerical simulations for different m/m^*, to analyze the

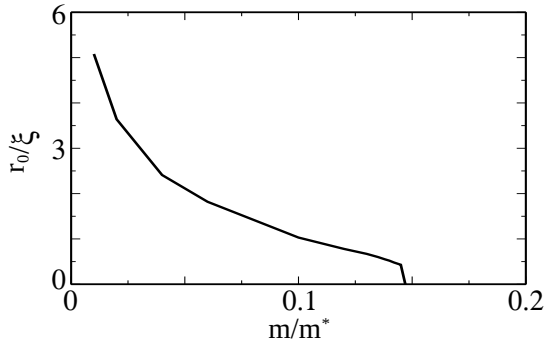

Figure 3.3: Helix amplitude r_0 (see text) as a function of m/m^* for $\beta = -0.8$.

behavior of the amplitude r_0 inside the unstable region and at the transition to the stable region. Our results (for $\beta = -0.8$) are depicted in figure 3.3. We observe a gradual decrease of r_0 when m/m^* approaches the stability border $(m/m^*)_{cr}$. For values close to the stability border, $r_0 \ll \xi$ and hence it becomes in practice (both numerically and experimentally) impossible to discern a significant vortex twisting. Our simulations are hence compatible with a second-order-like phase-transition from an helical into a straight lowest-energy vortex-line configuration.

Note that inside the instability region an increase of the lattice strength (i.e. a decrease of m/m^*) results in a larger bending which comes together with a shallower binding energy for the line. If the binding energy becomes lower than other typical energy scales involved in the system (inhomogeneity, boundary effects) then the 3D vortex line breaks into uncorrelated 2D vortices. The latter is, of course, also expected in the absence of dipole-dipole interaction if the tunneling becomes sufficiently small. Note that in figure 2.4 we did not consider any other additional energy scale, and hence the 3D vortex line could be considered all the way down to very small m/m^*. However, in our numerical simulations we do have boundary effects introduced by our finite cylindrical numerical box. As a consequence we have observed (also for the results of the next section) that for very small m/m^* inside the instability regime the boundary effects may completely unbound the vortex line into uncorrelated 2D vortices at each layer. However, here we are more concerned with the phase transition boundary, where the binding is still dominant even when the vortex is bent.

3.3 Snake-like vortex-lines

In chapter 2 and in the previous section 3.2, we have discussed the case in which the dipoles are oriented along the z-direction. In that situation, the cylindrical symmetry of the problem largely simplified the Bogoliubov

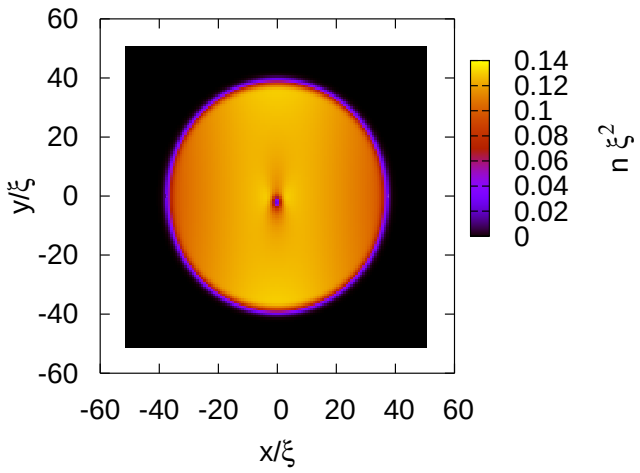

Figure 3.4: Anisotropic density distribution $n(x, y, z = 0)$ in the xy-plane of the ground state with a vortex for $\beta = -1.2$ and $m/m^* = 0.04$. The dipole is assumed in the y-direction and the unit of length is the healing length ξ.

analysis. The helical instability demands $\beta < 0$, and it is hence necessary the employ of the tuning mechanism discussed in the introductory section 1.5.1. However, the tuning is not strictly necessary to observe the destabilization of the straight vortex line. A perhaps experimentally simpler scenario is offered by the case in which the dipoles are oriented perpendicular to the vortex line (and hence also perpendicular to the over-imposed lattice potential). Then the dipole-dipole interaction is again repulsive in z-direction and competes with the kinetic energy in what concerns the stability of the straight vortex-line in a similar way as described in the previous sections. In this section we analyze this particular case (orientation along y). We show that the vortex line may be also destabilized in this experimentally less involved case.

As for section 3.2, we have evolved an initially straight vortex in imaginary time using equation (2.2) employing similar numerical conditions. However, the analysis in the new configuration is largely handicapped due to the distortion of the density of the condensate induced by the fact that the dipole is now on the xy plane, and hence breaks the polar symmetry. Figure 3.4 shows this anisotropy in the density profile. These density modulations may be reduced (but not fully eliminated) by considering larger numerical boxes. However, the latter may make the 3D numerical simulation prohibitively long.

In spite of these difficulties we observed the departure from the straight vortex line for sufficiently large β (note that in this configuration $\beta > 0$ and hence it may take values up to 2 before entering into the regime of

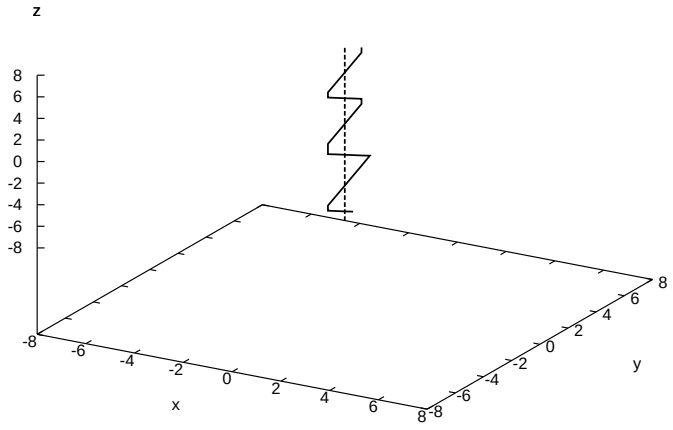

Figure 3.5: Vortex-line configurations of the ground state for $\beta = 1.2$ and $m/m^* = 0.075$ (straight) and $m/m^* = 0.04$ (snake-like), respectively. For both cases the dipole is assumed in the y-direction. The unit of length is $\sqrt{2}\xi$.

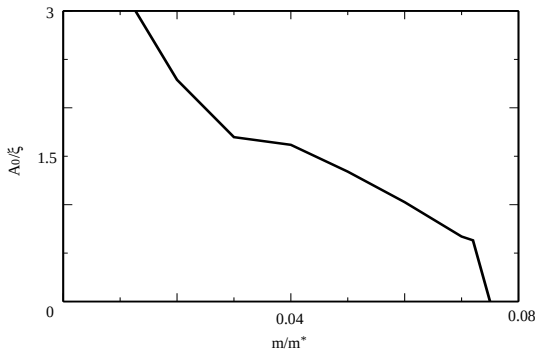

Figure 3.6: Snake amplitude A_0 (see text) as a function of m/m^* for $\beta = -1.2$.

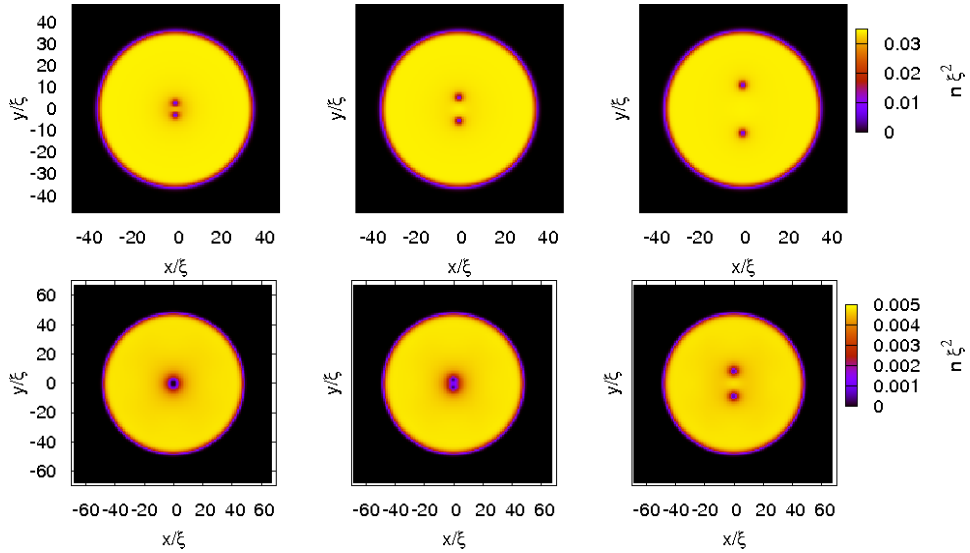

Figure 3.7: Density distributions $n(x, y, z = 0)$ in the xy-plane of a non-dipolar ($\beta = 0$)(top) and a strong dipolar ($\beta = 1.8$) (bottom) $n = 2$-vortex-configuration evolving in real time after 1,4 and 20 timesteps. The dipole is assumed in the z-direction and the unit of length is the healing length ξ. Remember, that ξ depends on the dipole (section 2.2).

phonon instability discussed in section 1.5.2). Due to the broken cylindrical symmetry, for sufficiently large β and small m/m^* the straight vortex line is destabilized into a snake-like configuration on the yz plane rather than into an helix, as in the previous section, as shown in figure 3.5. We have analyzed the amplitude of the helix when approaching the stability regime. Our results shown in figure 3.6 are compatible with a second-order-like behavior as in the previous section, although, as mentioned above, a rigorous analysis is largely handicapped by the appearance of strong density modulations in the simulations.

3.4 Doubly-quantized vortices in dipolar gases

As discussed in the introduction a doubly quantized vortex is unstable. This matches with the fact that two $n = 1$ vortices repel each other [93, 183], as discussed in the context of image-vortices in section 3.1. However, a doubly-quantized vortex can be stable in two-component Bose-Einstein condensates [186, 187]. In chapter 2 we saw that for the case of positive dipoles ($2 > \beta > 0$) the dipole-dipole interaction could stabilize the vortex-line. Hence, we want to investigate whether a strong dipole-dipole interaction may stabilize a doubly quantized vortex.

Therefore we create a doubly-quantized vortex and compute the ground-state configuration with the imaginary time evolution method (appendix A).

Then we let the ground-state configuration evolve in real time[1]. Figure 3.7 shows the results. The upper pictures show the evolution for the usual case without dipole-dipole interaction, while on the lower pictures one can observe the influence of the dipoles with $\beta = 1.8$. Even in the case of strong dipoles the vortices move apart from each other. Hence a doubly-quantized vortex cannot be stabilized by the dipole-dipole interaction. Recently this has been shown in [188] analyzing dipolar vortices for different trap geometries.

3.5 Conclusion

Summarizing, we have shown that the intrinsically dipole-induced instability discussed in chapter 2 opens the possibility for novel vortex-line configurations in dipolar BECs. In particular, we have shown with an intensive 3D numerical analysis that the presence of an additional optical lattice along the vortex line may allow for the observation of the dipole-induced destabilization of the straight vortex line due to the softening of a roton minimum in the Kelvin-wave spectrum. If this occurs the straight vortex-line configuration ceases to be that of minimal energy, and there is a second-order-like phase transition into an helical or snake-like vortex line, depending on the dipole orientation. In addition we have studied doubly-quantized vortices in dipolar gases and found that they are unstable as in usual short-range interacting gases.

[1]Technically we employ the real time evolution in the same way as the imaginary time evolution in 3D (appendix A)

Chapter 4

Hybrid multisite excitations in dipolar condensates in optical lattices

The long-range character of the dipole-dipole interaction leads to fundamentally new physics for quantum gases in optical lattices, since it induces interactions between neighboring sites. As a consequence, dipolar bosons in optical lattices are described by extended versions of the Bose-Hubbard Hamiltonian, and may present a wealth of novel phases, as supersolid [169] or Haldane-phases [189]. In addition, contrary to the case of short-range interactions, very deep optical lattices do not lead to independent low-dimensional gases, since non-overlapping atoms at different sites interact. As a consequence nonoverlapping BECs in two-well potentials may scatter [190], pair superfluidity may appear in ladder-like lattices [191], and even filament condensation may occur [192]. The effects of the intersite dipole-dipole interaction have been observed experimentally for the first time in very recent experiments in Florence on Bloch oscillations [124].

In this chapter we consider a stack of nonoverlapping quasi-two-dimensional condensates in an one-dimensional optical lattice (figure 4.1). We show that excitations in different lattice sites are coupled via the long-range dipole-dipole interaction. We study the influence of this coupling on the dispersion relation and the stability of the condensates for the case of attractive short-range interactions. In addition we discuss the observability of this effect in on-going experiments.

We start with an investigation of a single two-dimensional condensate. If the dipoles are oriented perpendicular to the condensate the dipole-dipole interaction in the plane is repulsive, and if sufficiently strong, it can prevent even a BEC with attractive contact-interaction from collapsing. The contact interaction can be tuned by using Feshbach resonances. In such a configuration the dispersion law could show a roton minimum so that the system may

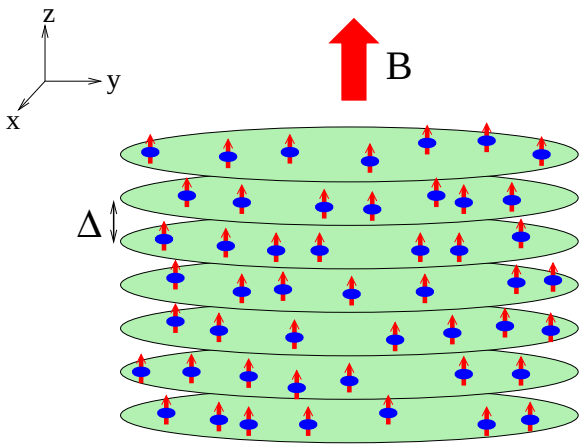

Figure 4.1: Scheme of the system under consideration.

be unstable, although the dipole-dipole interaction prevents the phonon instability. We have calculated the critical value of the dipolar moment, where the system is stable with respect to both kinds of instability.

Due to the anisotropic long-range character of the dipole-dipole interaction there is an attractive interaction between particles in different layers. Hence a second dipolar Bose-Einstein condensate placed at given distance is coupled to the first one via dipole-dipole interaction and excitations cannot considered separately anymore. A dispersion law for the coupled system is derived analogously to the single condensate and now the critical value of the dipolar moment is significantly larger, so that the second condensate could destablize the system with respect to roton-instability.

The increase of the critical dipole strength and the corresponding possible destablization is enhanced by taking more condensates into account. This is necessary in the case of a one-dimensional optical lattice, whereas at some point additional layers does not effect the dispersion law and the stability further, since the coupling becomes sufficiently small if the layers are to far away from each other. Then the critical dipolar strenght is saturated and we know the value where a stack of 50 to 100 pancake condensates appearing in related experiments is stable.

4.1 Single quasi-2D dipolar BEC

In the following, we consider a BEC of particles with mass m and electric dipole d (the results are equally valid for magnetic dipoles) oriented along z by an external field, and that hence interacts via a dipole-dipole potential as introduced in section 1.5.1: $V_d(\vec{r}) = d^2(1-3\cos^2(\theta))/r^3$, where θ is the angle formed by $\vec{r}$ with the z axis. At sufficiently low temperatures the physics of the dipolar BEC is provided by a non-local non-linear Schrödinger equation

(NLSE) of the form (1.69)

$$i\hbar\frac{\partial}{\partial t}\Psi(\vec{r},t) = \Bigg[-\frac{\hbar^2}{2m}\nabla^2 + V(\vec{r}) + g|\Psi(\vec{r},t)|^2 + \int d^3r' V_d(\vec{r}-\vec{r}')|\Psi(\vec{r}',t)|^2\Bigg]\Psi(\vec{r},t), \tag{4.1}$$

where $g = 4\pi\hbar^2 a/m$, with a the s-wave scattering length, and $V(\vec{r})$ is the trap potential. In the following, as in section 1.5.2, we use the convenient dimensionless parameter $\beta = g_d/g$, that charakterizes the strength of dipole-dipole interaction compared to the short range interaction, where $g_d = 8\pi d^2/3$. Note that β may be easily controlled experimentally by means of Feshbach resonances, as recently shown in Ref. [162].

Homogeneous solution

We consider first the case of a quasi-2D homogeneous BEC confined in z by the harmonic oscillator potential $V(\vec{r}) = m\omega_z^2 z^2/2$, which is sufficiently strong. As discussed in 1.3.1 the wave function is of the form

$$\Psi(\vec{r},t) = \Psi_\perp(\vec{\rho})\Phi_0(z)e^{-i(\mu/\hbar+w_z)t} \quad \text{with} \quad \Phi_0(z) = \frac{1}{\sqrt{\sqrt{\pi}l_z}}e^{-z^2/2l_z^2}, \tag{4.2}$$

where μ is the chemical potential and $\Phi_0(z)$ is the ground state of the transversal oscillator. The oscillator length $l_z = \sqrt{\hbar/m\omega_z}$ corresponds to the width of the lattice sites.

In order to solve the NLSE with this ansatz we multiply with $\Phi_0(z)$ and integrate over the whole z-axis

$$\mu\Psi_\perp(\vec{\rho}) = \Bigg\{-\frac{\hbar^2\vec{\nabla}_\rho^2}{2m} + \frac{g|\Psi_\perp(\vec{\rho})|^2}{\sqrt{2\pi}l_z} + \int dz\int d\vec{r'}|\Psi_\perp(\vec{\rho'})|^2 V_d(\vec{r}-\vec{r}')|\Phi_0(z')|^2|\Phi_0(z)|^2\Bigg\}\Psi_\perp(\vec{\rho}), \tag{4.3}$$

where the contact interaction part is rescaled by the prefactor $\int dz|\Phi_0(z)|^4 = (\sqrt{2\pi}l_z)^{-1}$ representing the quasi-two-dimenional character of the system. Using the convolution theorem the integral over d^3r' in the dipolar term reads as (section 1.5.1)

$$\int d\vec{r}'\,|\Psi(\vec{r}')|^2\,V_d(\vec{r}-\vec{r}') = \int \frac{d^3k}{(2\pi)^3}\,\widetilde{|\Psi(\vec{r}')|^2}\,\widetilde{V_d}(\vec{k})\,e^{i\vec{k}\vec{r}}. \tag{4.4}$$

The Fourier-transformation of the 3D density $\widetilde{|\Psi(\vec{r}')|^2}$ is simply the product of the Fourier-transformations of the 2D density $\tilde{n}_0(\vec{k}_\rho)$ and $\widetilde{|\Phi_0(z)|^2}(k_z) =$

$e^{-k_z^2 l_z^2/4}$. We insert these functions into (4.3), carry out the integrals over z and k_z and obtain

$$\mu\Psi_\perp(\vec{\rho}) = \left\{ -\frac{\hbar^2\vec{\nabla}_\rho^2}{2m} + \frac{(g+g_d)|\Psi_\perp(\vec{\rho})|^2}{\sqrt{2\pi}l_z} \right. \\ \left. -\frac{3g_d}{4}\int \frac{d^2k}{(2\pi)^2}\,\tilde{n}_0(\vec{k}_\rho)k_\rho \mathrm{erfc}[\frac{k_\rho l_z}{\sqrt{2}}]e^{k_\rho^2 l_z^2/2}e^{i\vec{k}_\rho\vec{\rho}} \right\}\Psi_\perp(\vec{\rho}), \qquad (4.5)$$

The ground state of a homogeneous 2D BEC is of the form $\Psi_\perp(\vec{\rho}) = \sqrt{n_0}$, where n_0 is the 2D density. Introducing this form into equation (4.5), one obtains

$$\mu = \frac{(g+g_d)n_0}{\sqrt{2\pi}l_z}. \qquad (4.6)$$

Note that the 2D condition is satisfied for $\mu \ll \hbar\omega_z$. This condition is always satisfied in our calculations.

Elementary excitations

In order to study the elementary excitations and the stability of the system we proceed as shown in the introduction 1.2.2. Inserting a plane wave ansatz

$$\Psi(\vec{r},t) = \left[\sqrt{n_0} + u_q\, e^{i\vec{q}\cdot\vec{\rho}-i\epsilon t/\hbar} - v_q^*\, e^{-i\vec{q}\cdot\vec{\rho}+i\epsilon t/\hbar}\right] \\ \times \Phi_0(z)\, e^{-i(\mu/\hbar+\omega_z)t} \qquad (4.7)$$

into the NLSE (4.1), linearizing in u_q, v_q, multiply with $\Phi_0(z)$ and integrate z we obtain

$$i\hbar\frac{\partial\chi(\vec{\rho},t)}{\partial t} = \left\{ -\frac{\hbar^2\nabla_\rho^2}{2m} - \mu + 2\tilde{g}n_0 + \tilde{g}_d n_0 \right\}\chi(\vec{\rho},t) + \tilde{g}n_0\chi^*(\vec{\rho},t) \qquad (4.8) \\ + \int dz \int d\vec{r'}|\Phi_0(z')|^2 V_d(\vec{r}-\vec{r}')\left[\chi(\vec{\rho}',t)+\chi^*(\vec{\rho}',t)\right]\Phi_0^2(z)n_0,$$

with $\tilde{g} = g/\sqrt{2\pi}l_z$ and $\tilde{g}_d = g_d/\sqrt{2\pi}l_z$, respectively. In order to shorten the expressions we have introduced

$$\chi(\vec{\rho},t) = u_q e^{i\vec{q}\vec{\rho}}e^{-i\epsilon t/\hbar} - v_q^* e^{-i\vec{q}\vec{\rho}}e^{i\epsilon t/\hbar} \qquad (4.9)$$

By using again the convolution theorem and the Fourier-transformations as above, the last dipolar term simplifies and (4.9) reduces to

$$i\hbar\frac{\partial\chi(\vec{\rho},t)}{\partial t} = \left\{ -\frac{\hbar^2\nabla_\rho^2}{2m} - \mu + 2\tilde{g}n_0 + \tilde{g}_d n_0 \right\}\chi(\vec{\rho},t) + \tilde{g}n_0\chi^*(\vec{\rho},t) \\ + \frac{g_d n_0}{2}\int\frac{d^2k}{(2\pi)^2}\int d\vec{\rho'}\left[\chi(\vec{\rho}',t)+\chi^*(\vec{\rho}',t)\right] \\ \times e^{i\vec{k}_\rho(\vec{\rho}-\vec{\rho}')}\left(\frac{2}{\sqrt{2\pi}l_z} - \frac{3k_\rho}{2}\mathrm{erfc}[\frac{k_\rho l_z}{\sqrt{2}}]e^{k_\rho^2 l_z^2/2}\right) \qquad (4.10)$$

We transform into dimensionless equations by expressing energies in units of the chemical potential (4.6) and using the corresponding length unit, the healing length $\xi = \hbar/\sqrt{m\mu}$.[1] The ansatz (4.9) defines an eigenvalue problem for the energies ϵ. So in order to find the dispersion relation $\epsilon(q)$ we have to diagonalize the matrix in

$$\epsilon \begin{pmatrix} u_q \\ v_q \end{pmatrix} = \begin{pmatrix} q^2 + 1 - f_\beta(q) & -1 + f_\beta(q) \\ 1 - f_\beta(q) & -(q^2 + 1 - f_\beta(q)) \end{pmatrix} \begin{pmatrix} u_q \\ v_q \end{pmatrix}, \tag{4.11}$$

with

$$f_\beta(q) = \frac{\beta}{1+\beta} \frac{3\sqrt{2\pi}}{4} |q| l_z \, \mathrm{erfc}[\frac{q l_z}{\sqrt{2}}] \, e^{q^2 l_z^2/2}. \tag{4.12}$$

We find

$$\epsilon(q) = \{q^2 \left[q^2 + 2(1 - f_\beta(q))\right]\}^{1/2} \tag{4.13}$$

Re-inserting dimensions we obtain the Bogoliubov spectrum of elementary excitations

$$\epsilon(q) = \{E_q \left[E_q + 2A\right]\}^{1/2} \tag{4.14}$$

where

$$E_q = \frac{\hbar^2 q^2}{2m} \qquad \text{and} \qquad A = \mu - \frac{g_d n_0}{\sqrt{2\pi} l_z} F(\frac{q l_z}{\sqrt{2}}), \tag{4.15}$$

with

$$F(x) = \frac{3\sqrt{\pi}}{2} |x| \mathrm{erfc}(x) e^{x^2}. \tag{4.16}$$

Note that without dipole-dipole interaction ($\beta = 0$) we recover the usual Bogoliubov spectrum for a 2D BEC with purely short-range interaction. In particular, if $a < 0$ and $\beta = 0$, $\epsilon(q)^2 < 0$ for $q \to 0$, recovering the well known phonon instability (and subsequent collapse) in homogeneous BEC with $a < 0$. If the dipole is sufficiently large, such that $g + g_d > 0$, then the dipole-dipole interaction prevents the instability at $q \to 0$. However, due to the q-dependence of the dipole-dipole interaction (given by the monotonously increasing character of the function F), the dispersion $\epsilon(q)$ may show for intermediate g_d values a roton-like minimum at a finite value of $q l_z$ (Fig. 4.2). For sufficiently low dipole-dipole interaction $\epsilon(q)^2 < 0$ at the roton-like minimum, leading to dynamical instability (roton instability). For $|\beta| > \beta_{cr}$ (with β_{cr} dependent on the ratio $g n_0 / l_z \hbar \omega_z$) roton instability is prevented, and the 2D homogeneous BEC is stable.

4.2 Two coupled quasi-2D dipolar BECs

In the following we show that β_{cr} is significantly modified in the presence of other neighboring quasi-2D dipolar BECs. We consider the case of an optical

[1] Note that the healing length depends on the dipolar coupling constant.

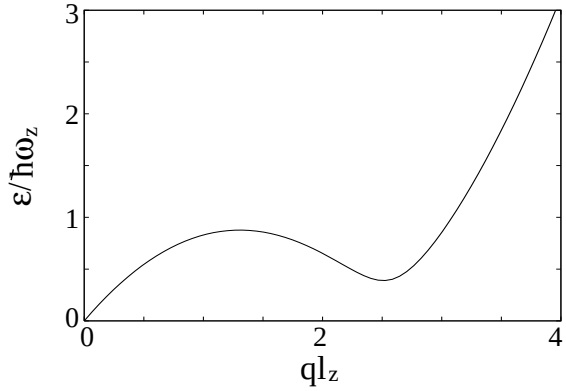

Figure 4.2: Roton minimum in the dispersion relation $\epsilon/\hbar\omega_z$ of a single 2D BEC with $\beta = -1.072$, $l_z = 0.09\mu$m, $a = -2$ nm, and a 3D density of $n_0/\sqrt{2\pi}l_z = 10^{14}\text{cm}^{-3}$.

lattice along z (Fig. 4.1) described by a potential $V(\vec{r}) = sE_r \sin^2(\pi z/\Delta)$, where Δ is the intersite spacing, and s provides the lattice depth in units of the recoil energy $E_r = \hbar^2\pi^2/2m\Delta^2$. As in the previous discussion we consider no trapping on the xy-plane (we discuss the potentially important role of the harmonic confinement on the xy-plane at the end of this chapter). As discussed in section 1.3.2, at each lattice node, $V(\vec{r})$ may be approximated by an effective harmonic oscillator potential $V_{eff}(z)$, with effective oscillator length $l_z \approx \Delta s^{-1/4}/\pi$. The lattice is considered strong enough so that we can assume that there is no spatial overlap between wave-functions in different lattice sites, and hence we may neglect any hopping. We assume the dipole-dipole interaction small enough to neglect pairing [191] or filamentation [192].

We start our discussion on inter-site effects with the two-well case. This simplified scenario already captures many features of the effect discussed. In addition, two-well potentials may be experimentally realized and are currently of considerable interest [193, 194]. The quasi-2D BEC in the i-th layer is given by the extended NLSE:

$$i\hbar\frac{\partial}{\partial t}\Psi_i(\vec{r},t) = \Bigg[-\frac{\hbar^2}{2m}\nabla^2 + V_{eff}(z) + g|\Psi_i(\vec{r},t)|^2 + \sum_j \int d^3r' V_d(\vec{r}-\vec{r}')|\Psi_j(\vec{r}',t)|^2\Bigg]\Psi(\vec{r},t), \tag{4.17}$$

where for a two-well potential, $i,j = 1,2$. Note that, crucially, the dipole-dipole interaction couples now the i-th layer to the j-th one.

Homogeneous solution

As for the single-site discussion, we consider a strong z-confinement at each site, and hence we may employ a quasi-2D ansatz

$$\Psi_i(\vec{r}) = \Psi_\perp(\vec{\rho}, t)\Phi_0(z - z_i)\, e^{-i(\mu/\hbar + w_z)t}, \tag{4.18}$$

where we consider the same 2D density at both sites, $\Phi_0(z)$ has the form discussed above, and z_i is the position of the i-th lattice node. We insert this ansatz into the NLSE (4.17). The dipole-dipole interaction couples the i-th layer to the j-th one, and hence instead of the dipolar term in equation (4.3) we have

$$\begin{aligned}\int dz \int d\vec{r'} |\Psi_\perp(\vec{\rho'})|^2 V_d(\vec{r} - \vec{r'}) |\Phi_0(z')|^2 |\Phi_0(z)|^2 \Psi_\perp(\vec{\rho}) \quad \rightarrow \\ \sum_j \int dz \int d\vec{r'} |\Psi_\perp(\vec{\rho'})|^2 V_d(\vec{r} - \vec{r'}) |\Phi_0(z' - z_j)|^2 |\Phi_0(z - z_i)|^2 \Psi_\perp(\vec{\rho})\end{aligned} \tag{4.19}$$

Fourier-transforming and using the convolution theorem, this term reduces to

$$\begin{aligned}&\int dz \int d\vec{r'} |\Psi_\perp(\vec{\rho'})|^2 V_d(\vec{r} - \vec{r'}) |\Phi_0(z' - z_j)|^2 |\Phi_0(z - z_i)|^2 \Psi_\perp(\vec{\rho}) = \\ &\frac{g_d}{2} \int \frac{d^2k}{(2\pi)^2}\, \tilde{n}_0(\vec{k}_\rho) e^{i\vec{k}_\rho \vec{\rho}} \int \frac{dk_z}{2\pi} \left(2 - \frac{3k_\rho^2}{k_\rho^2 + k_z^2}\right) e^{-k_z^2 l_z^2/2} e^{-ik_z|z_i - z_j|} \Psi_\perp(\vec{\rho})\end{aligned} \tag{4.20}$$

The exponential $e^{-ik_z|z_i - z'_j|}$ leads to a prefactor in the dipolar coupling between BECs in different layers depending on the distance $|z_i - z_j| = |i - j|\Delta$ between them. Since we consider the same 2D density at both sites the ground state of both homogeneous condensates is as in the previous section $\Psi_\perp(\vec{\rho}) = \sqrt{n_0}$. Introducing this ansatz into (4.20) and proceeding as in the single site case we obtain the 2D chemical potential

$$\tilde{\mu} = \mu + \lambda(\Delta), \tag{4.21}$$

with μ the chemical potential of an individual well and

$$\lambda(\Delta) = \frac{g_d n_0}{\sqrt{2\pi} l_z}\, e^{-\Delta^2/2l_z^2}. \tag{4.22}$$

Note that the inter-site interaction is a Gaussian function of the inter-site spacing and not of the form $1/\Delta^3$. The Gaussian dependence appears since the inter-site interactions are actually between two planes with an extension much larger (in our homogeneous approximation infinitely larger) than the inter-site distance.

Elementary excitations

As above we are interested in the elementary excitation of these systems. For $\Delta \to \infty$ the Bogoliubov modes at each site are independent and described by the single-site expression (4.14). For finite Δ the inter-site coupling leads to an hybridization of the modes at both sites with significant consequences, as we discuss below. As for the single-site discussion we insert a plane wave ansatz

$$\begin{aligned}\Psi_i(\vec{r},t) &= \left[\sqrt{n_0} + u_{qi}\, e^{i\vec{q}\cdot\vec{\rho}-i\epsilon t/\hbar} - v_{qi}^*\, e^{-i\vec{q}\cdot\vec{\rho}+i\epsilon t/\hbar}\right] \\ &\quad \times \Phi_0(z-z_i)\, e^{(-i(\tilde{\mu}/\hbar+\omega_z)t} \end{aligned} \tag{4.23}$$

into the NLSE (4.17), and linearize in u_{qi}, v_{qi}. The excitations in each layer can be described by the 2D Bogoliubov-equation (4.9). This implies one equation for each layer. But additionally one has several coupling terms. The excitations in the i-th layer χ_i are coupled via dipole-dipole interaction to the densities $|\Psi_{0j}|^2$ in all the other layers and the i-th ground-state Ψ_{0i} is coupled to all the other excitations χ_j and χ_j^*. Then in the case of two BECs one has three additional dipolar terms in the Bogoliubov-equation. The first of these three terms is calculated in the same way as the contribution of the second layer to the equation for the ground state (4.20). Hence it reduces to

$$\begin{aligned}\int dz \int d\vec{r'} |\Psi_\perp(\vec{\rho'})|^2 V_d(\vec{r}-\vec{r'}) |\Phi_0(z'-z_2)|^2 |\Phi_0(z-z_1)|^2 \chi_1(\vec{\rho},t) \\ = \frac{g_d n_0}{\sqrt{2\pi} l_z} e^{-\Delta^2/l_z^2} \chi_1(\vec{\rho},t),\end{aligned} \tag{4.24}$$

where we have used again

$$\chi_i(\vec{\rho},t) = u_{qi} e^{i\vec{q}\vec{\rho}} e^{-i\epsilon t/\hbar} - v_{qi}^* e^{-i\vec{q}\vec{\rho}} e^{i\epsilon t/\hbar} \tag{4.25}$$

The computation of the contribution of the other two terms is more involved. Using the convolution theorem and Fourier-transforming of the density and the dipolar potential, we obtain after carrying out the dz and the dk_z integral

$$\begin{aligned}&\int dz \int d\vec{r'} |\Phi_0(z'-z_2)|^2 V_d(\vec{r}-\vec{r'}) \left[\chi_2(\vec{\rho'},t) + \chi_2^*(\vec{\rho'},t)\right] \Phi_0^2(z-z_1) n_0 \\ &= \frac{g_d n_0}{\sqrt{2\pi} l_z} e^{-\Delta^2/l_z^2} \left[\chi_2(\vec{\rho},t) + \chi_2^*(\vec{\rho},t)\right] \\ &\quad - \frac{3 g_d n_0}{8} \int \frac{d^2k}{(2\pi)^2} \int d\vec{\rho'} \left[\chi_2(\vec{\rho'},t) + \chi_2^*(\vec{\rho'},t)\right] e^{i\vec{k}_\rho(\vec{\rho}-\vec{\rho'})} F_1(k_\rho),\end{aligned} \tag{4.26}$$

where we have introduced the function

$$F_1(k_\rho) = k_\rho\, e^{\frac{k_\rho^2 l_z^2}{2}} \left[e^{-k_\rho \Delta} \mathrm{erfc}\left(\frac{k_\rho l_z}{\sqrt{2}} - \frac{\Delta}{\sqrt{2} l_z}\right) + e^{k_\rho \Delta} \mathrm{erfc}\left(\frac{k_\rho l_z}{\sqrt{2}} + \frac{\Delta}{\sqrt{2} l_z}\right)\right].$$

Introducing these additional terms as well as the new chemical potential (4.21) we get instead of (4.10)

$$\begin{aligned} i\hbar\frac{\partial\chi_1(\vec{\rho},t)}{\partial t} &= \left[-\frac{\hbar^2\nabla_\rho^2}{2m}+\mu_0\right]\chi_1(\vec{\rho},t)+\mu_0\chi_1^*(\vec{\rho},t) \qquad (4.27)\\ &\quad +\frac{g_d n_0}{\sqrt{2\pi}l_z}e^{-\frac{\Delta^2}{l_z^2}}\left[\chi_2(\vec{\rho},t)+\chi_2^*(\vec{\rho},t)\right]\\ &\quad -\frac{3g_d n_0}{4}\int\frac{d^2k}{(2\pi)^2}\int d\vec{\rho'}\left[\chi_1(\vec{\rho}',t)+\chi_1^*(\vec{\rho}',t)\right]e^{i\vec{k}_\rho(\vec{\rho}-\vec{\rho}')}k_\rho\,\mathrm{erfc}[\frac{k_\rho l_z}{\sqrt{2}}]\,e^{\frac{k_\rho^2 l_z^2}{2}}\\ &\quad -\frac{3g_d n_0}{8}\int\frac{d^2k}{(2\pi)^2}\int d\vec{\rho'}\left[\chi_2(\vec{\rho}',t)+\chi_2^*(\vec{\rho}',t)\right]e^{i\vec{k}_\rho(\vec{\rho}-\vec{\rho}')}F_1(k_\rho)\\ i\hbar\frac{\partial\chi_2(\vec{\rho},t)}{\partial t} &= (1\leftrightarrow 2) \qquad (4.28) \end{aligned}$$

where $\mu_0=(g+g_d)n_0/\sqrt{2\pi}l_z$ is the chemical potential of one 2D BEC. The short form $(1\leftrightarrow 2)$ indicates that wherever an index 1 appears on χ in the first equation, it has to be replaced by an index 2 and vice versa. Rewriting these equations in terms of u_i and v_i we obtain from the first equation two equations for the positive and negative frequency part, respectively.

$$\begin{aligned} \epsilon u_{1q} &= \left[\frac{\hbar^2q^2}{2m}+\mu_0\right]u_{1q}-\mu_0 v_{1q}+\frac{g_d n_0}{\sqrt{2\pi}l_z}e^{-\frac{\Delta^2}{l_z^2}}\left[u_{2q}-v_{2q}\right] \qquad (4.29)\\ &\quad -\frac{3g_d n_0}{4}\left[u_{1q}-v_{1q}\right]|q|\,\mathrm{erfc}[\frac{|q|l_z}{\sqrt{2}}]\,e^{\frac{q^2l_z^2}{2}}-\frac{3g_d n_0}{8}\left[u_{2q}-v_{2q}\right]F_1(k_\rho)\\ \epsilon v_{1q} &= -\left[\frac{\hbar^2q^2}{2m}+\mu_0\right]v_{1q}+\mu_0 u_{1q}+\frac{g_d n_0}{\sqrt{2\pi}l_z}e^{-\frac{\Delta^2}{l_z^2}}\left[u_{2q}-v_{2q}\right] \qquad (4.30)\\ &\quad -\frac{3g_d n_0}{4}\left[u_{q1}-v_{q1}\right]|q|\,\mathrm{erfc}[\frac{|q|l_z}{\sqrt{2}}]\,e^{\frac{q^2l_z^2}{2}}-\frac{3g_d n_0}{8}\left[u_{2q}-v_{2q}\right]F_1(k_\rho) \end{aligned}$$

The second equation behaves in the same way. In section 4.1 we wrote everything in units of the chemical potential and the healing length. But as commented already, the healing length depends on the dipolar coupling constant. Hence we choose now the lattice spacing Δ as the length unit, which is fixed by the external potential and the corresponding energy scale $E_0=\hbar^2/(m\Delta^2)=\frac{2}{\pi^2}E_R$ as the unit of energy. In these units, equations (4.29) define the eigenvalue problem

$$\epsilon\begin{pmatrix}u_{1q}\\ v_{1q}\\ u_{2q}\\ v_{2q}\end{pmatrix}=M\begin{pmatrix}u_{1q}\\ v_{1q}\\ u_{2q}\\ v_{2q}\end{pmatrix}. \qquad (4.31)$$

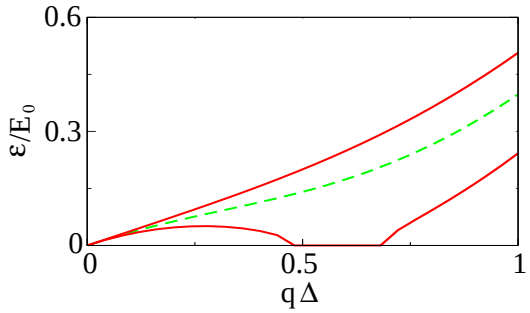

Figure 4.3: Dispersion law (in units of $E_0 = \hbar^2/m\Delta^2$) for a single site (dashed) and for two wells (solid) for $\beta = -1.2$, $\Delta = 0.53$ μm, $s = 13.3$, $a = -2$ nm, and $n_0/\sqrt{2\pi}l_z = 10^{14}/\mathrm{cm}^3$.

with the (4×4)-matrix

$$M = \begin{pmatrix} \frac{q^2}{2} + A - G_0 & -A + G_0 & C_1 - G_1 & -C_1 + G_1 \\ A - G_0 & -\frac{q^2}{2} - A + G_0 & C_1 - G_1 & -C_1 + G_1 \\ C_1 - G_1 & -C_1 + G_1 & \frac{q^2}{2} + A - G_0 & -A + G_0 \\ C_1 - G_1 & -C_1 + G_1 & A - G_0 & -\frac{q^2}{2} - A + G_0 \end{pmatrix}$$

with

$$A = (1+\beta)\frac{\tilde{g}n_0}{\sqrt{2\pi}l_z} \qquad \text{and} \qquad C_1 = \beta\frac{\tilde{g}n_0}{\sqrt{2\pi}l_z}e^{-\frac{\Delta^2}{l_z^2}} \tag{4.32}$$

and the functions

$$G_0(q) = \beta\frac{3\tilde{g}n_0}{4}|q|\,\mathrm{erfc}[\frac{|q|l_z}{\sqrt{2}}]\,e^{\frac{q^2l_z^2}{2}} \tag{4.33}$$

$$G_1(q) = \beta\frac{3\tilde{g}n_0}{8}|q|\,e^{\frac{q^2l_z^2}{2}}\left[e^{-q\Delta}\mathrm{erfc}\left(\frac{ql_z}{\sqrt{2}} - \frac{\Delta}{\sqrt{2}l_z}\right) + e^{q\Delta}\mathrm{erfc}\left(\frac{ql_z}{\sqrt{2}} + \frac{\Delta}{\sqrt{2}l_z}\right)\right]$$

The term $\tilde{g}n_0$ (with dimensions) is given by the scattering length a and the 3D density n_{3D} as $\tilde{g}n_0 = \frac{4\pi a}{\Delta}\,n_{3D}\,\Delta^3\sqrt{2\pi}l_z$. The diagonalization of the matrix in (4.31) yields two positive energy eigenvalues

$$\epsilon_\pm(q) = \frac{1}{2}\{q^2\left[q^2 + 4A - 4G_0(q) \pm 4(C_1 - G_1(q))\right]\}^{1/2}, \tag{4.34}$$

which are the Bogoliubov modes and can be rewritten with the proper dimensions in a form similar to equation (4.14)

$$\epsilon_\pm(q) = \{E_q\left[E_q + 2A \pm 2C(\Delta)\right]\}^{1/2}, \tag{4.35}$$

where

$$C(\Delta) = \lambda(\Delta) - \frac{g_d n_0}{\sqrt{2\pi}l_z}\tilde{F}\left(\frac{ql_z}{\sqrt{2}}, \frac{\Delta}{\sqrt{2}l_z}\right), \tag{4.36}$$

with

$$\tilde{F}(x,y) = \frac{3\sqrt{\pi}xe^{x^2}}{4} \sum_{\alpha=\pm 1} e^{-2\alpha xy}\mathrm{erfc}(x-\alpha y). \tag{4.37}$$

Note that for $\Delta \to \infty$, $C(\Delta) = 0$ and we recover two degenerate independent modes. For finite Δ the modes at the two wells hybridize, and two different branches appear for each q, one stiffer than the modes for $\Delta \to \infty$, and the other softer. The latter is particularly interesting, since the soft mode is more prone to rotonization (figure 4.3). Interestingly, under proper conditions, two parallel non-overlapping BECs may become roton-unstable even if they were stable separately. As a consequence, a larger β_{cr} is necessary to stabilize the two-well system.

4.3 Stack of N_s quasi-2D dipolar BECs coupled via dipole-dipole interaction

The hybridization (and consequent destabilization) in two-well potentials becomes even more pronounced for the case of dipolar BECs at $N_s > 2$ sites of a 1D optical lattice, since a site i couples with all its neighbors j (of course with decreasing strength for growing $|i-j|$). For simplicity of our analysis we consider the case in which all lattice sites present the same 2D density n_0. In that case, one may generalize the two-site analysis to the multi-site case, to reach a set of coupled Bogoliubov-de Gennes in dimensionless units

$$\epsilon \begin{pmatrix} u_{1q} \\ v_{1q} \\ \vdots \\ u_{Nq} \\ v_{Nq} \end{pmatrix} = M \begin{pmatrix} u_{1q} \\ v_{1q} \\ \vdots \\ u_{Nq} \\ v_{Nq} \end{pmatrix}, \tag{4.38}$$

with the $(2N_s \times 2N_s)$-matrix [2]

$$M = \begin{pmatrix} \frac{q^2}{2}+M_0 & -M_0 & M_1 & -M_1 & \dots & M_{N-1} & -M_{N-1} \\ M_0 & -\frac{q^2}{2}-M_0 & M_1 & -M_1 & \dots & M_{N-1} & -M_{N-1} \\ M_1 & -M_1 & \frac{q^2}{2}+M_0 & -M_0 & \dots & M_{N-2} & -M_{N-2} \\ M_1 & -M_1 & M_0 & -\frac{q^2}{2}-M_0 & \dots & M_{N-2} & -M_{N-2} \\ \vdots & \vdots & \vdots & \vdots & \ddots & \vdots & \vdots \\ M_{N-1} & -M_{N-1} & M_{N-2} & -M_{N-2} & \dots & \frac{q^2}{2}+M_0 & -M_0 \\ M_{N-1} & -M_{N-1} & M_{N-2} & -M_{N-2} & \dots & M_0 & -\frac{q^2}{2}-M_0 \end{pmatrix},$$

with $M_0 = A - G_0$ and $M_i = C_i - G_i$, where

$$A = (1+\beta)\frac{\tilde{g}n_0}{\sqrt{2\pi}l_z} \qquad \text{and} \qquad C_n = \beta\frac{\tilde{g}n_0}{\sqrt{2\pi}l_z}e^{-\frac{n\Delta^2}{l_z^2}} \tag{4.39}$$

[2] In the matrix we denote the number of sites with $N \equiv N_s$.

and the functions

$$G_0(q) = \beta\frac{3\tilde{g}n_0}{4}|q|\,\mathrm{erfc}[\frac{|q|l_z}{\sqrt{2}}]\,e^{\frac{q^2l_z^2}{2}} \tag{4.40}$$

$$G_n(q) = \beta\frac{3\tilde{g}n_0}{8}|q|\,e^{\frac{q^2l_z^2}{2}}\left[e^{-qn\Delta}\mathrm{erfc}\left(\frac{ql_z}{\sqrt{2}}-\frac{n\Delta}{\sqrt{2}l_z}\right)\right.$$
$$\left.+e^{qn\Delta}\mathrm{erfc}\left(\frac{ql_z}{\sqrt{2}}+\frac{n\Delta}{\sqrt{2}l_z}\right)\right] \tag{4.41}$$

Note that the entries of the matrix M are functions of its index, which makes it numerically accessible for arbitrary number of lattice sites N_s. If we consider only the first (4×4)-block-matrix we recover the matrix from (4.31). After diagonalizing M numerically, we obtain the corresponding band-like set of N_s elementary excitations (figure 4.4).

Note that the band-like spectrum has an upper phonon-like boundary. Rewriting the Bogoliubov de-Gennes equations (4.38) in terms of $f_{qi} = u_{qi} + v_{qi}$

$$\epsilon^2 f_{qi} = E_q(E_q+2A)f_{qi} + 2E_q\sum_{j\neq i}C(\Delta|i-j|)f_{qj}. \tag{4.42}$$

we find, for large N_s an approximate sound velocity

$$c_s \simeq \sqrt{[A+\sum_n C(\Delta|n|))/m]} \tag{4.43}$$

for the upper mode. The lower mode of the N_s-manifold becomes significantly softer than the individual modes for independent sites. As a consequence the roton instability extends to larger β_{cr} when N_s increases, until saturating for a sufficiently large N_s (due to the decreasing dipole-dipole interaction for increasing distance between sites).

Figure 4.5 summarizes our results on the stability as a function of β (we recall that $g<0$). As mentioned above if $g+g_d<0$ ($|\beta|<1$) the system is unstable against phonon instability. For $1<|\beta|<|\beta_{cr}(N_s)|$ the system is unstable against roton instability. $|\beta_{cr}|$ increases when N_s grows until saturating for sufficiently large N_s. For $|\beta|>|\beta_{cr}(N_s)|$ the quasi-2D BECs are stable.

The value of q_{rot} when the roton becomes unstable is of particular importance. Figure 4.6 shows a typical variation in $q_{rot}\Delta$ at the curve $\beta=\beta_{cr}(N_s)$ as a function of N_s. Note that q_{rot} at β_{cr} shows a maximum for small N_s. For small N_s, β_{cr} (and hence the on-site repulsive dipole-dipole interaction) increases significantly, and hence the value of q_{rot} at β_{cr} increases. For larger N_s β_{cr} tends to saturate, as mentioned above, and the repulsive on-site dipole-dipole interaction remains approximately constant along the curve $\beta_{cr}(N_s)$. As a consequence, the increase in N_s just increases the attractive contribution of the dipole-dipole interaction of neighboring sites,

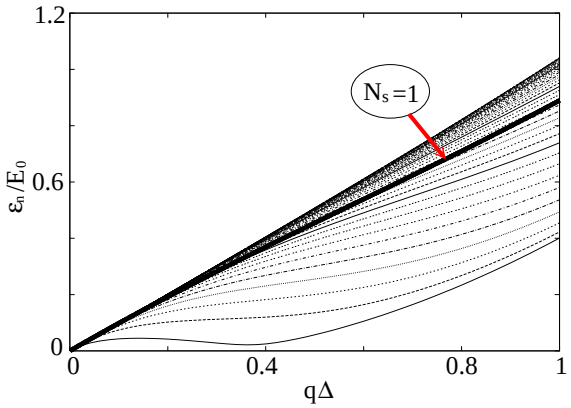

Figure 4.4: Band-like dispersion (in units of $E_0 = \hbar^2/m\Delta^2$) for $N_s = 40$ and $\beta = -2.44$. Other parameters are as in Fig. 4.3. We indicate the dispersion law for $N_s = 1$.

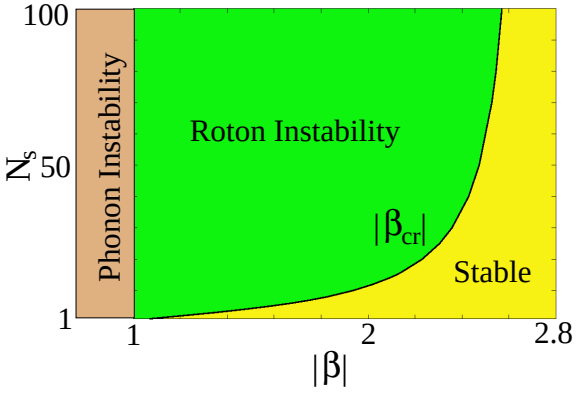

Figure 4.5: Stable and unstable regimes for N_s dipolar 2D BECs. We employ the same parameters as in figure 4.3.

and the dipole-dipole interaction becomes less effective in compensating the attractive on-site short-range interaction. As a result of that, q_{rot} decreases until saturating at a value lower than that for a single site.

4.4 Experimental realization

Typical experiments work with an harmonic xy-trapping (of frequency ω_{xy}). Although we have assumed homogeneous quasi-2D gases, we may estimate the effect of the xy-trapping by considering an effective cut-off at low momenta $q_{cut} \simeq 1/l_{xy}$, where $l_{xy} = \sqrt{\hbar/m\omega_{xy}}$ is the harmonic oscillator length characterizing the xy-trap. Note that this estimation is actually quite conservative, since for weak transversal confinements the transversal size of the interacting condensate is actually larger than l_{xy}, approaching the Thomas-

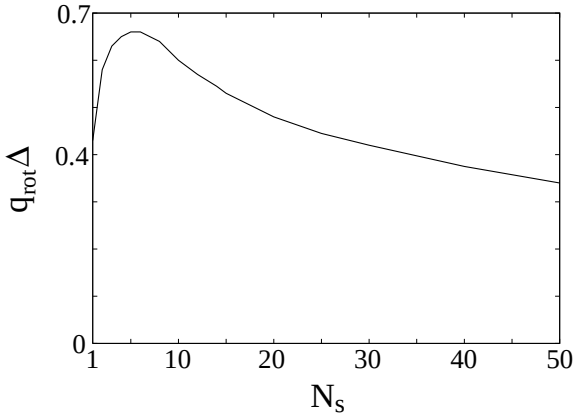

Figure 4.6: Roton momentum q_{rot} when the roton minimum touches zero as a function of the number of sites N_s. We employ the same parameters as in Fig. 4.3.

Fermi radius in the Thomas-Fermi regime. In a good approximation we may consider that all features occurring at momenta $q < q_{cut}$ are suppressed by the trap. As a consequence one expects that the xy confinement suppresses roton instability for frequencies $\omega_{xy} > \omega_{cut}$. For typical densities 10^{14}cm^{-3}, and typical intersite separation $\Delta = 0.53\mu$m, we estimate for ^{52}Cr that for a single site β_{cr} is achieved at a scattering length $a \simeq -31a_0$, and that for this case $\omega_{cut} \simeq 66$Hz. For the same case but $N_s = 4$ (which is the maximum of the corresponding q_{rot} curve), β_{cr} is achieved for $a \simeq -24a_0$, and $\omega_{cut} \simeq 160$Hz. For the latter case an instability rate of $\Gamma^{-1} \simeq 5$ms is expected for $a = -24.5a_0$. For ^{39}K, the numbers are more restrictive (due to the lower magnetic moment). For $N_s = 25$ (maximum of the q_{rot} curve), β_{cr} is achieved for $a \simeq -0.52a_0$, and $\omega_{cut} \simeq 4$Hz. For this case, one expects $\Gamma^{-1} \simeq 180$ms at $a = -0.53a_0$.

Note that the fact that q_{rot} shows a maximum may have interesting consequences in experiments, since this suggests that for some intermediate trapping frequencies the instability may be just present for a given window of values of N_s. Note also that the previous discussion just refers to the destabilization when the roton touches zero. For even larger values of $|a|$, a larger region of q may become unstable. However if the xy-trap just allows for the resolution of the upper boundary of the unstable region and not the lower one, roton and phonon instability may become experimentally undistinguishable.

4.5 Conclusion

The nonlocal character of the dipole-dipole interaction leads to a novel scenario where non-overlapping gases at different sites interact significantly.

Contrary to the case of pure short-range interaction, the dipole-dipole interaction leads to the hybridization of the excitations at different sites, which acquire a collective band-like character. In particular, the hybridization of the modes leads to a significant enhancement of the rotonization of the excitations, and may induce roton-instability for values of the short-range interaction at which a single site is stable. Finally, we have discussed the experimental requirements for the observation of the roton instability.

Recently, using a similar analysis, [195] discussed the roton-softening due to intersite interactions in the context of recent experiments in Florence [124]. Although we consider that roton softening plays no significant role in the damping observed in Ref. [124] due to the xy-confinement, a weaker ω_{xy} (along the lines discussed above) could allow for the instability discussed by Wang and Demler, and by us in this thesis.

Chapter 5

Bose-Fermi mixtures of self-assembled filaments of fermionic polar molecules

As discussed in the introduction dipolar quantum gases of heteronuclear molecules, especially at their lowest rovibrational state, may present a very large electric dipole moment ($\gtrsim 1$ Debye) [130, 131, 132]. Although quantum degeneracy has not been yet achieved, the rapid pace of development allows to expect degenerate gases of polar molecules in the next future. These gases are expected to be largely dominated by the dipole-dipole interaction.

Deep 1D optical lattices may slice a gas into non-overlapping samples. As mentioned already in the previous chapter, the dipole-dipole interaction leads to intersite effects. There we considered weak dipoles (e.g. atomic magnetic dipoles) and studied collective excitations shared by non-overlapping sites [196]. For bosonic polar molecules the non-local dipolar effects are much stronger, leading to interesting effects as pair-superfluidity for ladder-like lattices [191] and filament Bose-Einstein condensdation [192].

Filamentation is indeed an interesting possibility introduced by the dipole-dipole interaction. This phenomenon, first suggested in the context of ferrofluids by de Gennes and Pincus [197], has attracted a considerable theoretical interest for the case of classical dipoles (For a review see e.g. [198]. Dipolar chains in classical ferrofluids were recently observed in superparamagnetic iron colloids [199] and single-domain magnetite colloids [200]. In Ref. [192] it was shown that a similar filamentation process may occur for bosonic polar molecules in deep lattices, which may organize into chains sustained by an attractive inter-site dipole-dipole interaction, forming a dipolar chains liquid (DCL) which may Bose-condense [192]. (We discuss this issue in more detail in section 5.2.)

In this chapter we consider DCLs of fermionic polar molecules. Far from being a trivial extension of the bosonic case, fermionic polar molecules

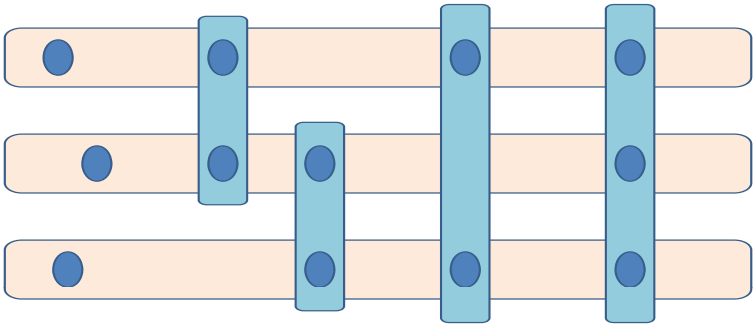

Figure 5.1: Polar fermionic molecules in a three-well potential may remain unpaired, form fermionic trimers, or bosonic dimers between nearest neighbors or next-nearest neighbors.

lead to a very different and rich physics. Whereas for bosonic molecules the chains are obviously bosons, for fermionic molecules the bosonic or fermionic character of the filaments depends on the number of molecules in the chain. This has particularly relevant consequences when the number of available lattice sites is odd. Here we focus on the simplest non-trivial case, namely a three-well potential (figure 5.1). For simplicity we restrict our discussion to the ideal gas regime, where inter-filament interactions are neglected. Although this approximation is of limited quantitative validity (and would demand mesoscopic samples in specific 1D arrangements as discussed below), it contains already many of the qualitatively new features which may be expected for more general scenarios of polar Fermi molecules in deep 1D and 2D optical lattices. In particular, the competition between trimer/dimer binding and trimer Fermi energy results in a non-trivial dependence of the character of the DCL as a function of the number of molecules per site N. If N is smaller than a critical N_c the DCL is a Fermi-degenerate gas of trimers. However for $N > N_c$ the trimers coexists with a Bose mixture formed by pseudo-spin-1/2 dimers and spinless dimers, leading to a peculiar Bose-Fermi mixture. We show that these Bose-Fermi DCLs may be probed by monitoring the spatial distribution of the molecules.

5.1 Single filaments of polar molecules

We consider polar molecules with mass m and electric dipole d in a deep three-well potential along the z-direction, with inter-site spacing Δ. This arrangement may be created by e.g. selectively emptying all sites of a strong 1D optical lattice except three neighboring ones. The potential barriers are large-enough to prevent any inter-site hopping. Due to reasons discussed below, the analysis of the problem simplifies notably if the gas is considered as strongly confined along the y-direction (e.g. in a single node of a lattice as that in the z-direction). Along the remaining x-direction we consider

a shallow harmonic confinement with frequency ω. The molecules interact via the dipole-dipole interaction $V_d(\mathbf{r}) = d^2(1-3\cos^2\theta)/r^3$, where θ is the angle formed by $\vec{r}$ with the dipole orientation. We assume that the dipoles form an angle α with the z direction, such that $\sin^2\alpha = 1/3$. Although this particular orientation and the 1D character of the sites are not needed for the formation of the DCL gas, which may occur also in stacks of 2D sites [192], this particular scenario allows both for a strong attraction between dipoles placed on top of each other and for a vanishing dipole-dipole interaction between molecules at the same site. This largely reduces the inter-filament interaction, allowing for a simplified ideal gas scenario, as discussed below.

The attraction between polar molecules placed on top of each other may be strong-enough to bind two or more polar molecules into self-assembled chains (figure 5.1). Whereas for bosonic molecules these chains are in any case bosons [192], for fermionic molecules the fermionic/bosonic character of the filaments depends on the odd/even number of molecules in a given chain. In particular, the three-well configuration allows for fermionic trimers (and of course monomers), and two different kinds of bosonic dimers, namely those between two molecules at nearest neighbors (type I dimers), and those between two molecules at the uppest and lowest site (type II dimers) (figure 5.1). Note that dimers I are actually pseudo-spin-1/2 bosons, since dimers in sites 1 and 2 are not equivalent to dimers in sites 2 and 3.

The ground-state of a single filament of M molecules is calculated similarly as for bosonic molecules [192]. Let $\hat{\mathbf{r}}_j$ be the position[1] and $\hat{\mathbf{p}}_j$ the momentum operator of a molecule at site j. Introducing $\hat{\mathbf{P}} = \sum_{j=1}^{M} \hat{\mathbf{p}}_j/M$, $\mathbf{R} = \sum_{j=1}^{M} \mathbf{r}_j/M$, $\mathbf{q}_j = \mathbf{p}_j - \mathbf{P}$, $\mathbf{s}_j = \mathbf{r}_j - \mathbf{R} = \{x_j, y_j, z_j\}$, the Hamiltonian splits into $\hat{H} = \hat{H}_{CM} + \hat{H}_{rel}$, where $\hat{H}_{CM} = \hat{\mathbf{P}}^2/2Mm + Mm\omega^2 R_x^2/2$ describes the filament center-of-mass and

$$\hat{H}_{rel} = \sum_{j=1}^{M} \left[\frac{\hat{\mathbf{q}}_j^2}{2m} + \frac{m}{2}\left(\omega_\perp^2 (y^2 + z_j^2) + \omega^2 x^2\right) \right] + \sum_{i,j>i} V_d\left[\mathbf{s}_i - \mathbf{s}_j\right]. \qquad (5.1)$$

the relative motion. The on-site yz confinement is approximated by a strong isotropic harmonic oscillator of frequency $\omega_\perp$. The wavefunction of the j-th molecule is chosen as $\psi_j(x_j - x_{j0})\varphi_j(y_j)\varphi_j(z_j - z_{j0})$, where $\varphi_j(\eta) = \exp\left(-\eta^2/2l_\perp^2\right)/\sqrt{l_\perp\sqrt{\pi}}$, with $l_\perp = \sqrt{\hbar/m\omega_\perp}$ and

$$\psi_j(\eta) = \frac{1}{\sqrt{\sqrt{\pi}R_0}}\, e^{-\eta^2/2R_0^2}, \qquad (5.2)$$

where R_0 is the variational width of the x wavepackets[2]. For deep lattices one may approximate $l_\perp \to 0$ (energy corrections are $\lesssim 1\%$ for depths > 14

[1] For the case of operators we use the bold font to denote the vector character.

[2] If U_0 is sufficiently large a molecule is locally bound in the dipolar potential induced by the molecule in the next layer and the wave-function should be a good ansatz.

recoil energies $\hbar^2\pi^2/2m\Delta^2$). The variational parameter R_0 is determined by minimizing the energy of the relative motion of a filament with M molecules

$$E = \sum_{j=1}^{M} \frac{\hbar}{2mR_0^2} + \sum_{j=1}^{M} \frac{m}{2}\omega R_0^2 + \sum_{i,j>i}^{M} \int dx dx' \frac{V_d\,(x-x', j-i)}{\pi R_0^2}\, e^{-(x-x_{j0})^2/R_0^2}\, e^{(x'-x_{i0})^2/R_0^2}, \tag{5.3}$$

where for the case of dipoles forming an angle α with the z direction, such that $\sin^2\alpha = 1/3$, the dipolar potential reads

$$V_d(x,z) = \frac{d^2}{(x^2+z^2)^{3/2}}\left(1 - \frac{(\sqrt{2}z+x)^2}{x^2+z^2}\right). \tag{5.4}$$

From this expression we see that for dipoles sitting site by site in the same layer ($z = 0$) the dipole-dipole interaction vanishes. Minimizing the energy of straight filaments ($x_{j0} = x_{i0} = 0$) with respect to R_0 we obtain the filament binding energy [3]. We denote as $-E_T$, $-E_{D,I}$ and $-E_{D,II}$ the binding energies for, respectively, trimers, dimers I, and dimers II. These energies grow with the dipole strength $U_0 = md^2/\hbar^2\Delta$. There exists a critical U_0^* such that for $U_0 < U_0^*$ the composites unbind ($R_0 \gtrsim l_{HO} = \sqrt{\hbar/m\omega}$). In free space a bound state exists even for arbitrarily small values of U_0 [201]. Note that $U_0^*(T) < U_0^*(D,I) \ll U_0^*(D,II)$ (figure 5.2) due to the different strength of the dipole-dipole interaction in each composite. In the following we consider the regime $U_0 > U_0^*(D,II)$, where $R_0 \ll l_{HO}$ for all of the possible composites of figure 5.1.

Transverse filament excitations contribute to the gas entropy, being relevant at finite temperature T. In addition, and much more as for the case of bosonic molecules [192], transverse modes are important for fermionic molecules also at very low T since they may significantly reduce the trimer Fermi energy. For a chain of M molecules, we obtain the low-lying modes $\xi_{\nu=1,\ldots,M}$ after expanding the chain energy E around its minimum, and diagonalizing $A_{nn'} = \partial^2 E/\partial x_n \partial x_{n'}$, where $n, n' = 1, \ldots, M$. From equation (5.3) we calculate the diagonal entries of this matrix

$$A_{nn} = \frac{1}{2}\sum_{i=1, i\neq n}^{M} \int dx dx' \frac{V_d\,(x-x', n-i)}{\pi R_0^2} \frac{2}{R_0^2}\left(2\frac{x^2}{R_0^2} - 1\right) e^{-x^2/R_0^2}\, e^{x'^2/R_0^2} \tag{5.5}$$

and the off-diagonal ($n \neq n'$) entries

$$A_{nn'} = \frac{1}{2}\int dx dx' \frac{V_d\,(x-x', n-n')}{\pi R_0^2} \frac{4}{R_0^4} x x'\, e^{-x^2/R_0^2}\, e^{x'^2/R_0^2}. \tag{5.6}$$

[3] For simplicity we neglect that the minimal-energy configuration is slightly tilted from the vertical with an angle $\sim \pi/10$.

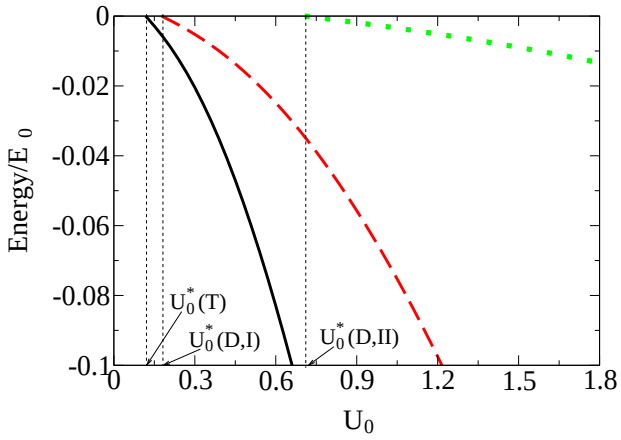

Figure 5.2: Binding energy (in units of $E_0 = \hbar^2/m\Delta^2$) of the different composites of figure 5.1 as a function of $U_0 = md^2/\hbar^2\Delta$.

The tranverse excitation modes are $\xi_{\nu=1,\ldots,M} = \sqrt{a_\nu}$, where a_ν are the eigenvalues of $A_{nn'}$

Summarizing, a filament is characterized by its length M and corresponding binding energy E_M, by a transversal excitation mode ξ_ν and by the energy level n, which it occupies in the external harmonic oscillator trap.

5.2 Bosonic filaments

In this section we discuss as a starting point the statistcal analysis of bosonic polar molecules as performed in [192]. We consider two-dimensional gases of bosonic polar molecules placed at the different sites of a one-dimensional optical lattice. In [192] it was shown that for a sufficiently low temperature ($T < T_C$) a Bose-Einstein condensate of the longest filaments available occur. We recovered the result from [192] and extended it by investigating the influence of the transversal modes on the statistics of bosonic polar molecules. The modes were obtained performing a two-dimensional variant of the procedure shown in section 5.1 [202]. Since the energies of the lowest modes are very small in comparison with the thermal energy $k_B T_C$, the filaments can easily occupy these states and the development of a BEC is handicapped. Our analysis confirms this fact, and as shown in figure 5.3, the presence of the transverse modes significantly reduces the value of T_C. However, this effect on the critical temperature vanishes for huge values of U_0, where the energy of the lowest modes is already as large as $k_B T_C$.

As discussed below the ideal-gas treatment is of limited validity. From an estimation of the total interaction energy similar to (5.15) one can show that a two-dimensional filament gas with long filaments as discussed in [192] and in [202] always violates the ideal gas condition for realistic traps and densities. The analysis in [192] has in addition some other serious problems.

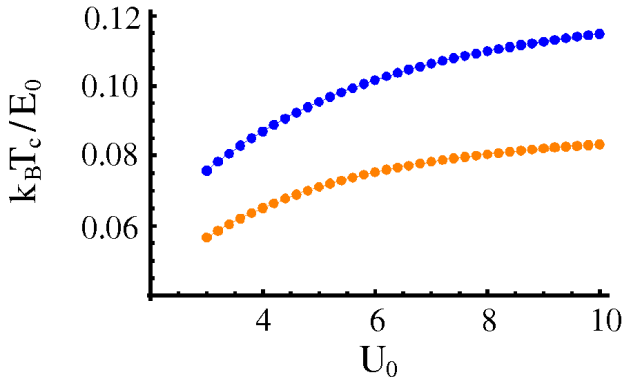

Figure 5.3: Condensation temperature as a function of U_0 for a filament gas of $N = 40000$ bosonic polar molecules ($m = 100$amu) with (orange) and without (blue) transversal bending modes for a system of $L = 81$ two-dimensional layers in an external trap of $\omega/2\pi = 3.5$Hz.

It completely neglects all filaments with holes, which are of the form of our type II dimers. From the model for the single filaments described in the previous section it follows that the binding energy of such filaments can be larger than the binding energy of shorter filaments without holes. In addition [192] considers only one chemical potential for the whole system. Since we neglect tunneling the number of particles per site is conserved and as we discuss later we need a chemical potential for each lattice site. In the remainder of this chapter we focus on fermionic polar molecules in three-well potentials confined to one dimension.

5.3 Quantum statistics of filaments

In the following we consider the filament statistics of fermionic molecules, assuming an ideal filament gas. This largely simplifies the analysis of the problem, while allowing for the discussion of key qualitative features of these systems, in particular the competition between different Bose and Fermi composites. This approximation is just quantitatively valid for mesoscopic samples in the arrangement discussed above, as we discuss at the end of this paper.

The fermionic or bosonic character of the chains is reflected by the average occupations for trimers, dimers I, dimers II and monomers:

$$N_T(n,\nu_T) = \left[e^{\beta[-E_T+\xi_{\nu_T}+\epsilon_n-(2\mu_1+\mu_2)]}+1\right]^{-1} \tag{5.7}$$

$$N_{D,I}(n,\nu_{D,I}) = \left[e^{\beta[-E_{D,I}+\xi_{\nu_{D,I}}+\epsilon_n-(\mu_1+\mu_2)]}-1\right]^{-1} \tag{5.8}$$

$$N_{D,II}(n,\nu_{D,II}) = \left[e^{\beta[-E_{D,II}+\xi_{\nu_{D,II}}+\epsilon_n-2\mu_1]}-1\right]^{-1} \tag{5.9}$$

$$N_{S,j}(n) \;=\; \left[e^{\beta[\epsilon_n-\mu_j]}+1\right]^{-1} \tag{5.10}$$

where $N_{S,j}$ denotes the average occupation of individual molecules at site j, $\xi_{\nu_{T;D,I;D,II}}$ the transverse filaments modes of the different composites, $\epsilon_n = \hbar\omega(n+1/2)$ the harmonic oscillator levels and $\beta = 1/k_BT$ the inverse temperature. In the previous expressions we have assumed symmetric configurations such that the number of dimers I in sites 1–2 is the same as the number of dimers I in sites 2–3, and equal to $N_{D,I}(n,\nu_{D,I})$. Note that $\mu_1 = \mu_3$ is the chemical potential for molecules at the uppest and lowest sites, whereas μ_2 denotes the chemical potential for molecules in the middle site. These different chemical potentials are necessary to fulfill the normalization conditions, in which we assume N molecules per lattice site. Imposing symmetry between the uppest and the lowest sites, these conditions acquire the form:

$$N \;=\; N_T + N_{D,I} + N_{D,II} + N_{S,1}, \tag{5.11}$$

$$N \;=\; N_T + 2N_{D,I} + N_{S,2}, \tag{5.12}$$

where N_T, $N_{D,I}$, $N_{D,II}$, $N_{S,1}$ and $N_{S,2}$ denote respectively the total number of trios, dimers I in sites 1–2 (or 2–3), dimers II, monomers in site 1 (or 3) and monomers in site 2. We insert the occupation numbers (5.7–5.10) and sum over all degrees of freedom, harmonic oscillator levels n and the tranversal bending modes ν. In order to simplify the expressions we calculate the sums over the harmonic oscillator levels in the continuum limit $\hbar\omega \ll k_BT$ by using the integral

$$\int \frac{dx}{\beta\hbar\omega}\,\frac{1}{e^{\beta a}\,e^{x}\pm 1} = \mp\frac{k_BT}{\hbar\omega}\,\ln\left(1\pm e^{-\beta a}\right). \tag{5.13}$$

Then we obtain $\mu_1(N,T)$ and $\mu_2(N,T)$ numerically with a root finding method [184] and from (5.7–5.10) the occupation numbers. The occupation numbers and hence the quantum statistics depend on the external parameters: temperature T, number of particles per site (filling) N, strength of the dipole-dipole interaction U_0 and the frequency of the external harmonic oscillator trap ω. In the following we discuss the influence of these parameters. We start with fixed dipolar coupling and trap frequency and analyze the quantum statistics at sufficiently low temperatures for different fillings.

Due to the attractive dipole-dipole interaction between molecules in the filament, the most bound chain is the trimer. The difference in binding between dimers and trimers induces that for sufficiently small N and at low-enough T the DCL becomes a degenerate Fermi gas of trimers. The trimers fill up oscillator levels (and also transverse trimer modes) up to the corresponding Fermi energy $E_F(N)$, which equals $N\hbar\omega$ for rigid filaments but it is actually smaller due to the transverse trimer modes (figure 5.4). However, if the number of molecules per site is sufficiently large, the growth

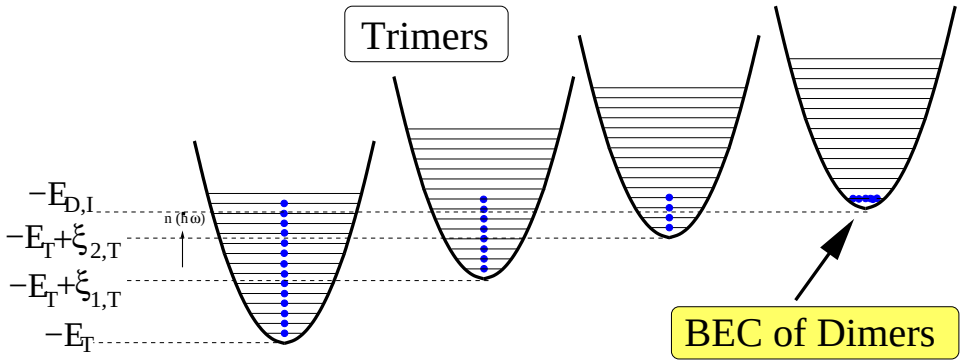

Figure 5.4: Occupation numbers at very low temperatures for $N > N_c$. The Fermi energy is larger than the difference in binding energy and the particles start to occupy dimers.

in Fermi energy overcomes the binding energy difference. This transition may be easily estimated by comparing the average energy per molecule for the case of two trimers and that for the case of 2 dimers I and one dimer II. This leads to a condition for the critical number of molecules per site $N_c(U_0, \omega)$,

$$E_F(N_c) = 2E_T - 3(E_{D,I} + E_{D,II})/2 \tag{5.14}$$

(which we have confirmed numerically). Note that N_c grows with growing U_0 and decreasing ω. For $N < N_c$ the DCL is a degenerate trimer gas, whereas for $N > N_c$ the trimer gas coexists (figure 5.4) with a mixture of pseudo-spin-1/2 bosons (dimers I) and spin-less bosons (dimers II).

5.4 Spatial density distributions

The peculiar properties of the DCL translate into the spatial molecular distribution integrated over the three sites. For $N < N_c$ and $N < \xi_{1_T}/\hbar\omega$, only trimers in their internal ground state are formed, and hence the gas behaves as a spin-less Fermi gas of particles of mass $3m$, presenting a Thomas-Fermi density profile $(1-(x/R)^2)^{1/2}$ with $R/l_{HO} = \sqrt{2N/3}$ (figure 5.5, top). For $\xi_{1_T}/\hbar\omega < N < N_c$, the DCL is still a trimer gas, but transversal modes may be populated.

In that case the density profile departs from the Thomas-Fermi profile (figure 5.5, center), due to the appearance of internally excited trimers in low harmonic oscillator levels. For $N > N_c$ the density profile changes dramatically. Note that since we consider 1D gases, dimer BEC is strictly speaking precluded. However, due to finite size the dimers quasi-condense (at low-enough T) occupying the few lowest levels of the harmonic oscillator. Hence when N surpasses N_c a Bose cloud nucleates at the trap center. As

a result the distribution of the polar molecules shows a Gaussian-like peak at the trap center (figure 5.5, bottom).

For $N \gg N_c$ and $U_0 > U_0^*(D, II)$ the DCL is at low T a basically pure Bose gas of dimers I and II (except for a small trimer fraction). Since both dimers have mass $2m$, the difference between them cannot be discerned from the analysis of the integrated density profile of the molecules. However the different binding energy and excited dimer modes for both types of dimers may be studied spectroscopically to reveal the dual nature of the mixture. If $N \gg N_c$ but $U_0^*(D, I) \ll U_0 < U_0^*(D, II)$, dimers II are precluded, and hence the DCL will become at low T a Bose-Fermi mixture of dimer-I bosons and degenerate monomers at sites 1 and 3 (which act as a pseudo-spin-1/2 fermions). Again, this exotic mixture could be revealed from the corresponding dual density profile.

5.5 Finite temperature analysis

The DCL presents as well an intriguing finite temperature physics due to the role of filament modes and the different binding energy of dimers and trimers. This is particularly clear from a finite T analysis of a DCL with $N < N_c$ (figure 5.6). Note that whereas at very low T the DCL is purely a trimer Fermi gas, at finite T it becomes more favorable to populate dimers than to populate higher excited trimer states. As a consequence the system presents a striking thermal enhancement of the bosonic modes. Interestingly, contrary to the standard situation, this leads to a maximal central peak density for a given finite T as shown in figure 5.7. For even larger T the central density decreases again due to the occupation of dimers at higher oscillator modes, and the breaking of the filaments into individual molecules.

5.6 Validity of the ideal gas approach

The discussed ideal gas analysis allows for a relatively easy understanding of key qualitative features characterizing fermionic polar molecules in deep optical lattices under more general conditions, as the competition between filament-binding energy and Fermi energy of fermionic chains, the relevant role of the filament modes at zero and finite T, or the formation of peculiar mixtures of different types of composite bosons and fermions. However, the quantitative validity of the ideal gas approximation is rather limited (also for bosonic molecules [192]), even for the previously discussed 1D arrangement with the particular choice for the dipole orientation. We may estimate the importance of the inter-filament interactions by comparing the inter-trimer interactions with the Fermi energy of rigid trimers ($\epsilon_F = N\hbar\omega$). For deeply bound chains ($R_0 \sim \Delta/2$) and at inter-filament distances $x > \Delta$ we may approximate the interaction between molecules at different chains as that

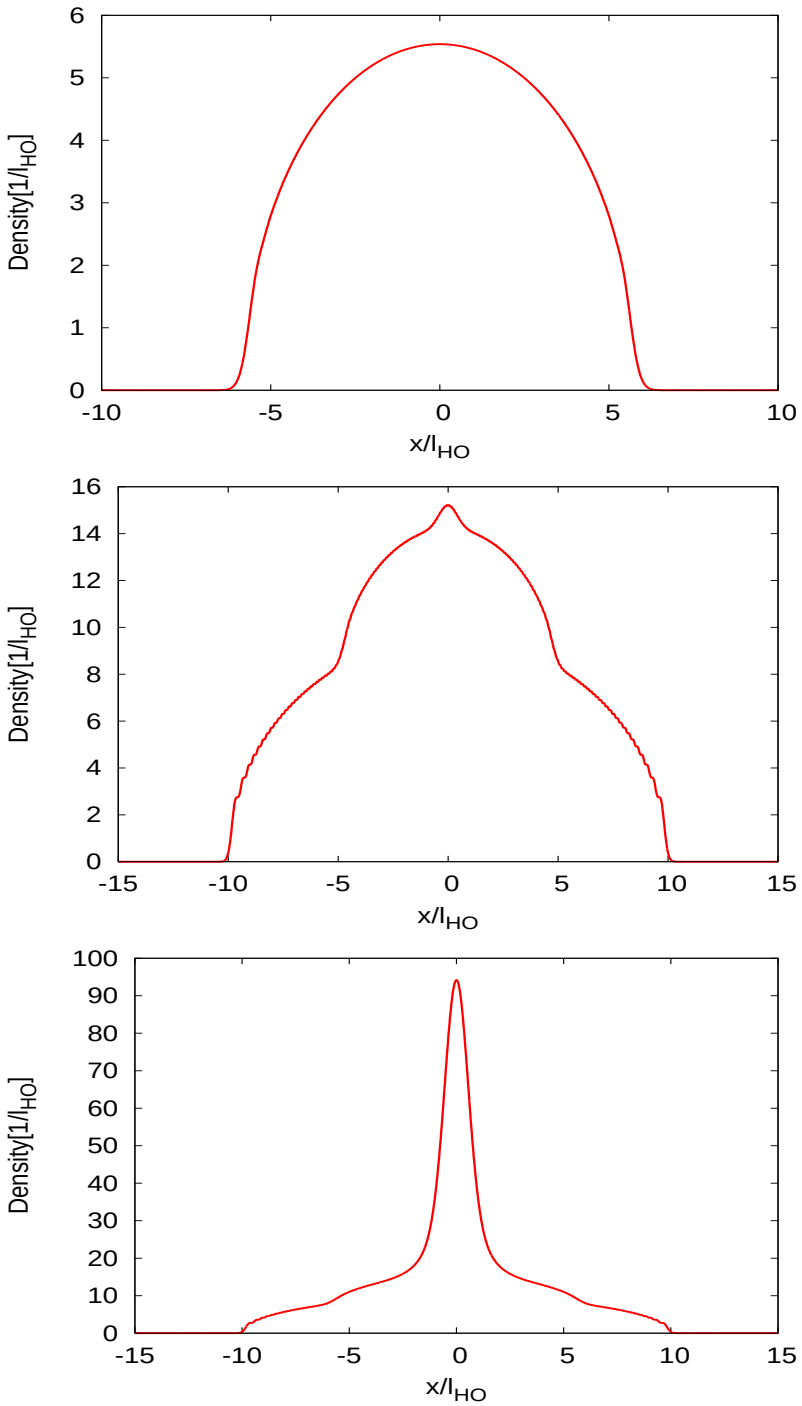

Figure 5.5: Integrated density profiles of the molecules, for $N < \xi_{1_T}/\hbar\omega < N_c$ (top), $\xi_{1_T}/\hbar\omega < N < N_c$ (center), and $N > N_c$ (bottom). We consider $U_0 = 2$, $\omega/2\pi = 1$Hz, $m = 100$amu, which lead to $N_c = 230$.

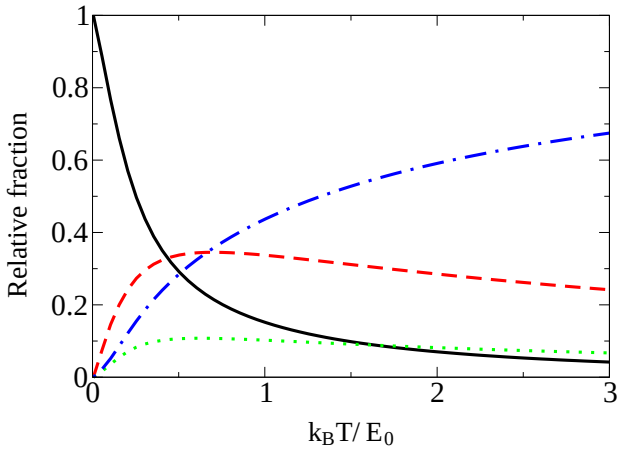

Figure 5.6: Temperature dependence of the fraction of molecules in trimers (solid), dimers I (dashed), dimers II (dotted) and monomers (dashed-dotted). We consider the parameters of figure 5.5 with $N < N_c$.

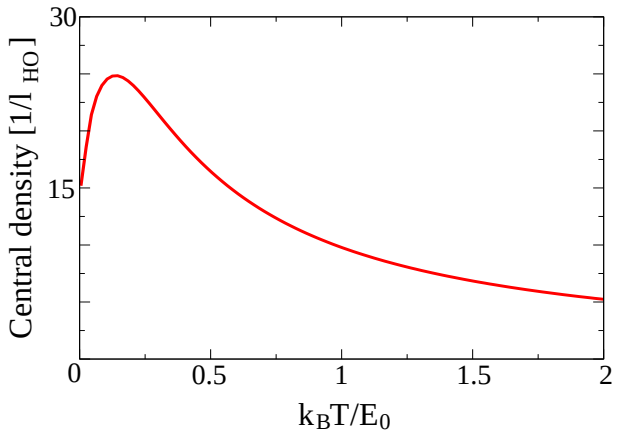

Figure 5.7: Temperature dependence of the central density. We consider the parameters of figure 5.5 with $N < N_c$.

between two point dipoles (1.71). Adding up these interactions we may estimate the mean inter-trimer dipole-dipole interaction

$$V_{ff}(\bar{x}) = -2\frac{d^2}{4\pi\epsilon_0}\Delta^2\left(\frac{1}{(\Delta^2+\bar{x}^2)^{5/2}} + \frac{2}{(4\Delta^2+\bar{x}^2)^{5/2}}\right), \tag{5.15}$$

where $\bar{x}$ is the mean inter-trimer distance. For the case of $d = 0.8$ Debye, $m = 100$ atomic mass units, $\Delta = 0.5\mu$m, and $\omega/2\pi = 1$Hz, we obtain $U_0 \simeq 2$, and $N_c \simeq 230$. For this value $\bar{x} \simeq 1.7\Delta$ and $V_{ff} \simeq 0.33\epsilon_F$. The ideal gas approximation is hence quantitatively valid only for dilute mesoscopic samples (as those considered in our numerical calculations). Once the dimer Bose gas nucleates at the trap center the ideal gas condition is quickly violated, due to the larger bosonic densities, although the formation of the dual density profile (similar to that in figure 5.5) still holds. For stacks of 2D sites the ideal gas approximation fails even for extremely low 2D densities. However, the formation of dimer mixtures beyond a given critical density should also occur for 2D arrangements. These mixtures may be considered as weakly-interacting for 2D densities n such that $nr_*^2 < 1$ with $r_* = md^2/\hbar^2$. For the previous values this demands $n \lesssim 1.1\times10^8\text{cm}^{-2}$. For $N \gg N_c$ (and $U_0 > U_0^*(D,II)$) weakly-interacting dimers will form a BEC of three different bosons (dimers I in 1–2, I in 2–3, and II), whose properties will largely depend on the precise determination of the different inter-dimer interactions, which will be the subject of a future work.

5.7 Conclusion

Fermionic polar molecules in three-well potentials are expected to form a rather peculiar filament gas. Depending on the filling per site and the interaction strength we expect that the character of the chain gas ranges from a pure trimer gas at low fillings, to a bosonic mixture of pseudo-spin-1/2 and spin-less dimers for large-enough fillings and dipole strengths. Note, finally, that molecules in even larger number of sites may form a quantum gas mixture of increasing complexity. Dipolar chain liquids are hence an exciting perspective for on-going experiments with polar fermionic molecules.

Chapter 6

Conclusion and Outlook

In this thesis we have studied novel properties of quantum gases in deep optical lattices induced by the dipole-dipole interaction. Because of its long-range and anisotropic character the dipole-dipole interaction may significantly change the physics of ultracold quantum gases. We have shown that in the presence of an additional one-dimensional optical lattice, the influence of the of the dipole-dipole interaction is crucially enhanced. In particular, concerning vortex lines in Bose-Einstein condensates it may lead to an instability of transverse excitations and novel ground-state configurations of the vortex filament. In combination with the long-range behaviour of the dipole-dipole interaction it may lead to roton-instability in a stack of non-overlapping BECs and one can observe band-like excitation spectra because of the dipolar coupling between the lattice sites. Last but not least we have shown that sufficiently strong dipoles like polar molecules placed at the different sites of an optical lattice may bind into composites and obey for the case of fermions a very interesting and rich quantum statistics.

In the following, we give a brief outlook on possible future projects based on the results of this thesis.

In chapters 2 and 3 we discussed in detail the physics of the vortex line in a dipolar gas. However, we have not considered several vortex lines interacting with each other. It should be interesting to study the dipolar influence on these vortex line interactions and in particular the interaction between two helical vortex filaments. Recently, the physics of dipolar vortices in harmonic traps and the influence of the trap geometry has been studied in [188] (also for the $n = 2$-vortex).

As mentioned already in chapter 4 an analysis of the roton-instability is interesting for ongoing experiment in Florence and Stuttgart. However, for simulating an experiment, a more careful quantitative analysis is necessary, taking into account both the xy-trapping, and the z-trapping, which we plan to investigate in a further work. The first step extending our work, namely the numerical calculation of the ground state with an imaginary

time evolution method in a trapped situation has been done by now in [203]. However, the roton-instability can be discussed only considering elementary excitations which is still an open problem in the trapped case.

The quantum gas of self-assembled chains of fermionic polar molecules investigated in chapter 5 provides a variety of phases already in the ideal gas regime. Hence it would be fascinating to analyse the filament gas in one or two dimensions in a weakly or even strongly interacting regime with numerical methods. In a first step we study at the moment two weakly interacting two-dimensional gases of fermionic dipoles in a double well potential. Since the Fermi gases are attractively coupled via the dipole-dipole interaction, they may form, for the case of weak dipolar interactions, weakly bound Cooper pairs and the system can be described by BCS theory. If the dipoles are sufficiently strong the Fermions may bound into bosonic dimers as in chapter 5 and can form a dimer-BEC. In this way one could find by slowly increasing the strength of the dipole-dipole interaction a continuous BCS-BEC crossover. However, it is crucial to understand first the scattering properties in detail.

All in all, one can state that dipolar gases in deep optical lattice will provide fascinating and novel physics also in the near future.

Appendix A

Imaginary time evolution method

The imaginary time evolution method (ITE) is used in order to find the ground state of a physical system. The time-dependence of the system is determined by the Hamiltonian H.

We consider an initial state $|\psi_{ini}\rangle$. Evolving during a short time Δt,

$$|\psi(\Delta t)\rangle = e^{-iH\Delta t}|\psi_{ini}\rangle \tag{A.1}$$

If $|\psi_{ini}\rangle$ is not an eigenstate of H one can write

$$e^{-iH\Delta t}|\psi_{ini}\rangle = \sum_n e^{-iE_n\Delta t}|\phi_n\rangle\langle\phi_n|\psi_{ini}\rangle \tag{A.2}$$

where E_n are the eigenvalues and $|\phi_n\rangle$ the eigenstates of H. If $|\psi_{ini}\rangle$ is not too different from the ground-state $|\phi_0\rangle$ it has some overlap ($\langle\phi_0|\psi_{ini}\rangle \neq 0$) and one can separate

$$e^{-iH\Delta t}|\psi_{ini}\rangle = e^{-iE_0\Delta t}|\phi_0\rangle\langle\phi_0|\psi_{ini}\rangle + \sum_{n\neq 0} e^{-iE_n\Delta t}|\phi_n\rangle\langle\phi_n|\psi_{ini}\rangle \tag{A.3}$$

If we now evolve in imaginary time ($i\Delta t \to \Delta t$) we can get rid of the $n \neq 0$-states after a sufficient number of time-steps since $E_n > E_0$. The system converges into the ground state $|\phi_0\rangle$ with energy E_0.

As discussed in the introduction, the time-dependence of the ground-state $|\phi_0\rangle$ in a quantum gas is determined by the chemical potential μ, such that $E_0 \equiv \mu$.

A chemical potential $\tilde{\mu}$ can be calculated at each imaginary time step from the normalization condition

$$Norm \equiv \langle\psi(t+\Delta t)|\psi(t+\Delta t)\rangle = e^{-2\tilde{\mu}\Delta t}\langle\psi(t)|\psi(t)\rangle, \tag{A.4}$$

where $|\psi_(t)\rangle$ should be normalized. Then

$$\tilde{\mu} = \frac{-\ln(Norm)}{2\Delta t}. \tag{A.5}$$

When the imaginary time evolution has converged to the ground state, the chemical potential calculated in this way $\tilde{\mu}$ corresponds to the real chemical potential μ of the system. This gives us the truncation condition,

$$\mu_{rel} \equiv \left| \frac{\tilde{\mu}(t+\Delta t) - \tilde{\mu}(t)}{\tilde{\mu}(t+\Delta t)} \right| < \epsilon, \tag{A.6}$$

for a very small ϵ (e.g. $\epsilon = 10^{-12}$). If the relative chemical potential μ_{rel} tends to zero the state has converged into the ground state $\psi(t) = |\phi_0\rangle$ and $\tilde{\mu} = \mu$.

Summarizing, for the imaginary time evolution method one has to perform the following steps:

1. Start with a normalized state $|\psi_{ini}\rangle$ and some value for $\tilde{\mu}$.
2. Evolve a short step Δt in imaginary time and calculate $|\psi(t+\Delta t)\rangle$.
3. Calculate the $Norm$ and the new value for $\tilde{\mu}$ and check whether μ_{rel} is smaller than ϵ.
4. If μ_{rel} is larger than ϵ, normalize $|\psi(t+\Delta t)\rangle$ and go back to step 2. Repeat steps 2-4 until $\mu_{rel} < \epsilon$.

Imaginary time evolution in 1D

In one dimension we discretize the operator H as follows. We consider $|\psi(\Delta t)\rangle$ in position space $\psi(x,t)$ and split the time-evolution operator in equation (A.1)

$$e^{iH\Delta t/2}\psi(x,\Delta t) = e^{-iH\Delta t/2}\psi_{ini}(x) \tag{A.7}$$

Since Δt is very small we can expand the exponential and obtain in imaginary time

$$(1 + H\Delta t/2)\psi(x,\Delta t) = (1 - H\Delta t/2)\psi_{ini}(x) \tag{A.8}$$

By discretizing the x-axis we identify

$$M\vec{\psi}(\Delta t) = \vec{R}, \tag{A.9}$$

where the vector $\vec{R}$ is the known right-hand site in equation (A.8), $\vec{\psi}(\Delta t)$ is unknown and M is the matrix $(1 + H\Delta t/2)$ which is usually tridiagonal because of the second derivative appearing in the kinetic energy. In order to determine $\vec{\psi}(\Delta t)$ one can take in this case for instance the routine "tridag" from Numerical Recipes [184]. This procedure was used in the calculation of the straight vortex line (sections 1.4.2 and 2.2) in order to solve (1.55) and (2.6).

Imaginary time evolution in 3D

In chapter 3 we perform an imaginary time evolution in three dimensions. In this section we discuss in detail how to do the time evolution (step 2) for this case. Instead of solving a tridiagonal matrix equation we use Fourier transformations to handle the kinetic energy terms in the Hamiltonian. Therefore we write $|\psi(\Delta t)\rangle$ in position space as $\psi(\vec{r}, \Delta t)$ and seperate

$$H = \frac{p^2}{2m} + V(\vec{r}) \tag{A.10}$$

Applying the Baker-Campbell-Hausdorff $e^{A+B} = e^A\, e^B\, e^{-[A,B]/2}$ formula we neglect the commutator terms since they are of the order of Δt^2 and hence equation (A.1) reads in imaginary time

$$\psi(\vec{r}, \Delta t) = e^{-p^2/2m\Delta t}\, e^{-V(\vec{r})\Delta t}\psi_{ini}(\vec{r}) + O(\Delta t^2) \tag{A.11}$$

where the second exponential containing the potential energy acts just as a multiplication at each position $\vec{r}$. After this multiplication we call the vector $\psi_V(\vec{r}) \equiv e^{-V(\vec{r})\Delta t}\psi_{ini}(\vec{r})$ and rewrite equation (A.11)

$$\psi(\vec{r}, \Delta t) = e^{-p^2/2m\Delta t}\, \psi_V(\vec{r}). \tag{A.12}$$

In order to evaluate the action of the momentum operator in the exponential we apply a Fast Fourier transformation (FFT) [184] on $\psi_V(\vec{r})$ multiply and transform back to position space

$$\psi(\vec{r}, \Delta t) = \mathrm{FFT}^{-1}\left[e^{-p^2/2m\Delta t}\, \mathrm{FFT}\left[\psi_V(\vec{r})\right]\right]. \tag{A.13}$$

Appendix B

Dipolar gases in one-dimensional lattices

In this appendix we discuss in detail the derivation of the coarse-grained Hamiltonian employed in chapters 2 and 3. A BEC in a deep one dimensional optical lattice (section 1.3.2) is described by a discretisized wave-function and obeys a discrete nonlinear Schrödinger equation. We will show in detail that this equation can be transformed into a continuous equation, where the influence of the lattice is taken into account only by an effective mass m^* for motions in lattice direction and a renormalized coupling constant for the short-range interactions $\tilde{g}$.

Gross-Pitaevskii equation

In the following we consider an interacting system with the following two-body interaction

$$U(\vec{r}) = g\delta^3(\vec{r}) + V_d(\vec{r}), \tag{B.1}$$

where the first term is the contact interaction and the second is the dipole-dipole interaction (dipoles oriented in z-direction) (1.66)

$$V_d(r) = d^2 \frac{x^2 + y^2 - 2z^2}{r^5} \tag{B.2}$$

with the Fourier transform (1.68)

$$\tilde{V}_d(k) = \frac{g_d}{2}\left(3\frac{k_z^2}{k_\rho^2 + k_z^2} - 1\right) = \frac{g_d}{2}\left(2 - 3\frac{k_\rho^2}{k_\rho^2 + k_z^2}\right) \tag{B.3}$$

where $g_d = 8\pi d^2/3$. At sufficiently low temperatures the physics of the dipolar condensate is provided by the Gross-Pitaevskii equation (GPE) (1.69)

$$i\hbar\frac{\partial\Psi(\vec{r})}{\partial t} = \left[-\frac{\hbar^2\nabla^2}{2m} + V_{ext}(\vec{r}) + g|\Psi(\vec{r})|^2 + \int d\vec{r}'\,|\Psi(\vec{r}')|^2\,V_d(\vec{r}-\vec{r}')\right]\Psi(\vec{r}), \tag{B.4}$$

Discrete Gross-Pitaevskii equation

In the following we consider a BEC placed in a 1D lattice along the z-direction (1.33)

$$V_{ext}(z) = sE_R\,\sin^2(Qz)\,, \tag{B.5}$$

where $E_R = \hbar^2Q^2/2m$ the recoil energy. In the tight-binding regime (for a sufficiently strong lattice potential) we can write (1.35)

$$\Psi(\vec{r},t) = \sum_j w(z-bj)\psi_j(\vec{\rho},t), \tag{B.6}$$

where $b = \pi/Q$ is the lattice spacing, $\vec{\rho}$ the position in the xy-plane and $w(z)$ is the Wannier function associated with the lowest band. The GPE equation (discrete nonlinear Schrödinger equation) of the dipolar BEC reads analogously to (1.36) [84]

$$i\hbar\frac{\partial}{\partial t}\psi_j(\vec{\rho},t) = \left[-\frac{\hbar^2}{2m}\nabla^2_{\vec{\rho}} + \bar{g}|\psi_j(\vec{\rho},t)|^2 + V_{dd}(\vec{\rho},j,t)\right]\psi_j(\vec{\rho},t) - J(\psi_{j-1}(\vec{\rho},t) - 2\psi_j(\vec{\rho},t) + \psi_{j+1}(\vec{\rho},t)), \tag{B.7}$$

where (1.37)

$$J = \int dz\,w(z)\left[-\frac{\hbar^2}{2m}\frac{d^2}{dz^2} + V_{ext}(z)\right]w(z+b) \equiv \frac{2b^2}{\hbar^2}\,\frac{m}{m^*} \tag{B.8}$$

$$n_j(\rho,t) = |\psi_j(\rho,t)|^2, \tag{B.9}$$

$$f_j(z) = f(z-bj) = |w(z-bj)|^2, \tag{B.10}$$

$$\bar{g} = gb\int dz\,w(z)^4, \tag{B.11}$$

$$V_{dd} = \int V(\vec{r}-\vec{r}')\sum_{j'} n_{j'}(\rho',t)f_{j'}(z')d^3r'\,f_j(z)dz. \tag{B.12}$$

Approximation #1 In deriving the discrete GPE we have made the assumption in the interaction term that in the tight-binding regime we approximate $w(z+bj)w(z+bj') \approx \delta_{jj'}f(z+bj))$ [179]. We use the convolution theorem to rewrite

$$V_{dd}(\vec{\rho},j,t) = \int V(\vec{r}-\vec{r}')\sum_{j'} n_{j'}(\rho',t)f_{j'}(z')d^3r'\,f_j(z)dz \tag{B.13}$$

$$= \frac{1}{(2\pi)^3}\int d^3k\tilde{V}(\vec{k})|\tilde{f}(k_z)|^2\sum_{j'}\tilde{n}_{j'}(k_\rho,t)e^{\left[ik_zd(j-j')+i\vec{k}_\rho\vec{\rho}\right]},$$

where $\tilde{V}(\vec{k})$, $\tilde{f}(k_z)$ and $\tilde{n}_{j'}(k_\rho)$ denote the Fourier transform of $V(\vec{r})$, $f(z)$ and $n_j(\vec{\rho})$,respectively. We define the disctrete Fourier transform

$$\tilde{\mathfrak{n}}(\vec{k}) = \sum_j \exp\left[-ik_z bj\right] \tilde{n}_j(k_\rho) \tag{B.14}$$

which fulfills

1. $\tilde{\mathfrak{n}}(k\rho, k_z + 2\pi m/b) = \tilde{\mathfrak{n}}(k_\rho, k_z)$ with $m = 0, \pm 1, \pm 2, ...$
2. $\dfrac{b}{2\pi}\displaystyle\int_{IBZ} \tilde{\mathfrak{n}}(\vec{k})\ \exp\left[ik_z bj\right]\ dk_z = \tilde{n}_j(k_\rho)$

where IBZ is the first Brillouin zone $(-\pi/b, \pi/b)$. We split the integral of k_z in the following way

$$\int_{-\infty}^{+\infty} F(k_z) \exp\left[ik_z bj)\right] dk_z = \sum_m \int_{IBZ} F(k_z + 2\pi m/b) \exp\left[ik_z bj)\right] dk_z \tag{B.15}$$

to obtain that

$$V_{dd}(\rho, j) = \int_{IBZ} \tilde{\mathcal{V}}(\vec{k}) \tilde{\mathfrak{n}}(\vec{k}) \exp\left[i\vec{k_\rho}\vec{\rho} + ik_z bj\right] d^3k \tag{B.16}$$

with

$$\tilde{\mathcal{V}}(\vec{k}) = \sum_m \tilde{V}(k_\rho, k_z + 2\pi m/b) |\tilde{f}(k_z + 2\pi m/b)|^2 \tag{B.17}$$

Approximation #2: We assume that b is the smallest scale of distance. Since the vortex core has a size of the order of the healing length, the dominant contribution is provided by $k_\rho \sim 1/\xi$, where ξ is the healing length. We assume $b \ll \xi$.

Approximation #3: In addition, we will be interested (when performing the Bogoliubov analysis) in k_z-momenta q such that $q \sim 1/\xi$ (figure 2.1). Therefore for $m \neq 0$, $\tilde{V}(k_\rho, k_z + 2\pi m/b) \approx \tilde{V}(0, k_z + 2\pi m/b) = g_d$. Then

$$\tilde{\mathcal{V}}(\vec{k}) = \tilde{V}(\vec{k}) |\tilde{f}(k_z)|^2 + \mathcal{C}_{dd}(k_z), \tag{B.18}$$

with

$$\begin{aligned}
\mathcal{C}_{dd}(k_z) &= g_d \sum_{m\neq 0} |\tilde{f}(k_z + 2\pi m/b)|^2 \\
&\approx g_d \sum_{m\neq 0} \exp\left[-(k_z + 2\pi m/b)^2 \sigma^2/2\right] \\
&\approx g_d \sum_{m\neq 0} \exp\left[-(2\pi m/b)^2 \sigma^2/2\right] \\
&= g_d \left(\Theta_3\left[0, \exp\{-2\pi^2\sigma^2/b^2\}\right] - 1\right) \equiv \mathcal{G}_d,
\end{aligned} \tag{B.19}$$

where Θ is the elliptic theta function. In the previous expressions we have assumed, as usual, a Gaussian form (with width $\sigma \simeq b/\pi s^{1/4}$) for the function f. Note, that for typical parameters $\mathcal{G}_d$ is a very small number. The final form of the discrete GPE reads

$$\begin{aligned} i\hbar\frac{\partial}{\partial t}\psi_j(\vec{\rho},t) &= -J(\psi_{j-1}(\vec{\rho},t)-2\psi_j(\vec{\rho},t)+\psi_{j+1}(\vec{\rho},t)) \\ &+\left[-\frac{\hbar^2}{2m}\nabla^2_{\vec{\rho}}+\bar{g}|\psi_j(\vec{\rho},t)|^2\right]\psi_j(\vec{\rho},t) \\ &+\int_{IBZ}\tilde{V}(\vec{k})|\tilde{f}(k_z)|^2\tilde{\mathtt{n}}(\vec{k},t)\exp\left[i\vec{k_\rho}\vec{\rho}+ik_zbj\right]\frac{d^3k}{(2\pi)^3}\,\psi_j(\vec{\rho},t) \end{aligned} \tag{B.20}$$

where we redefine the contact interaction

$$\bar{g}+\frac{\mathcal{G}_d}{b}\to\bar{g}; \tag{B.21}$$

Effective continuous model

Since we consider (in our Bogoliubov analysis) $k_z \ll \pi/b$ we can actually consider an effective continuous model. To this aim we rewrite the tunneling part [179]

$$-J(\psi_{j+1}-2\psi_j+\psi_{j-1})\to -Jb^2\partial_z^2\psi\equiv-\frac{\hbar^2}{2m^*}\partial_z^2\psi \tag{B.22}$$

where we have employed the effective mass associated with the lowest band $E(\kappa)=-2J\,\cos(\kappa b)$ at quasi-momentum $\kappa\to 0$, namely $\hbar^2/2m=Jb^2$. We redefine

$$\frac{1}{\sqrt{b}}\psi_j(\vec{\rho})\to\psi(\vec{r}), \tag{B.23}$$

where now $\psi(\vec{r})$ is the new coarse-grained wavefunction. As a consequence

$$\bar{g}n\to\tilde{g}n, \tag{B.24}$$

where $\tilde{g}=\bar{g}b$ and

$$\int_{IBZ}\tilde{V}(\vec{k})|\tilde{f}(k_z)|^2\tilde{\mathtt{n}}(\vec{k})\,e^{i\vec{k_\rho}\vec{\rho}+ik_zbj}\frac{d^3k}{(2\pi)^3}\to\int\tilde{V}(\vec{k})\tilde{n}(\vec{k})\,e^{i\vec{k}\vec{r}}\frac{d^3k}{(2\pi)^3}. \tag{B.25}$$

In this expression we have employed that since, as discussed above, we consider that at most $k_z\sim 1/\xi$, and $\xi\gg\sigma$, then $|\tilde{f}(k_z)|\simeq 1$. Additionally, in the last equation we have used that

$$\tilde{\mathtt{n}}(\vec{k})\to\int\exp\left[ik_zz\right]\tilde{n}(\vec{k_\rho},z)dz=\tilde{n}(\vec{k}). \tag{B.26}$$

In conclusion, the final effective continuous GPE (which we consider in chapters 2 and 3) read

$$\begin{aligned} i\hbar\frac{\partial\Psi(\vec{r})}{\partial t} &= \left\{-\frac{\hbar^2\nabla_\perp^2}{2m}-\frac{\hbar^2\nabla_z^2}{2m^*}+\tilde{g}|\Psi(\vec{r})|^2+\right. \\ &\left.\int d\vec{r}'|\Psi(\vec{r}')|^2V_d(\vec{r}-\vec{r}')\right\}\Psi(\vec{r}), \end{aligned} \tag{B.27}$$

where we have applied the convolusion theorem in the dipolar term. The renormalized coupling constant is

$$\begin{aligned} \tilde{g} &= gb\int|f(z)|^2dz+\mathcal{G}_d \\ &\approx \frac{g}{\sqrt{2\pi}}\left(\frac{b}{\sigma}\right)+g_d\left(\Theta_3\left[0,\exp\{-2\pi^2\sigma^2/b^2\}\right]-1\right), \end{aligned} \tag{B.28}$$

where in the last equation we have assumed, as above, a Gaussian approximation for the Wannier function.

Appendix C

Calculations to the dipolar vortex line

When studying vortex lines we have used several times the integral representation of the Bessel functions of the first kind [180], which is particularly important when performing Fourier transformations with cylindrical symmetry

$$\int_0^{2\pi} d\phi \, e^{\pm i\, z \cos(\phi-\phi')} \, e^{in\phi} = 2\pi(\pm i)^n J_n(z) \, e^{in\phi'}, \tag{C.1}$$

for integer n. The Bessel functions satisfy the orthonomality condition

$$\int_0^{\infty} \mathrm{d}k_\rho \, k_\rho J_0(k_\rho\rho')J_0(k_\rho\rho) = \frac{1}{\rho}\delta(\rho-\rho'). \tag{C.2}$$

Since the Fourier transform of the dipole-dipole interaction potential (1.68) is crucial for the calculations shown in this appendix we specify it again

$$\tilde{V}_d(k) = \frac{g_d}{2}\left(3\frac{k_z^2}{k_\rho^2+k_z^2}-1\right) = \frac{g_d}{2}\left(2-3\frac{k_\rho^2}{k_\rho^2+k_z^2}\right) \tag{C.3}$$

with $g_d = 8\pi\alpha d^2/3$, where α is a possible prefactor induced by the dipolar tuning (section 1.5.1).

Straight vortex line

The straight vortex line ($n = 1$) has the form (2.4)

$$\Psi_0(\vec{r},t) = \phi_0(\rho)\, e^{i\varphi}\, e^{-i\mu t/\hbar}, \tag{C.4}$$

As a typical example how to treat the dipole-dipole interaction potential we discuss in detail equation (2.5), which gives the dipolar contribution to

the physics of the straight vortex line.

$$\begin{aligned}
\int d\vec{r}' \, |\Psi_0(\vec{r}')|^2 \, V_d(\vec{r}-\vec{r}') &= \int \frac{d^3k}{(2\pi)^3} \, \widetilde{|\Psi_0(\vec{r}')|^2} \, \widetilde{V_d}(\vec{k}) \, e^{i\vec{k}\vec{r}} \\
&= \int \frac{d^3k}{(2\pi)^3} \, \widetilde{|\phi_0(\rho)|^2} 2\pi\delta(k_z) \, \widetilde{V_d}(\vec{k}) \, e^{i\vec{k}\vec{r}} \\
&= \int \frac{d^2k}{(2\pi)^2} \widetilde{|\phi_0(\rho)|^2} \, \widetilde{V_d}(\vec{k_\rho}, 0) \, e^{i\vec{k_\rho}\vec{\rho}} \\
&= \int \frac{d^2k}{(2\pi)^2} \widetilde{|\phi_0(\rho)|^2} \, \left(-\frac{\alpha d^2 4\pi}{3} \right) e^{i\vec{k_\rho}\vec{\rho}} \\
&= -\frac{\alpha d^2 4\pi}{3} |\phi_0(\rho)|^2 \qquad \text{(C.5)}
\end{aligned}$$

Kelvin modes

In order to derive the eigenvalue equations for the Kelvin modes (2.11) and (2.12), one can proceed analogously. We start with the linearized differential equation (2.9) for the vortex line excitations $\chi(\vec{r})$

$$\begin{aligned}
i\hbar\partial_t \chi(\vec{r},t) &= \Big[-\frac{\hbar^2}{2m}\nabla_\perp^2 - \frac{\hbar^2}{2m^*}\nabla_z^2 - i\frac{\hbar^2}{m\rho^2}\partial_\varphi + \frac{\hbar^2}{2m\rho^2} - \mu \\
&\quad + (2\tilde{g} - \frac{g_d}{2}) \, |\phi_0(\rho)|^2 \Big] \, \chi(\vec{r}) \; + \tilde{g}\phi_0^2(\rho)\chi^*(\vec{r}) \qquad \text{(C.6)} \\
&\quad + \int d\vec{r}' V(\vec{r}-\vec{r}')\phi_0(\rho')\phi_0(\rho) \left[\chi^*(\vec{r}') + \chi(\vec{r}') \right],
\end{aligned}$$

In order to be more accurate in this calculation we write the excitations at first in the form [52]

$$\chi(\vec{r}) = \sum_{l,k} b_l(q,\rho) \, \mathrm{e}^{\,\mathrm{i}\,qz} \, \mathrm{e}^{\,\mathrm{i}\,l\varphi}, \qquad \text{(C.7)}$$

characterized by the quantum numbers l and q. Later we will rewrite them and recognize expression (2.10). We simplify the dipolar term using again Fourier transformation and the convolution theorem, and find

$$\int \mathrm{d}\vec{r'} \, V(\vec{r}-\vec{r}')\phi_0(\rho')b_l(q,\rho') \, \mathrm{e}^{\,\mathrm{i}\,qz'} \, \mathrm{e}^{\,\mathrm{i}\,l\varphi'} \qquad \text{(C.8)}$$

$$= \int \frac{\mathrm{d}^3k}{(2\pi)^3} \, \widetilde{V}(k_\rho, k_\varphi, k_z+q) \, \widetilde{h}(\vec{k}) \, \mathrm{e}^{\,\mathrm{i}\,qz} \, \mathrm{e}^{\,\mathrm{i}\,\vec{k}\vec{r}}, \qquad \text{(C.9)}$$

where

$$\begin{aligned}
\widetilde{h}(\vec{k}) &= \int \mathrm{d}^3r \, \phi_0(\rho') \, b_l(q,\rho') \, \mathrm{e}^{\,\mathrm{i}\,l\varphi'} \, \mathrm{e}^{\,-\mathrm{i}\,\vec{k}\vec{r}'} \qquad \text{(C.10)} \\
&= 2\pi\delta(k_z) \int_0^\infty \mathrm{d}\rho' \, \rho'\phi_0(\rho') \, b_l(q,\rho') \int_0^{2\pi} \mathrm{d}\varphi' \, \mathrm{e}^{\,\mathrm{i}\,l\varphi'} \, \mathrm{e}^{\,-\mathrm{i}\,q_\rho\rho\cos(\varphi'-q_\varphi)}
\end{aligned}$$

Using the Bessel function of the first kind we get

$$\widetilde{h}(\vec{k}) = (2\pi)^2\delta(k_z)\,\mathrm{e}^{\,\mathrm{i}lk_\varphi}\int_0^\infty \mathrm{d}\rho'\,\rho'\phi_0(\rho')\,b_l(q,\rho')J_l(k_\rho\rho') \tag{C.11}$$

Now we are able to calculate the dipolar part (C.8)

$$\begin{aligned}
&\int \mathrm{d}\vec{r'}\,V(\vec{r}-\vec{r'})\phi_0(\rho')b_l(q,\rho')\,\mathrm{e}^{\,\mathrm{i}qz'}\,\mathrm{e}^{\,\mathrm{i}l\varphi'}\\
&\quad= \int \frac{\mathrm{d}^3k}{(2\pi)^3}\,\widetilde{V}(k_\rho,k_\varphi,k_z+q)\,(2\pi)^2\delta(k_z)\,\mathrm{e}^{\,\mathrm{i}lk_\varphi}\,\mathrm{e}^{\,\mathrm{i}qz}\,\mathrm{e}^{\,\mathrm{i}\vec{k}\vec{r}}\\
&\qquad\quad\times\int_0^\infty \mathrm{d}\rho'\,\rho'\phi_0(\rho')\,b_l(q,\rho')J_l(k_\rho\rho')\\
&\quad= \int_0^\infty \mathrm{d}\rho'\,\rho'\phi_0(\rho')\,b_l(q,\rho')\int_0^\infty \frac{\mathrm{d}k_\rho}{2\pi}\,k_\rho J_l(k_\rho\rho')\,\widetilde{V}(k_\rho,k_\varphi,q)\\
&\qquad\quad\times\int_0^{2\pi}\mathrm{d}k_\varphi\,\mathrm{e}^{\,\mathrm{i}l(k_\varphi-\varphi)}\,\mathrm{e}^{\,\mathrm{i}\,k_\rho\rho\cos(k_\varphi-\varphi)}\,\mathrm{e}^{\,\mathrm{i}qz}\,\mathrm{e}^{\,\mathrm{i}l\varphi}\\
&\quad= \int_0^\infty \mathrm{d}\rho'\,\rho'\phi_0(\rho')\,b_l(q,\rho')\,\mathrm{e}^{\,\mathrm{i}qz}\,\mathrm{e}^{\,\mathrm{i}l\varphi}\\
&\qquad\quad\times\alpha d^2\frac{4\pi}{3}\int_0^\infty \mathrm{d}k_\rho\,k_\rho J_l(k_\rho\rho')J_l(k_\rho\rho)\left[\frac{3q^2}{k_\rho^2+q^2}-1\right].
\end{aligned}\tag{C.12}$$

Note that the equations do not mix different q's and l's. Hence we consider the equations for one q and one l

$$\begin{aligned}
\mathrm{i}\hbar\,\dot{b}_l(q,\rho) \;=\;& \left[-\frac{\hbar^2}{2m}\left(\frac{1}{\rho}\partial_\rho+\partial_\rho^2\right)+\frac{\hbar^2(l+1)^2}{2m\rho^2}+\frac{\hbar^2q^2}{2m^*}-\mu\right.\\
&\left.+(2\tilde{g}-\alpha d^2\frac{4\pi}{3})\,|\phi_0(\rho)|^2\right]\,b_l(q,\rho)+\tilde{g}\phi_0(\rho)^2\,b^*_{-l}(-q,\rho)+\\
&\alpha d^2\frac{4\pi}{3}\int_0^\infty \mathrm{d}\rho'\,\rho'\phi_0(\rho')\,\{b_l(q,\rho')+b^*_{-l}(-q,\rho')\}\\
&\times\int_0^\infty \mathrm{d}k_\rho\,k_\rho J_l(k_\rho\rho')J_l(k_\rho\rho)\left[\frac{3q^2}{k_\rho^2+q^2}-1\right]\phi_0(\rho).
\end{aligned}\tag{C.13}$$

We separate equation (C.13) into positive and negative frequency parts

$$b_l(q,\rho) \;=\; u(\rho)\,\mathrm{e}^{\,-\mathrm{i}\epsilon t/\hbar} \tag{C.14}$$

$$b^*_{-l}(-q,\rho) \;=\; -v(\rho)\,\mathrm{e}^{\,\mathrm{i}\epsilon^* t/\hbar}. \tag{C.15}$$

and simplify the dipolar term finally using the following integral [181]

$$\int_0^\infty \mathrm{d}k_\rho\,k_\rho J_l(k_\rho\rho')J_l(k_\rho\rho)\left[\frac{3q^2}{k_\rho^2+q^2}-1\right]=3q^2\,F_l(q\rho,q\rho')-\frac{1}{\rho}\delta(\rho-\rho'), \tag{C.16}$$

with the product of modified Bessel functions

$$F_l(q\rho, q\rho') = \begin{cases} I_l(q\rho')\, K_l(q\rho) & \text{if} \quad \rho' < \rho \\ K_l(q\rho')\, I_l(q\rho) & \text{if} \quad \rho' > \rho \end{cases} . \tag{C.17}$$

Then equation (C.13) reduces to the Bogoliubov de-Gennes equations (2.11) and (2.12) discussed in chapter 2

$$\begin{aligned} \epsilon u_l(\rho) &= \left[\frac{\hbar^2}{2m}\left(-D_\rho + \frac{(l+1)^2}{\rho^2} + \frac{m}{m^*}q^2\right) - \mu + 2\bar{g}\phi_0(\rho)^2\right] u_l(\rho) \\ &\quad -\bar{g}\phi_0(\rho)^2 v_l(\rho) \qquad (C.18) \\ &\quad +\frac{3\beta}{2-\beta}\bar{g}q^2 \int_0^\infty d\rho'\rho'\phi_0(\rho')\phi_0(\rho)\left[u_l(\rho') - v_l(\rho')\right] F_l(q\rho, q\rho') \\ \epsilon v_l(\rho) &= -\left[\frac{\hbar^2}{2m}\left(-D_\rho + \frac{(l-1)^2}{\rho^2} + \frac{m}{m^*}q^2\right) - \mu + 2\bar{g}\phi_0(\rho)^2\right] v_l(\rho) \\ &\quad +\bar{g}\phi_0(\rho)^2 u_l(\rho) \qquad (C.19) \\ &\quad +\frac{3\beta}{2-\beta}\bar{g}q^2 \int_0^\infty d\rho'\rho'\phi_0(\rho')\phi_0(\rho)\left[u_l(\rho') - v_l(\rho')\right] F_l(q\rho, q\rho'), \end{aligned}$$

with $\bar{g} = \tilde{g} - g_d/2$ according to equation (2.7) and $\beta = g_d/\tilde{g}$.

Numerical calculation of the Kelvin modes

We solve at this point the coupled integral-differential equations for $u_l(\rho)$ and $v_l(\rho)$. Fortunately they are linear, such that we can transform them easily in an eigenvalue problem by discretizising the ρ-axis. Then $u_l(\rho)$ and $v_l(\rho)$ correspond to the eigenvectors and ϵ are the eigenvalues.

However, before solving the Bogoliubov de-Gennes equations (2.11) and (2.12) numerically one should get rid of the centrifugal barrier by a rescaling similar to that employed in the case of the straight vortex discussed in section 1.4.2

$$\begin{aligned} \phi_0(\rho) &= \rho\,\bar{\phi}_0(\rho) && (C.20) \\ u(\rho)_l &= \rho^{l+1}\bar{u}_l(\rho) && (C.21) \\ v(\rho)_l &= \rho^{l-1}\bar{v}_l(\rho) && (C.22) \end{aligned}$$

This implies for the terms containing the derivatives

$$\begin{aligned} \left[-\left(\frac{1}{\rho}\partial_\rho + \partial_\rho^2\right) + \frac{(l+1)^2}{\rho^2}\right] u_l(\rho) &= -\rho^{l+1}\left[\frac{(2l+3)}{\rho}\partial_\rho + \partial_\rho^2\right] \bar{u}_l(\rho) \\ \left[-\left(\frac{1}{\rho}\partial_\rho + \partial_\rho^2\right) + \frac{(l-1)^2}{\rho^2}\right] v_l(\rho) &= -\rho^{l-1}\left[\frac{(2l-1)}{\rho}\partial_\rho + \partial_\rho^2\right] \bar{v}_l(\rho). \end{aligned}$$

We insert these expressions into equations (2.11) and (2.12) and divide by ρ^{l+1} in the first equation and by ρ^{l-1} in the second one. In addition we transform into dimensionless units similar as in section 1.4.2.

$$\phi_0(\rho) \to \sqrt{n_0}\,\phi_0(\rho) \qquad \text{with} \qquad \rho \to \frac{\rho}{\rho_0} \qquad \text{and} \qquad \rho_0^2 = \frac{\hbar}{2m\bar{g}n_0},$$

Note, that $\sqrt{2}\rho_0 = \xi$ is the healing length with the shifted coupling constant $\bar{g}$. Then the dimensionless rescaled Bogoliubov de-Gennes equations reads as

$$\begin{aligned}
\epsilon\bar{u}_l(\rho) &= \left[-\left(\frac{(2l+3)}{\rho}\partial_\rho + \partial_\rho^2\right) + \frac{m}{m^*}q^2 - \mu + 2\bar{g}\rho^2\bar{\phi}_0(\rho)^2\right]\bar{u}_l(\rho) \\
&\quad -\bar{g}\bar{\phi}_0(\rho)^2\bar{v}_l(\rho) \quad + \frac{3\beta}{2-\beta}\bar{g}q^{2+l} \qquad \text{(C.23)} \\
&\quad \times \int_0^\infty d\rho'\rho'^{l+1}\bar{\phi}_0(\rho')\bar{\phi}_0(\rho)\left[\bar{u}_l(\rho')\rho^2 - \bar{v}_l(\rho')\right]\frac{F_l(q\rho, q\rho')}{(q\rho)^l} \\
\epsilon\bar{v}_l(\rho) &= \left[-\left(\frac{(2l-1)}{\rho}\partial_\rho + \partial_\rho^2\right) + \frac{m}{m^*}q^2 - \mu + 2\bar{g}\rho^2\bar{\phi}_0(\rho)^2\right]\bar{v}_l(\rho) \\
&\quad +\bar{g}\rho^4\bar{\phi}_0(\rho)^2 u_l(\rho) \quad + \frac{3\beta}{2-\beta}\bar{g}q^{2+l} \qquad \text{(C.24)} \\
&\quad \times \int_0^\infty d\rho'\rho'^{l+1}\bar{\phi}_0(\rho')\bar{\phi}_0(\rho)\left[\rho^2\bar{u}_l(\rho') - \bar{v}_l(\rho')\right]\frac{F_l(q\rho, q\rho')}{(q\rho)^l},
\end{aligned}$$

where μ and $\phi(\rho)$ are results of the imaginary time evolution of the straight vortex line. The chemical potential μ and $\bar{g}n_0$ are very close to one as they should be in these units.

It seems to be the case that there still appear a divergent term in (C.23) for $\rho \to 0$. But then $\rho' > \rho$ and the relevant term behaves as

$$\lim_{\rho\to 0}\frac{F_l(q\rho, q\rho')}{(q\rho)^l} = \lim_{\rho\to 0}\frac{I_l(q\rho)\,K_l(q\rho')}{(q\rho)^l}, \qquad \text{(C.25)}$$

which gives with l'Hospital

$$\lim_{\rho\to 0}\frac{I_l(q\rho)\,K_l(q\rho')}{(q\rho)^l} = \frac{1}{\Gamma(l+1)}\left(\frac{1}{2}\right)^l K_l(q\rho'). \qquad \text{(C.26)}$$

That is a finite value and there are no divergencies. Hence it is not too hard to solve the rescaled dimensionless Bogoliubov-de Gennes equations (C.23) numerically.

We solved these equations for $l = 1$ for given dipole β and lattice m/m^* and for differerent values of q to obtain the dispersion relation $\epsilon(q)$. Multiplying the resulting $\epsilon(q)$ with -1 leads to the Kelvin mode dispersion for $l = -1$. As one can see directly from (2.11) and (2.12) it is equivalent

to change $l \rightarrow -l$ and to interchange $u_l(\rho)$ and $v_l(\rho)$ in combination with $\epsilon \rightarrow -\epsilon$. This means an interchange of the (+) and (-) families of the excitations discussed in the introduction below equation (1.29).

Bibliography

[1] S. N. Bose, Z. Phys. **26**, 178 (1924).

[2] A. Einstein, Sitzber. Kgl. Preuss. Akad. Wiss. **1**, 3 (1925).

[3] D. Pines, *The Many-Body Problem* (W. A. Benjamin, New York, 1962).

[4] A. Fetter and J. Walecka, *Quantum Theory of Many-Paricle Systems* (McGraw-Hill, New York, 1971).

[5] S. Chu, Rev. Mod. Phys. **70**, 685 (1998).

[6] C. N. Cohen-Tannoudji, Rev. Mod. Phys. **70**, 707 (1998).

[7] W. D. Phillips, Rev. Mod. Phys. **70**, 721 (1998).

[8] K. B. Davis, M. O. Mewes, M. R. Andrews, N. J. Vandruten, D. S. Durfee, D. M. Kurn and W. Ketterle, Phys. Rev. Lett. **75**, 3969 (1995).

[9] M. H. Anderson, J. R. Ensher, M. R. Matthews, C. E. Wiemann and E. Cornell, Science **269**, 198 (1995).

[10] C. C. Bradley, C. A. Sackett, J. J. Tollett and R. G. Hulet, Phys. Rev. Lett. **75**, 1687 (1995).

[11] E. A. Cornell and C. E. Wiemann, Rev. Mod. Phys. **74**, 875 (2002).

[12] W. Ketterle, Rev. Mod. Phys. **74**, 1131 (2002).

[13] B. DeMarco and D. S. Jin, Science **285**, 1703 (1999).

[14] A. G. Truscott, K. E. Strecker, W. I. McAlexander, G. B. Partridge and R. Hulet, Science **291**, 2570 (2001).

[15] F. Schreck, L. Khaykovic, K. Corwin, G. Ferrari, T. Bourdel, J. Cubizolles and C. Salomon, Phys. Rev. Lett. **87**, 080403 (2001).

[16] Z. Hadzibabic, C. Stan, K. Diekmann, S. Gupta, M. Zwierlein, A. Görlitz and W. Ketterle Phys. Rev. Lett. **88**, 160401 (2002).

[17] F. Dalfovo, S. Giorgini, L. P. Pitaevskii and S. Stringari, Rev. Mod. Phys. **71**, 463 (1999).

[18] S. Giorgini, L. P. Pitaevskii and S. Stringari, Rev. Mod. Phys. **80**, 1215 (2008).

[19] P. G. de Gennes, *Superconductivity in metals and alloys*, (W. A. Benjamin, 1966).

[20] M. Randeria, in *Bose-Einstein Condensation*, edited by A. Griffin, D. W. Snoke and S. Stringari (Cambridge University Press, Cambridge, 1995).

[21] T.-L. Ho, Phys. Rev. Lett. **81**, 742 (1998).

[22] T. Ohmi, K. Machida, J. Phys. Soc. Jpn **67**, 1822 (1998).

[23] D. Jaksch, H.-J. Briegel, J. I. Cirac, C. W. Gardiner and P. Zoller, Phys. Rev. Lett. **82**, 1975 (1999).

[24] A. Peters, K. Y. Chung and S. Chu, Nature **400**, 849 (1999).

[25] G. Lamporesi *et al.*, Phys. Rev. Lett. **100**, 050801 (2008).

[26] P. R. Berman, *Atom Interferometry* (Academic Press 1997).

[27] H. Müller *et al.*, Phys. Rev. Lett. **100**, 031101 (2008).

[28] O. Morsch and M. Oberthaler, Rev. Mod. Phys. **78**, 179 (2006).

[29] D. Jaksch *et al.*, Phys. Rev. Lett. **81**, 3108 (1998).

[30] M. Greiner *et al.*, Nature **415**, 39 (2002).

[31] O. Morsch *et al.*, Phys. Rev. Lett. **87**, 140402 (2001).

[32] T. Lahaye, C. Menotti, L. Santos, M. Lewenstein and T. Pfau, Rep. Prog. Phys. **72**, 126401 (2009).

[33] M. A. Baranov, Physics Reports **464**, 71 (2008).

[34] F. Schwabl, *Statistische Mechanik*, (Springer, 2000).

[35] A. J. Leggett, *Quantum Liquids* (Oxford University Press, Oxford, 2006).

[36] C. Cohen-Tannoudji, B. Diu and F. Laloë, *Quantenmechanik I* (de Gruyter, Berlin, 1999).

[37] O. Penrose and L. Onsager, Phys. Rev. **104**, 576 (1956).

[38] C. N. Yang, Revs. Mod. Phys. **34**, 694 (1962).

[39] A. J. Leggett, in *Bose-Einstein Condensation*, edited by A. Griffin, D. W. Snoke and S. Stringari (Cambridge University Press, Cambridge, 1995).

[40] A. J. Leggett and F. Sols, Found. Phys. **21**, 353 (1991)

[41] M. Nakahara, *Geometry, Topology and Physics* (Taylor & Francis, London, 2003).

[42] J. W. Kane and L. P. Kadanoff, Phys. Rev. **155**, 80 (1967).

[43] N. Bogoliubov, J. Phys. USSR **11**, 23 (1947).

[44] A. J. Leggett, Rev. Mod. Phys. **73**, 307 (2001)

[45] C. J. Pethik and H. Smith, *Bose-Einstein Condensation in Dilute Gases* (Cambridge University Press, Cambridge, 2002).

[46] S. Stringari and L. P. Pitaevskiii, *Bose-Einstein Condensation*, (Oxford University Press, 2003).

[47] T. Köhler, K. Gòral and P. S. Julienne, Rev. Mod. Phys. **78**, 1311 (2006).

[48] C. Chin, R. Grimm, P. S. Julienne and E. Tiesinga, e-print arXiv: 0812.1496v2 (accepted in Rev. Mod. Phys.).

[49] S. Inouye, M. R. Andrews, J. Stenger, H. J. Miesner, D. M. Stamper-Kurn and W. Ketterle, Nature **392**, 151 (1998).

[50] P. Courteille, R. S. Freeland, D. J. Heinzen, A. F. van Abeelen and B. J. Verhaar, Phys. Rev. Lett. **81**, 69 (1998).

[51] E. P. Gross, J. Math. Phys. **4**, 195 (1963).

[52] L. P. Pitaevskii, Sov. Phys. JETP **13**, 451 (1961).

[53] A. Fetter and A. Svidzinsky, J. Phys.: Condens. Matter v. **13**, R135 (2001).

[54] I. S. Aranson and L. Kramer, Rev. Mod. Phys. **74**, 99 (2002).

[55] C. Sulem and P. L. Sulem, *The Nonlinear Schrödinger Equation* (Springer, New York, 1999).

[56] E. M. Lifshitz and L. P. Pitaevskii, *Statistical Physics II* (Nauka, Moscow, 1978).

[57] F. Schwabl, *Quantenmechanik für Fortgeschrittene*, (Springer, 2004).

[58] Y. Castin, in *Coherent atomic matter waves*, Lecture Notes of Les Houches Summer School, p.1-136, edited by R. Kaiser, C. Westbrook, and F. David, (EDP Sciences and Springer-Verlag, 2001)

[59] E. L. Raab, M. Prentiss, A. Cable, S. Chu and D. E. Pritchard, Phys. Rev. Lett. **59**, 2631 (1987).

[60] A. L. Migdall, J. V. Prodan, W. D. Phillips, T. H. Bergeman and H. J. Metcalf, Phys. Rev. Lett. **54**, 2596 (1985).

[61] T. H. Bergeman, G. Erez and H. J. Metcalf, Phys. Rev. A **35**, 1535 (1987).

[62] T. Mayer-Kuckuk, *Atomphysik*, (Teubner, Stuttgart, 1997).

[63] R. Grimm, M. Weidemüller and Yu. B. Ovchinnikov, Adv. At. Mol. Opt. Phys. **42**, 95 (2000).

[64] D. M. Stamper-Kurn, M. R. Andrews, A. P. Chikkatur, S. Inouye, H.-J. Miesner, J. Stenger and W. Ketterle, Phys. Rev. Lett. **80**, 2027 (1998).

[65] M. D. Barrett, J. A. Sauer and M. S. Chapman, Phys. Rev. Lett. **87**, 010404 (2001).

[66] J. Weiner, V. S. Bagnato, S. Zilio and P. S. Julienne, Rev. Mod. Phys. **71**, 1 (1999).

[67] I. Bloch, Nature Phys. **1**, 23 (2005).

[68] I. Bloch, J. Phys. B **38**, 629 (2006).

[69] M. R. Andrews *et al.*, Science **275**, 637 (1997).

[70] D. S. Petrov, G. V. Shlyapnikov and J. T. M. Walraven, Phys. Rev. Lett. **85**, 3745 (2000).

[71] J. O. Anderson, U. A. Khawaja and H. T. C. Stoof, Phys. Rev. Lett. **88**, 070407 (2002).

[72] U. A. Khawaja, J. O. Andersen, N. P. Proukakis and H. T. C. Stoof, Phys. Rev. A **66**, 013615 (2002).

[73] C. Mora and Y. Castin, Phys. Rev. A **67**, 053615 (2003).

[74] D. S. Petrov, M. A. Baranov and G. V. Shlyapnikov, Phys. Rev. A **67**, 031601 (2003).

[75] A. Görlitz *et al.*, Phys. Rev. Lett. **87**, 130402 (2001).

[76] M. Greiner, I. Bloch, O. Mandel, T. W. Hänsch and T. Esslinger, Phys. Rev. Lett. **87**, 160405 (2001).

[77] S. Burger *et al.*, Europhys. Lett. **57**, 1 (2002).

[78] V. Vuletic *et al.* Phys. Rev. Lett. **81**, 5768 (1998).

[79] H. Moritz, T. Stöferle, K. Günter, M. Köhl and T. Esslinger, Phys. Rev. Lett. **94**, 210401 (2005).

[80] N. Read and D. Green, Phys. Rev. B **61**, 10267 (1999).

[81] M. Randeria, J.-M. Duan, L.-Y. Shieh, Phys. Rev. B **41**, 327 (1989).

[82] M. Lewenstein, A. Sanpera, V. Ahufinger, B. Damski, A. Sen, U. Sen, Adv. Phys. **56**, 243 (2007).

[83] I. Bloch, J. Dalibard and W. Zwerger, Rev. Mod. Phys. **80**, 885 (2008).

[84] A. Trombettoni, and A. Smerzi, Phys. Rev. Lett. **86**, 2353 (2001).

[85] R. P. Feynman, in *Progress in Low Temperature Physics*, edited by C. J. Gorter (North-Holland, Amsterdam, 1955).

[86] L. Onsager, Nuovo Cimento **6**, 249 (1949).

[87] W. F. Vinen, in *Superconductivity* edited by R. D. Parks (Marcel Dekker, New York, 1969) Chap. 20.

[88] R. J. Donnelly, *Quantized Vortices in Helium II* (Cambridge, 1991).

[89] A. Fetter, Rev. Mod. Phys. **81**, 647 (2009).

[90] M. R. Matthews *et al.*, Phys. Rev. Lett. **83**, 2498 (1999).

[91] K. W. Madison *et al.*, Phys. Rev. Lett. **84**, 806 (2000).

[92] J. R. Abo-Shaeer *et al.*, Science **292**, 476 (2001).

[93] N. Manton and P. M. Sutcliffe, *Topological Solitons* (Cambridge University Press, Cambridge, 2004).

[94] N. D. Mermin, Rev. Mod. Phys. **51**, 591 (1979)

[95] V. P. Mineev, Sov. Sci. Rev. A **2**, 173 (1980)

[96] G. Toulouse, J. Physique Lett. **37**, L149 (1976)

[97] Yu. N. Ovchinnikov and I. M. Sigal, Nonlinearity **11**, 1277 (1998).

[98] Yu. N. Ovchinnikov and I. M. Sigal, Physica A **261**, 143 (1998).

[99] D. Vollhardt and P. Wölfle, *The Superfluid Phases of Helium 3* (Taylor & Francis,London, 1990).

[100] J. J. Garcia-Ripoll *et al.*, Phys. Rev. A **61**, 053609 (2000).

[101] T. H. R. Skyrme, Proc. R. Soc. Lond. A **260**, 127 (1961).

[102] T.-L. Ho, Phys. Rev. Lett. **81**, 742 (1998).

[103] R. A. Battye, N. R. Cooper, P. M. Sutcliffe, Phys. Rev. Lett. **88**, 080401 (2002).

[104] L. E. Sadler *et al.*, Nature **443**, 312 (2006)

[105] A. Vilenkin and E. P. S. Shellard *Cosmic Strings and Other Topological Defects* (Cambridge University Press, Cambridge, 1994).

[106] J. Goldstone, Nuovo Cimento **19**, 154 (1961).

[107] P. W. Higgs, Phys. Lett. **12**, 132 (1964).

[108] R. L. Davis and E. P. S. Shellard, Phys. Rev. Lett. **63**, 2021 (1989).

[109] B. Gradwohl, G. Kälbermann, T. Piran and E. Bertschinger, Nuc. Phys. B **338**, 371 (1990).

[110] P. G. Saffman *Vortex Dynamics* (Cambridge University Press, Cambridge 1997).

[111] F. V. Dolzhanskii, V. A. Krymov and D. Yu. Manin, Sov. Phys. Usp. **33**, 495 (1990).

[112] D. M. Sedrakyan and K. M. Shakhabasyan, Sov. Phys. Usp. **34**, 555 (1991).

[113] V. L. Ginzburg and L. P. Pitaevskii, JETP **34**, 1240 (1958).

[114] A. A. Abrikosov, JETP **5**, 1174 (1957).

[115] V. Schweikhard *et al.*, Phys. Rev. Lett. **93**, 210403 (2004).

[116] V. Schweikhard *et al.*, Phys. Rev. Lett. **92**, 040404 (2004).

[117] N. R. Cooper, E. H. Rezayi, and S. H. Simon, Phys. Rev. Lett. **95**, 200402 (2005).

[118] N. R. Cooper, N. K. Wilkin and J. M. F. Gunn, Phys. Rev. Lett. **87**, 120405 (2001).

[119] N. K. Wilkin and J. M. F. Gunn, Phys. Rev. Lett. **84**, 6 (2000).

[120] N. R. Cooper and N. K. Wilkin, Phys. Rev. B **60**, R 16279 (1999).

[121] A. Griesmaier *et al.*, Phys. Rev. Lett. **94**, 160401 (2005).

[122] Q. Beaufils *et al.*, Phys. Rev. A **77**, 061601(R) (2008).

[123] M. Vengalattore *et al.*, Phys. Rev. Lett. **100**, 170403 (2008).

[124] M. Fattori *et al.*, Phys. Rev. Lett. **101**, 190405 (2008).

[125] S. E. Pollack *et al.*, Phys. Rev. Lett. **102**, 090404 (2009).

[126] H.-L. Bethelem and G. Meijer, Int. Rev. Phys. Chem.**22**, 73 (2003).

[127] C. Haimberger *et al.*, Phys. Rev. A. **70**, 021402(R) (2004).

[128] J. M. Sage *et al.*, Phys. Rev. Lett. **94**, 203001 (2005).

[129] C. Ospelkaus *et al.*, Phys. Rev. Lett. **97**, 120402 (2006).

[130] S.Ospelkaus *et al.*, Natur Phys. **4**, 622 (2008).

[131] J. Deiglmayr *et al.*, Phys. Rev. Lett. **101**, 133004 (2008).

[132] K. K. Ni *et al.*, Science **322**, 231 (2008).

[133] D. Tong *et al.*, Phys. Rev. Lett. **93**, 063001 (2004).

[134] D. Jaksch *et al.*, Phys. Rev. Lett. **85**, 002208 (2000).

[135] S. Yi and L. You, Phys. Rev. A 61, 041604 (2000).

[136] K. Góral, K. Rzążewski, and T. Pfau, Phys. Rev. A **61**, 051601 (2000).

[137] L. Santos, G. V. Shlyapnikov, P. Zoller and M. Lewenstein, Phys. Rev. Lett. **85**, 1791 (2000).

[138] L. Santos, G. V. Shlyapnikov, and M. Lewenstein, Phys. Rev. Lett. **90**, 250403 (2003).

[139] S. Giovanazzi, and D. H. J. O'Dell, Eur. Phys. J. D **31**, 439 (2004).

[140] S. Komineas and N. R. Cooper, Phys. Rev. A 75, 023623 (2007).

[141] S. Ronen, D. C. E. Bortolotti, and J. L. Bohn, Phys. Rev. Lett. **98**, 030406 (2007).

[142] M. A. Baranov, M. S. Marenko, V. S. Rychkov and G. V. Shlyapnikov, Phys. Rev. A **66**, 013606 (2002).

[143] M. A. Baranov *et al.*, Phys. Rev. Lett. **92**, 250403 (2004).

[144] G. M. Bruun and E. Taylor, Phys. Rev. Lett. **101**, 245301 (2008).

[145] N. R. Cooper and G. V. Shlyapnikov, Phys. Rev. Lett. **103**, 155302 (2009).

[146] J. Quintanilla, S.T. Carr and J.J. Betouras, Phys. Rev. A **79**, 031601 (2009).

[147] K. Góral, L. Santos, and M. Lewenstein, Phys. Rev. Lett. **88**, 170406 (2002).

[148] M. A. Baranov, K. Osterloh, and M. Lewenstein, Phys. Rev. Lett. **94**, 070404 (2005).

[149] E. H. Rezayi, N. Read, and N. R. Cooper, Phys. Rev. Lett. **95**, 160404 (2005).

[150] H. P. Büchler *et al.*, Phys. Rev. Lett. **98**, 060404 (2007).

[151] C. Menotti, C. Trefzger and M. Lewenstein, Phys. Rev. Lett. **98**, 235301 (2007).

[152] J. Stuhler *et al.*, Phys. Rev. Lett. **95**, 150406 (2005).

[153] T. Lahaye *et al.*, Nature **448**, 672 (2007).

[154] A. G. Litvak *et al.*, Sov. J. Plasma Phys. **1**, 60 (1975).

[155] M. Peccianti *et al.*, Nature **432**, 733 (2004).

[156] P. G. de Gennes and J. Prost, *The Physics of Liquid Crystals* (Oxford University Press, Oxford, 1995).

[157] R. Rosenzweig, *Ferrohydrodynamics* (Cambridge University Press, 1985).

[158] H. Knieling, R. Richter, I. Rehberg, G. Matthies and A. Lange, Phys. Rev. E **76**, 066301 (2007).

[159] P. Pedri and L. Santos, Phys. Rev. Lett. **95**, 200404 (2005).

[160] I. Tithonenkov, B. A. Malomed, and A. Vardi, Phys. Rev. Lett. **100**, 090406 (2008).

[161] R. Nath, P. Pedri and L. Santos, Phys. Rev. Lett. **101**, 210402 (2008).

[162] T. Lahaye *et al.*, Phys. Rev. Lett. **101**, 080401 (2008).

[163] R. Nath, P. Pedri and L. Santos, Phys. Rev. Lett. **102** 050401 (2009).

[164] L. D. Landau, J. Phys. U.S.S.R. **11**, 91 (1947).

[165] R. P. Feynman, Phys Rev. **94**, 262 (1954).

[166] S. Giovanazzi, A. Görlitz, and T. Pfau, Phys. Rev. Lett. **89**, 130401 (2002).

[167] D. Wang, New J. Phys. **10**, 053005 (2008).

[168] S. Yi and L. You, Phys. Rev. A **63**, 053607 (2001).

[169] K. Góral and L. Santos, Phys. Rev. A **66**, 023613 (2002).

[170] O. Dutta and P. Meystre, Phys. A **75**, 053604 (2007).

[171] D. H. O'Dell and C. Eberlein, Phys. Rev. A **75**, 013604 (2007).

[172] S. Yi and H. Pu, Phys. Rev. A **73**, 061602 (2006).

[173] N. R. Cooper, E. H. Rezayi, and S. H. Simon, Phys. Rev. Lett. **95**, 200402 (2005).

[174] J. Zhang and H. Zhai, Phys. Rev. Lett. **95**, 200403 (2005).

[175] W. Thompson, Phil. Mag. **10**, 155 (1880).

[176] R. A. Ashton and W. I. Glaberson, Phys. Rev. Lett. **42**, 1062 (1979).

[177] R. I. Epstein and G. Baym, Astrophys. Jour. **387**, 276 (1992).

[178] V. Bretin *et al.*, Phys. Rev. Lett. **90**, 100403 (2003).

[179] M. Krämer, L. Pitaevskii, and S. Stringari, Phys. Rev. Lett. **88**, 180404 (2002).

[180] I. A. Stegun and M. Abramowitz *Handbook of Mathematical Functions* (Dover Publications, 1964)

[181] I. S. Gradshteyn and I. M Ryzhik, *Table of Integrals, Series and Products* (Academic Press, 2000).

[182] M. Klawunn, R. Nath, P. Pedri and L. Santos, Phys. Rev. Lett. **100**, 240403 (2008).

[183] A. L. Fetter, Phys. Rev. **138**, A429 (1965).

[184] W. H. Press, S. A. Teukolsky, W. T. Vetterling and B. P. Flannery, *Numerical Recipes in C (Second Edition)* (Cambridge University Press, 1992).

[185] S. Ronen, D. C. E. Bortolotti, and J. L. Bohn ,Phys. Rev. A **74**, 013623 (2006).

[186] P. Öhberg and L. Santos, Phys. Rev. A **66**, 013616 (2002).

[187] S. A. McGee and M. J. Holland, Phys. Rev. A **63**, 043608 (2001).

[188] Ryan M. Wilson *et al.*, Phys. Rev. A **79**, 013621 (2009)

[189] E. G. Dalla Torre, E. Berg, and E. Altman, Phys. Rev. Lett. 97, 260401 (2006).

[190] R. Nath, P. Pedri, and L. Santos, Phys. Rev. A **76**, 013606 (2007).

[191] A. Argüelles and L. Santos, Phys. Rev. A **75**, 053613 (2007).

[192] D. Wang, M. D. Lukin, E. Demler, Phys. Rev. Lett. **97**, 180413 (2006).

[193] T. Schumm *et al.*, Nature Physics **1**, 57 (2005).

[194] J. Esteve *et al.*, Nature **455**, 1216 (2008).

[195] D. W. Wang and E. Demler, e-print arXiv: 0812.1838 (2008).

[196] M. Klawunn and L. Santos, Phys. Rev. A **80**, 013611 (2009).

[197] P. G. de Gennes and P. A. Pincus, Phys. Kondens. Mater. **11**, 189 (1970).

[198] P. I. C. Teixeira, J. M. Tavares and M. M. Telo da Gama, J. Phys. Condens.Matter **12**, R411 (2000).

[199] K. Butter *et al.*, Nature Materials **2**, 88 (2003).

[200] M. Klokkenburg *et al.*, Phys. Rev. Lett. **96**, 037203 (2006).

[201] B. Simon, Annals of Physics **97**, 279 (1976).

[202] J. Duhme, *Ultracold filament gases of polar molecules* (Diploma thesis, Hannover, 2009).

[203] P. Köberle and G. Wunner, Phys. Rev. A **80**, 063601 (2009).

List of Publications

The results of the present thesis have generated the following publications:

1. M. Klawunn, J. Duhme and L. Santos, *Bose-Fermi mixtures of self-assembled chains of fermionic polar molecules*, arXiv: 0907.4612 (cond-mat.quant-gas), (accepted in Phys. Rev. A).

2. M. Klawunn and L. Santos, *Hybrid multisite excitations in dipolar condensates in optical lattices*, Phys. Rev. A **80**, 013611 (2009).

3. M. Klawunn and L. Santos, *Phase transition from straight into twisted vortex lines in dipolar Bose-Einstein condensates*, New J. Phys. **11**, 055012 (2009), (Part of "Focus on Cold and Ultracold Molecules").

4. M. Klawunn, R. Nath, P. Pedri and L. Santos, *Transverse instability of straight vortex lines in dipolar BECs*, Phys. Rev. Lett, **100**, 240403 (2008).

Other publications of the author:

1. M. Klawunn, O. Lechtenfeld and S. Petersen, *Moduli-space dynamics of noncommutative abelian sigma-model solitons*, JHEP, **06** (2006) 032.

Acknowledgements

This work would not have been possible without the support of many people. It is therefore a pleasure for me to acknowledge their help.

First of all, I would like to express my thanks to my supervisor Luis Santos for giving me the opportunity to do my Ph.D. studies in Hannover and for introducing me to one of the most fascinating areas of physics. I thank him for his help with advice and expertise, and for numerous helpful discussions. He was willing to listen to all my questions and concerns and I am grateful for guiding my way as much as necessary. It was always very welcome to me to work in his very nice and active international research group and I would like to thank in this context Rejish Nath, Paolo Pedri and Jörg Duhme for enjoyable collaborations.

I am also grateful to Eric Jeckelmann for kindly agreeing to referee this thesis and for Wolfgang Ertmer for being the head of the examination board.

In addition I am very thankful to Tobias Wirth, Arturo Argüelles and Carsten von Zobeltitz for their patient help on various computer-related problems.

Special thanks goes to Kirsten Vogeler and Alex Pikovski for proofreading parts of this thesis and their useful feedback. Furthermore I would like to thank the following people for their help and useful discussions: Hendrik Adorf, Jörg Duhme, Philipp Hyllus, Rejish Nath, Alexander Pikovski, Alexander Seel, Oliver Topic, Kirsten Vogeler and Tobias Wirth.

I express my gratitude to our whole group for a great time in Hannover: Arturo Argüelles, Nils Bornemann, Ulrich Ebling, Garu Gebreyesus, Karen Rodriguez, Giovanni Mazzarella, Andreas Jakob, Philipp Hyllus, Maria Colome-Tatche, Jörg Duhme Frank Deuretzbacher, Kazimierz Lakomy, Alexander Pikovski. Apart from the people mentioned I am grateful to all the people working at the ITP for the nice working atmosphere in the institute.

I am greatly thankful to the financial support provided by SPP1116 and QUEST. Without that this thesis would not have been finished.

I also thank my parents and my family for giving me the possibility to have rest and recreate at the weekends. Finally, I want to express my deepest gratitude to Maria Beelte. I would not have been in the position to carry out this work at all without her love and encouragement.

Curriculum Vitae

19.8.1981	geboren in Hildesheim
1987 - 1991	Grundschule Algermissen
1991 - 1993	Orientierungsstufe St.-Augustinus-Schule, Hildesheim
1993 - 2000	Bischöfliches Gymnasium Josephinum, Hildesheim
2000	Schulabschluss: Abitur
2000 -2001	Wehrdienst
2001 - 2003	Grundstudium in Physik an der Leibniz Universität Hannover
2003	Vordiplom in Physik
2003 - 2006	Hauptstudium in Physik an der Leibniz Universität Hannover
2005 - 2006	Diplomarbeit am Institut für Theoretische Physik (Leibniz Universität Hannover)
2006	Abschluss als Diplom-Physiker
2006 - 2009	Promotionsstudium in Physik an der Leibniz Universität Hannover

Selbstständigkeitserklärung

Hiermit versichere ich, die vorliegende Doktorarbeit selbstständig und unter ausschließlicher Verwendung der angegebenen Hilfsmittel angefertigt zu haben.

Hannover, den 30. Oktober 2009

Michael Klawunn